REPUBLIQUE DU CAMEROUN
Paix-Travail-Patrie

****

UNIVERSITE DE YAOUNDE I

****

CENTRE DE RECHERCHE ET DE FORMATION DOCTORALE EN SCIENCES, TECHNOLOGIES ET GEOSCIENCES

****

UNITE DE RECHERCHE ET DE FORMATION DOCTORALE EN PHYSIQUES ET APPLICATIONS

****

B.P 812 Yaoundé
Email: crfd_stg@uy1.uninet.cm

REPUBLIC OF CAMEROON
Peace-Work-Fatherland

****

THE UNIVERSITY OF YAOUNDE I

****

POSTGRADUATE SCHOOL OF SCIENCES, TECHNOLOGY AND GEOSCIENCES

****

RESEARCH AND POSTGRADUATE TRAINING UNIT FOR PHYSICS AND APPLICATIONS

****

P.O. BOX 812 Yaoundé
Email: crfd_stg@uy1.uninet.cm

LABORATOIRE DE MECHANIQUE, MATERIAUX ET STRUCTURES

LABORATORIE OF MECHANICS, MATERIALS AND STRUCTURES

Nonlinear dynamics of some electromechanical systems combining translational and rotational motions within a magnetic field

Thesis submitted and defended in partial fulfillment of the requirements for the award of Doctorat of Philosophy (PhD) degree in Physics

Speciality: *Fundamental Mechanics and complex systems*

By

NGATCHA TANLY Nelly Danielle
Registration number: 10W0577

Master of sciences in Physics

Under the supervision of:

WOAFO Paul

Professor
University of Yaounde I

Year: 2024

UNIVERSITÉ DE YAOUNDE I
THE UNIVERSITY OF YAOUNDE I

FACULTÉ DES SCIENCES
FACULTY OF SCIENCES

DÉPARTEMENT DE PHYSIQUE
DEPARTMENT OF PHYSICS

ATTESTATION DE CORRECTION DE LA THÈSE DE DOCTORAT/Ph.D

Nous, Professeur **DJUIDJE KENMOE Germaine** et Professeur **ESSIMBI ZOBO Bernard**, respectivement Examinateur et Président du jury de la Thèse de Doctorat/PhD de Madame **NGATCHA TANLY Nelly Danielle**, Matricule **10W0577**, préparée sous la direction du Professeur **WOAFO Paul** (Université de Yaoundé 1) intitulée : « **Nonlinear dynamics of some electromechanical systems combining translational and rotational motions within a magnetic field**», soutenue le vendredi, **19 Janvier 2024**, en vue de l'obtention du grade de Docteur/PhD en Physique, Spécialité **Mécanique, Matériaux et Structures,** option **Mécanique Fondamentale et Systèmes Complexes** attestons que toutes les corrections demandées par le jury de soutenance ont été effectuées.

En foi de quoi, la présente attestation lui est délivrée pour servir et valoir ce que de droit.

Fait à Yaoundé, le 26 FEV 2024

Examinateur	Le Président du jury	Le Chef de Département de Physique
Pr. DJUIDJE KENMOE	Pr. ESSIMBI ZOBO Bernard	Pr. NDJAKA Jean-Marie

UNIVERSITE DE YAOUNDE I FACULTE DES SCIENCES Le Chef de Département DEPARTEMENT DE PHYSIQUE

DEPARTMENT OF PHYSICS

Nonlinear dynamics of some electromechanical systems combining translational and rotational motions within a magnetic field

Thesis

Submitted and defended for the award of

Doctorat/ PhD in Physics

Specialty: Mechanics, materials and structures

Option: Fundamental mechanics and complex systems

by

NGATCHA TANLY Nelly Danielle

Registration Number:**10W0577**

MASTER DEGREE in Physics

supervised by

WOAFO Paul

Professor

Year 2024

Dedication

I dedicate this work to my lovely and hardworking parents **Mr and Mrs TANLY** who have always believed in this work through their encouragement and various supports.

Acknowledgements

First, I thank God the Almighty who is the author of this thesis. He gave me the strength daily to complete this work regardless of the difficulties. He inspired and taught me during this process. To Him be all the Glory. In addition, God has blesssed me with many supportive people during my thesis completion and I would like to express my gratitude to those people. I think notably to:

- **Professor Paul WOAFO** my supervisor who accepted me in his laboratory and created the research environment in which I performed my PhD studies. I also thank him for the encouragements, advice, orientations and supports in all aspects of this research. His patience, his rigor, his humility, his hard work ethics and his opening spirit particularly marked me.
- All the members of jury for the examination of this thesis.
- **Professor NANA NBENDJO Blaise** , Professor at the University of Yaounde I, Faculty of Science for his availability and his advice.
- **Professor Jean-Marie Bienvenu NDJAKA** , the Head of the Department of Physics, Faculty of Science, UYI and all **the teaching staff** and **personnel of the Department of Physics** for their valuable teachings and their fruitful advice from my first year of undergrad at the University until now.

- **Dr. TSAPLA FOTSA Rolande** for her scientific assistance and her availability during a part of this work.

- All my elders of the Laboratory of Modelling and Simulation in Engineering, Biomimetics and Prototypes (LaMSEBP) who supported this work with their knowledge: **Dr. CHAMGOUE André, Dr. NWAGOUM Peguy, Dr. THEPI Raoul, Dr. SIMO DOMGUIA, Dr. TCHAKUI Murielle, Dr. FANKEM Raissa, Dr. TALLA Francis** and **Professor SIFEU TAKOUGANG KINGNI**.

- All My labmates and PhD students with whom I share wonderful moments and particularly: **Dr. MBOU SOH Guy, Dr. YOUMBI FOUEGO Dorota, Dr. ESSAMBA MAH Ursule, Dr. MONKAM Ibriss Joel, Dr. MBOYO Réné, KOUAM Fidèle, TEMGOUA Pavel** and **KOUNCHIE Prosper** for fruitful interactions during the seminars and my presentations at the LaMSEBP.

- All the scientific organizations in which I have been involved and for the different financial support they provided to the group to carry out activities in secondary schools, universities and conferences that helped me to flourish scientifically during my PhD Studies notably **the Optical Society** (OSA),**the Society of Photonics, Instrumentation and Engineering**(SPIE), **the Institute of Electronics, Electricity and Engineering** (IEEE) **CPS student Chapter**.

- My friends **NGUETA Sandra, FANDO Sandrine, TOUOLACK Serge, KAMENI Guylli, DJEUTCHOU William, DJOMO Brice, NWOKAM Hermann, AMANAYENA Heidi, EBEGNE Lydie, DJEMEA Gabrielle** and **MBAKOP Nelly**, for their moral support, assistance, encouragements and prayers.

- **MOCHE Kesia, DOMKAM Christeva, MAKOU Vanesa, NGUEMOUO**

Carelle, TSUATA Evodie, KUATE Audrey and **KUATE Joelle** who have particularly constituted a team of prayer to see the achievement of this thesis.

- The great family of **Protestant Chaplancy University of Yaounde 1** for their encouragement and their academic and spiritual teachings .

- My parents **Mr. TANLY Decolo Barthelemy** and **Mrs. NJOBET Nicole** for their love, advice, encouragement, support in every way and particularly for their prayers to God to see this thesis achieved.

- My parents in law **Mr.** and **Mrs. MANGOUA KAMWA** for their encouragement.

- My brothers and sisters **TANLY Line Flore, TANLY Nadine, NGUIYA Passi, TANLY Joel** and **TANLY Armelle** who always believed in me and supported me in different ways.

- My husband **Mr. BEUNANG Klaus Carter** without whom I will never achieve this thesis. Thanks for your words which give me strength to go ahead, for your prayers days and nights, for your encouragements, for your presence and your love which helped me to gain more self-confidence.

- My children **BEUNANG Job Esdras** and **BEUNANG Joyce Yohannah** for their presence during this thesis completion.

All those whose names have not been mentioned here, but who have contributed in one or the other to the success of this work should hereby receive my sincere gratitude.

Contents

Dedication **i**

Acknowledgements **ii**

List of abbreviations **viii**

List of tables **ix**

List of figures **x**

Abstract **xiv**

Résumé **xvi**

GENERAL INTRODUCTION **1**

1 Litterature review **4**

1.1 Introduction 4

1.2 Generalities on electromechanical systems 4

1.2.1 Definition of electromechanical systems 4

1.2.2 Autonomous EMSs 5

1.2.3 Non-autonomous EMSs 5

1.2.4 Types of electromechanichal systems 6

1.3 Nonlinearities in electromechanical systems 8
1.3.1 Nonlinearity in the mechanical subsystem 9
1.3.2 Nonlinearity in electrical subsystem 11
1.3.3 Mathematical modelling of QZS mechanism 13
1.4 Rotational and translational electromechanical systems 15
1.4.1 Rotational electromechanical systems 15
1.4.2 Translational electromechanical systems 21
1.5 Problem statement of the work 22
1.6 Conclusion 23

2 Mathematical formalism, numerical methods and modelling of the mechanical systems 24

2.1 Introduction 24
2.2 Mathematical formalism 24
2.2.1 Lagrange's formalism 24
2.2.2 Linear Stability analysis of ordinary differential equations 25
2.2.3 Principle of Harmonic Balance Methods 27
2.3 Numerical Methods 27
2.3.1 Fourth-order Runge-Kutta method for ordinary differential equations 27
2.3.2 Hardware and software 29
2.4 Numerical tools for characterization of the dynamical states 29
2.4.1 Time traces and phase portrait 30
2.4.2 Bifurcation Diagram 30
2.4.3 Lyapunov exponent 31
2.5 Modelling of the mechanical systems 32

2.5.1 Systems delivering rotation and translation motion 32

2.5.2 Hybrid translational-pendulum electromechanical system with a non-linear spring 37

2.6 Conclusion 41

3 Results and discussion 42

3.1 Introduction 42

3.2 Dynamical behaviours of a coupled system made of rotary motor and mobile translating support 42

3.2.1 Oscillatory state in the linear case 42

3.2.2 Frequency response and bifurcation diagrams 46

3.3 Complex dynamics of a driven hybrid translational-pendulum electromechanical system subjected to a nonlinear spring 56

3.3.1 Frequency response 56

3.4 Conclusion 68

GENERAL CONCLUSION 70

Bibliography 72

List of publications 82

List of abbreviations

AC: Alternative Current

DC: Direct Current

EMS: Electromechanical System

FORTRAN: FORmula TRANslator

MaEMS: Macro Electro-Mechanical System

MATLAB: MATrix LABoratory

MEMS: Micro Electro-Mechanical System

NEMS: Nano Electro-Mechanical System

NODE: Nonlinear Ordinary Differential Equations

QZS: Quazi Zero Stiffness

List of Tables

2.1 Values of the electrical components in the circuit 33

2.2 Values of the spring constants, lengths and that of the rails 33

2.3 Values of the motor parameters 34

2.4 Parameter of the nonlinear inductance 34

2.5 Parameter values 38

List of Figures

1.1 Schematic representation of the spring system [50]. 10

1.2 Schematic representation of SEDC motor [61]. 16

1.3 Schematic representation of the electromechanical system [62]. 19

1.4 a)Schematic representation of the pendulum system and b) schematic representation of the motor with windings to measure the angular velocity and the rotational angular of the rotor [63]. 19

1.5 a)Schematic representation of the DC motor arm and (b) geometric representation of the magnetic forces acting on DC motor arm (in red) [64]. . . 20

1.6 Self-sustained electromechanical device [65]. 21

1.7 Self-sustained electromechanical device [66]. 22

2.1 Schematic representation of the electromechanical system 33

2.2 Schematic representation of the electromechanical device 38

3.1 Analytical (full line) and numerical (dot line) frequency-response curves: (a) amplitude of the electrical current; (b) amplitude of the rod displacement; (c) amplitude of the rod velocity; (d) amplitude of the angular displacement; (e) amplitude of the angular velocity. With $E_0 = 0.39$. 45

3.2 Analytical (star line) and numerical (dot line) frequency-response of: (a) amplitude of the electrical current; (b) amplitude of the rod displacement; (c) amplitude of the rod velocity; (d) amplitude of the angular displacement; (e) amplitude of the angular velocity. With $E_0 = 0.39$. 48

3.3 (a) Bifurcation diagram, (b) the corresponding Lyapunov exponent, versus the amplitude of the excitation with the parameters of Tables 1,2,3,4 and $\Omega = 0.1$. 49

3.4 Phase portraits obtain with parameter of Figure 3.3 and (a)$E_0 = 0.1$, (b) $E_0 = 1.5$, (c)$E_0 = 4$ and (d)$E_0 = 5$. 50

3.5 Analytical (star line) and numerical (dot line) frequency-response of: (a) amplitude of the electrical current; (b) amplitude of the rod displacement; (c) amplitude of the rod velocity; (d) amplitude of the angular displacement; (e) amplitude of the angular velocity. With $E_0 = 0.39$. 52

3.6 ((a)Bifurcation diagram and (b) Lyapunov exponent diagram against the amplitude of the excitation E with the parameter of Figure 3.6 and for $\Omega = 0.1$. 54

3.7 Phase portraits with the parameter of Figure 3.6. (a)$E_0 = 0.1$; (b) $E_0 = 1$; (c) $E_0 = 12$. 54

3.8 (a) Bifurcation diagram and (b) Lyapunov exponent diagram against the control parameter with the parameter of Figure 3.8 and . With $E_0 = 12$. . 55

3.9 Phase portraits obtained with the parameters of figure 3.8 and (a) $\eta = 0.3$; (b) $\eta = 1.33$ 55

3.10 Analytical (full line) and numerical (dot line) frequency-response curves: (a) amplitude of the rod displacement;(b) amplitude of the angular displacement; (c) amplitude of the rod velocity; (d) amplitude of the angular velocity. With and $E_0 = 0.07$ and $Q = 1.2$. 58

3.11 Analytical (full line) and numerical (dot line) frequency-response curves: (a) amplitude of the rod displacement;(b) amplitude of the angular displacement; (c) amplitude of the rod velocity; (d) amplitude of the angular velocity. With and $E_0 = 0.07$ and $Q = 1$. 59

3.12 Analytical (full line) and numerical (dot line) frequency-response curves: (a) amplitude of the rod displacement;(b) amplitude of the angular displacement; (c) amplitude of the rod velocity; (d) amplitude of the angular velocity. With and $E_0 = 0.07$ and $Q = 0.8$. 60

3.13 Analytical (star line) and numerical (dot line) frequency-response curves: (a) amplitude of the rod displacement, (b) amplitude of the angular displacement with and $E_0 = 0.07$ and $Q = 1.2$. 63

3.14 Analytical (star line) and numerical (dot line) frequency-response curves: (a) amplitude of the rod displacement, (b) amplitude of the angular displacement with and $E_0 = 0.07$ and $Q = 1$. 63

3.15 Analytical (star line) and numerical (dot line) frequency-response curves: (a) amplitude of the rod displacement, (b) amplitude of the angular displacement with and $E_0 = 0.07$ and $Q = 0.8$. 64

3.16 Analytical (star line) and numerical (dot line) frequency-response curves: (a) amplitude of the rod displacement, (b) amplitude of the angular displacement with and $E_0 = 0.07$ and $Q = 1$. 64

3.17 Analytical (dot line) and numerical (star line) frequency-response curves: (a) amplitude of the rod displacement, (b) amplitude of the angular displacement with $E_0 = 0.17$, $\Omega = 0.7$ and $Q = 0.8$. 65

3.18 (a) Bifurcation diagram, (b) the corresponding Lyapunov exponent, versus the amplitude of the excitation E with the parameters of Tables 1 and $\Omega = 2$ and $Q = 1$. 66

3.19 Phase portraits obtain with parameter of Figure 3.18 and (a)$E_0 = 2$, (b) $E_0 = 10$. 66

3.20 (a) Bifurcation diagram, (b) the corresponding Lyapunov exponent, versus the ratio with the parameters of Tables 1, $E_0 = 0.7$, $\Omega = 2$ and $Q = 1$. . . . 67

3.21 Phase portraits obtain with parameter of Figure 3.20 and (a) $\alpha = 0.1$, (b)$\alpha = 1.2$. 67

Abstract

This thesis deals with the dynamics of electromechanical systems combining translational motion with rotational motion. The rotational motion is ensured either by a motor or by a pendulum and the translational motion is ensured by a conducting rod free to move on Laplace's rails. The attention is focussed on the effects of the nonlinear spring and the hysteretic iron-core inductor introduced in the mechanical and electrical parts respectively. After the schematic representation and a detailed description of each prototype,the mathematical models are written and the appropriate theoretical methods are used to investigate their dynamical behaviors. The following main results are obtained:

- In the case of rotational motor-translational rod, the dynamical study based on time traces, phase portraits and bifurcation diagrams, shows that the device exhibits different behaviors like jump amplitude phenomenon, hysteresis phenomenon, periodic and chaotic oscillations.

- In the case where the rotational motion is ensured by a pendulum, the periodic and chaotic angular oscillations and rotations are obtained using both the mathematical and numerical methods. Resonant, antiresonant and jump phenomena are obtained. The bifurcation diagrams with the corresponding maximal Lyapunov exponent are plotted versus different parameters of the system. In most cases, the transition from periodic behavior to chaos appears suddenly.

Keywords: Electromechanical system, hybrid translational/rotational motion, non-linear spring, hysteretic iron-core inductor, chaos, rotation oscillations.

Résumé

Cette thèse analyse la dynamique des systèmes électromécaniques combinant un mouvement de translation et un mouvement de rotation. La rotation est assurée soit par un moteur, soit par un pendule et le mouvement de translation est assuré par une tige conductrice se déplaçant sur des rails de Laplace. L'attention est portée sur l'effet du ressort à réponse non linéaire introduit dans la partie mécanique et l'effet de la bobine non linéaire avec noyaux de fer d'Young introduite dans la partie électrique. Après la représentation schématique et la description de chaque prototype, les modèles mathématiques sont établis et les méthodes théoriques appropriées sont utilisées pour analyser la dynamique des systèmes proposés. Les principaux résultats obtenus sont les suivants :

- Dans le cas du système moteur rotatif-support translatif, l'étude de la dynamique basée sur la trace temporelle, les portraits de phase et les diagrammes de bifurcation montre que le système présente différents types de comportements tels que les sauts d'amplitude, le phénomène d'hystéresis, les comportements périodiques et chaotiques.

- Dans le cas où la rotation est assurée par un pendule, des oscillations angulaires et des rotations périodiques et chaotiques sont obtenues à l'aide des méthodes mathématiques et numériques. On obtient des phénomènes de résonance, d'antirésonance et de saut d'amplitudes. Le diagramme de bifurcation et l'exposant de Lyapunov

correspondant sont tracés en fonction de différents paramètres du système. Dans la plupart des cas, la transition du comportement périodique au chaos apparaît soudainement.

Mots-clés: Système électromécanique, mouvement hybride de translation/rotation, ressort non linéaire, inductance avec noyau de fer hystérétique, chaos, oscillations de rotation.

GENERAL INTRODUCTION

Electromechanical systems (EMSs) play an essential role in fulfilling the needs of modern technological applications. In recent years, many efforts have been focused on the development and improvement of EMSs [1–7]. Due to their various configurations, their robustness and reliability, EMSs are used in a variety of applications in industries and at home. At home, EMSs are used as machine tools for some laborious tasks. For example, the mixer or food processors are used to crush or to mash the seasoning, the vacuum cleaner to clean the sitting room, the washing machine to clean the dress and the dishwasher to clean the plates [3, 5, 7]. In industries, the EMSs as the conveyor belts and the robot arms play an essential role in the automation of industrial processes.

Since several years, nonlinear electromechanical systems have been widely studied. They can be found in a wide range of applications such as domestic equipments (mixers, robots) [8, 9], in biological organs (cardiovascular system) [10, 11] and engineering devices (shaker, production chains). In the modelling, nonlinear terms can arise from a mechanical part (material, geometric or inertial nonlinearities), from an electrical circuit (nonlinear inductor, nonlinear condenser, nonlinear resistance) and from the coupling (coupling between the electromagnets, saturation, hysteresis, nonlinear magnetic force, time delay). This leads to complex dynamical behaviors such as the jump, the hysteresis, subharmonic and superharmonic oscillations, frequency division or multiplication, multistability, grazing, switching, quasi-periodicity and chaos. Some of these behaviors resulting from nonlin-

ear dynamics can improve the processes in which the EMS are engaged such as industrial mixing processes [12], industrial shaking processes [13] and monitoring compaction [14,15].

Despite their common presence in literature, pendulum systems continue to attract a lot of attention for research and application since they exhibit many phenomena of nonlinear dynamics [16–31]. The pendulum models comprise downward pendulum [21], horizontal pendulum [22], rotating pendulum [23], inverted pendulum [24, 25] and they can be coupled to the electrical part and become electromechanical pendulums which are particularly interesting for applications in engineering devices, space exploration, manufacturing automation, construction, mining, hazardous operations, and many other areas. This is due to some particular dynamic state (oscillation and chaos) that they can generate because of intrinsic angular nonlinearity or due to natural or introduced nonlinearities in the electrical and mechanical parts [31–36]. Many works have been devoted to the study of pendulum with a horizontal moving support because it is an actuated system that is highly unstable and nonlinear. This system combines two motions which interact each other: the translation of the support and the rotation of the pendulum [37, 38]. Adding a nonlinear component to this system which is already nonlinear can generate more complex dynamics.

Almost all of the studies on EMS have paid attention either on EMS with only translational motion or on EMS with only rotational motions. Other systems convert the rotational movement into translational movement and vice versa. But, there are industrial automation, domestic appliances and even medical tasks where the EMS actions required simultaneously both rotation and translation. This might for instance be the case of some mixers which may translate and rotate during the mixing processes in order to cover the whole space occupied by the products to be mixed. Another application of interest is an electromechanical perforator which has many applications in mechanical and civil

engineering (for instance for the digging of wells for water, gas or petrol).

One of the objectives of this thesis is to design new electromechanical devices which are able to perform both rotational and translational motions. Same as it has been demonstrated that nonlinear dynamical behaviors present some benefits in increasing the efficiency of some activities, one can expect that mechanisms delivering combined complex rotational and translational motions can improve the efficiency while performing the targeted tasks. In the same line, the second objective of this work is to generate complex behaviours in the dynamics of the designed EMS by adding nonlinear components.

The present work is therefore organized within 3 chapters as follows. In **chapter one**, we present some generalities on EMS, research results on electromechanical systems with nonlinearities, and on rotational and translational systems. Afterwards the objectives and interest of the work are presented. In **chapter two**, we focus on the mathematical formalism and numerical methods used to characterize the dynamical states of the physical systems studied. **Chapter three** is devoted to results and discussions. We structure the chapter in two main parts. In the first part, we consider an electromechanical mechanism in which the rotational motion of a motor is combined to the translational motion of a plate carrying the motor through Laplace's rails. Here, we study the dynamics of the system in the oscillatory state, and the complex behavior of the system in presence of nonlinear spring and nonlinear inductance. In the second part, we deal with the complex dynamics of a driven hybrid translational-pendulum electromechanical system subjected to a nonlinear spring. The system and equations are given, the frequency response and bifurcation diagrams are obtained and analysed. The conclusion ends with a **general conclusion** where the main results of the work are summarized. The study also provides a brief outline of possible future research directions.

Chapter I

Litterature review

1.1 Introduction

This chapter is concerned with generalities on electromechanical systems (EMSs) and literature review on studies on these systems with nonlinearities. In section 1.2, we present the generalities on EMS. Attention is paid to the nonlinearities occurring in those systems in section 1.3. Section 1.4 deals with the presentation of rotational and translational EMS. Section 1.5 will give more details on the problems to be solved in this thesis. The conclusion of the chapter appears in section 1.6.

1.2 Generalities on electromechanical systems

1.2.1 Definition of electromechanical systems

EMS refers to a mechanical element coupled to electrical circuits via electromechanical transducers. The interest devoted to such a system is due to the fact that it is pervasive in modern life. EMSs play an essential role in fulfilling the needs of modern technological applications. They can be found out in a wide range of applications such as domestic equipments (mixers, robots), in biological organs (cardiovascular system) and engineering devices (shaker, chains of production). The electrical energy supplied to these systems is transformed into mechanical energy with an efficiency of 80 percent by electric drives [39].

In general way, according to the nature of excitation, EMSs can be divided into two categories respectively autonomous and non-autonomous systems.

1.2.2 Autonomous EMSs

Autonomous EMSs are systems which can operate without an external generator. This can considerably reduce the cost of manufacturing of such systems. In this perspective, some authors have used self-subtained oscillators such as Van der Pol, Duffing and Rayleigh oscillators to control mechanical devices. Nowadays, the development of autonomous EMS constitutes a big challenge for researchers. Nana Bonaventure and Woafo Paul investigated the dynamics of an autonomous electromechanical pendulum like system with experimentation [40]. Grassland Schimdt invented an Energy-autonomous electromechanical wireless switch used as a service switch [41].

1.2.3 Non-autonomous EMSs

When there is a need of an external excitation to run the system, the EMS is said to be a non-autonomous, forced or driven system. A disadvantage of forced EMS is the fact that their different frequencies are concentrated around the frequency of the external voltage or current sources. This reduces their potential application particularly as random number generators and in telecommunications where some properties of chaotic signals are used to secure communication [40]. Interesting works on forced systems were published. Let us enumerate some of them. In Ref. [42] Simo and Woafo analyzed bursting oscillations in a non-autonomous electromechanical systems consisting of a rigid beam coupled to a double well forced Duffing oscillator. Jianping Cai and Meili Lin adopted adaptative control technique to synchronize two identical non-autonomous system with unknown parameters in finite time [43].

1.2.4 Types of electromechanichal systems

Depending on their dimensions, EMSs are classified as follow: nanoelectromechanical systems (NEMSs) with dimensions at nanometer range, microelectromechanical systems (MEMSs) which generally range in size from 20 micrometres to a millimetre and macro-electromechanical systems (MaEMSs) whose dimensions are bigger than the one of MEMS.

a) Nanoelectromechanical systems(NEMs)

NEMs are devices that integrate electrical and mechanical functionality at the nanoscale. NEMs devices can theorically be applied in any electromechanical system. The first NEMs was build by Dawon Kahng and Mohamed M. Atalla at Bell Labs in 1960. It was a MOSFET(metal-oxide-semiconductor field effect transistor)with gate oxide hickness of 100nm.

NEMs has several fascinating attribues. It can provide access to fundamental frequencies in the microwave range [44], active masses in the femtograms range, heat capacities far below a yoctocalorie [45], mechanical quality factors, in the tens of thousands (and quite possibly much higher) [46], force sensitivities at the attonewton level [47], mass sensitivity at the levels of individual molecules. All these distinguished properties of NEMs devices pave the way to applications such as force sensors, chemical sensors, biological sensors and ultrahight frequency resonator. NEMs mostly contains apparatuses like actuators, sensors, resonators, beams and motors.

b) Microelectromechanical systems (MEMs)

The integration of mechanical elements, sensors, actuators and electronics on common silicon substrate through micro-fabrication technology leads to what is known as micro-electromechanical systems. MEMs is a process technology used to create tiny integrated

devices or systems that combine mechanical and electrical component. They are fabricated using integrated circuit batch processing technics and can range in size from a few micrometers. These systems can sense, control and activate mechanical processes on the micro scale, and function individually or in arrays to generate effects on the macro scale.

MEMs are used in a wide range of sensors, actuactors, generators, energy sources, biochemical and biomedical system and oscillator. Current MEMs devices include accelerometers for airbag sensor, inkjet printer heads, computer disk drive read/ write heads, projection display chip, blood pressure sensors, optical switches, microvalves, biosensors and many other products that are all manufactured and shipped in high commercial volume.

Some advantages of MEMs are: extremely scalable in manufacturing resulting in very low unit costs when mass- produced, MEMs sensors possess extremely high sensitivity, MEMs switches and actuators can attain very high frequency, MEMs devices require very low power consumption. Some disadvantages of MEMs are the following: very expensive during the research and development stage for any new MEMs design or devices, fabrication and assembly unit costs can be very high for low quantities, testing equipment to characterise the quality and performance can also be expensive.

c) Macroelectromechanical systems (MaEMS)

The devices of big sizes are called MaEMS. The macro systems however are very requested in engineering and in many others branches of science. They are easily integrated in engineering system with frequencies less than 100Hz such as industrial and domestic shakers. They can be found in various field such as: domestic equipment's manufacturing, communication and energy production [48]. Mechanical motion is typicaly converted into electrical energy and vice versa through various transducers mechanism such as piezo-

electricity, electromagnetic induction, electrostatic, magnetostrictive and biological processes [49].

1.3 Nonlinearities in electromechanical systems

Linearity is usually praised as a positive feature and property in many disciplines, and even in common language. It is considered synonymous to and associate with ease of use and predictability. In general, linear models are applicable only in a very restrictive domain like when the vibration amplitude is very small. Unlike linearity, nonlinearity is sometimes considered as a negative feature, as a hurdle, as an uncertainty and with a lack of ease. Designing nonlinear systems can be harder because nonlinear interactions or behaviours in the system must be taken into account. The behaviour of a nonlinear systems can be sensitive to the parameters of the systems and the initial conditions of the system. More specially, by changing a nonlinear system's parameters, the behaviour of the system can change qualitatively as well as quantitatively. The consequences of the lack of linearity are fundamental and substantial, and nonlinear systems differ completely from linear system.

Any physically realistic system involves nonlinearities. Indeed, interesting physical phenomena occur in structures in the presence of nonlinearities, which cannot be explained by linear models. These phenomena include jumps, hysteresis, subharmonic, superharmonic, and combination resonances, self-excited oscillations, modal interactions, and chaos. In reality, no physical system is strictly linear and hence linear models of physical systems have limitations of their own. Thus, to accurately identify and understand the dynamical behavior of structural systems under general loading conditions, it is essential that nonlinearities present in the system should also be modeled and studied.

Nonlinear phenomena have applications to a wide variety of fields, ranging from mathematics, physics, biology, and chemistry, to engineering, economics and medicine. One of the fields where nonlinearities can have positive interests is electromechanical engineering. However, the understanding of such electromechanical devices in nonlinear regime is essential for the improvement of industrial and domestic product.

The source of nonlinearities can be material or constitutive, geometric, inertia, body forces or friction. The constitutive nonlinearity occurs when the stresses are nonlinear functions of the strains. The geometric nonlinearity is associated with large deformations in solids, such as beams, plates, frames and shell, resulting in nonlinear strain displacement relation (mid-plane stretching, large curvatures of structural elements, large strains and large rotations of elements). The inertia nonlinearity may because by the presence of concentrated or distributed masses. The nonlinear body forces are essentially magnetic and electric forces. The friction nonlinearity occurs because of the displacement and velocity, such as dry friction and Backlash.

As far as EMSs are concerned, nonlinearity can be of electrical or mechanical origin. It can arise from various sources such as spring and damping mechanisms, resistive, inductive, and capacitive circuit elements.

1.3.1 Nonlinearity in the mechanical subsystem

a) Spring with nonlinear response

A nonlinear spring has a nonlinear relationship between force and displacement.The schematic representation of the spring force is displayed in figure 1.1.

The spring system comprises a longitudinal spring with linear stiffness k_v which is connected at point P with two linear springs with identical stiffness k_0 and initial length

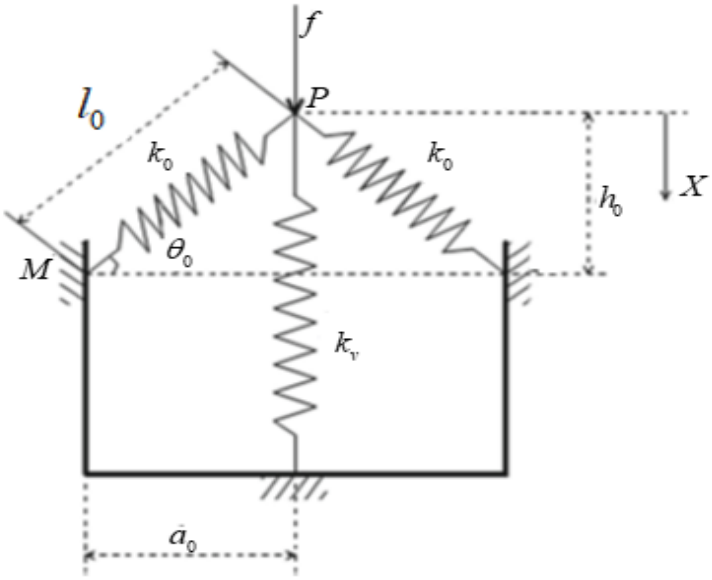

Figure 1.1: Schematic representation of the spring system [50].

l_0 mo unted obliquely. The two springs are initially inclined with a slope of angle θ_0 from the horizontal plane and hinged at points M and N respectively. The loading point P is initially located at height h_0 above the points M, N and at horizontal distance a_0 apart from these points. The elastic force f can be written as it was given in [50]:

$$f = k_v X - 2k_0 X \left(\frac{l_0}{\sqrt{a_0^2 + X^2}} - 1 \right) + k_v h_0 \tag{1.1}$$

b) Nonlinear stiffness

For hardening spring effect in mechanical problems, it is found experimentally that the stiffness is not constant but increases with the received constraint. It is approximately defined by the relation:

$$k(x) = k_0 + k_1 x^2 \tag{1.2}$$

k_0 is the stiffness for small stretching, x the elongation and k_1 a coefficient of nonlinearity. An example of an electromechanical device with a nonlinear spring has been studied recently by Notué et al in ref. [51].

1.3.2 Nonlinearity in electrical subsystem

Because the circuit element namely resistors, capacitors and inductors can be either linear or nonlinear depending upon their characteristic curves, the sources of nonlinearity in electrical subsystem can be introduced in three ways.

a) Capacitor

In nonlinear capacitor, capacitance value changes as voltage is applied, do the energy or stored charge is different from what was expected. The voltage of a capacitor is a nonlinear function of the instantaneous electrical charge:

$$v(q) = \frac{1}{C_0}q + a_2q^2 + a_3q^3 + ... \tag{1.3}$$

where C_0 is the linear value of C and a_i are the nonlinear coefficients depending of the type of capacitor in use. This is typical of nonlinear reactance components such as varactor diodes widely used in many areas of electrical engineering to design for instance parametric amplifiers, up-converters, mixers, low-power microwave oscillators...This type of capacitor has been use in [52, 53].

b) Resistor

Nonlinear resistors are those types of resistors where the electric current flowing through it changes with the exchange applied voltage or temperature and does not change according to Ohm's law. The voltage and current values vary depending upon other factors like temperature and light, but they may not be linear. There are several types of nonlinear resistors, but the most commonly used are varistor resistors.

If a resistor is characterized by a $v - i$ curve other than a straight line through the origin, it is called a nonlinear resistor. The characteristic curve of a typical nonlinear

resistor is given as:

$$v(i) = R_a i_a \left[-\left(\frac{i}{i_a}\right) + \frac{1}{3}\left(\frac{i}{i_a}\right)^3 \right] \tag{1.4}$$

where R_a and i_a are respectively the normalization resistance and current, i is the value of current corresponding for the limit resistor voltage. In this case, the model have the property to exhibit self-excited oscillations. This is due to the presence of the nonlinear resistor whose current-voltage charateristic curve shows a negative slope and the fact that the model incorporate through its nonlinear resistance a dissipative mechanism to damp oscillations that grow too large and a source of energy to pump up those that become small. Because of this particular behavior, we can qualify our physical system with nonlinear resistor as a self-sustained oscillator. The nonlinear resistance is successfully use to get specific features like sensors, limiters, ESD protection, self-balancing stabilisation etc. using still a relatively simple and reliable passive component. The nonlinear resistor can be also realized using a block consisting of two transistors.

c) Inductor

- **Inductor with ferromagnetic material**

  Nana et al in [54] demonstrated experimentally that under some conditions, the inductance of an inductor with a magnetic core can depend on the current and has the following mathematical expression:

$$L = \frac{\mu_0 N^2 A}{l} + \frac{B_s N A}{i} \tanh\left(\frac{\alpha N i}{2l} - \frac{\delta}{2}\right) \tag{1.5}$$

  with $\delta = \beta sign\left(\frac{di}{dt}\right)$.

  B_s is the saturation flux density. A and l are respectively the cross sectional area and the average length of the magnetic material. N is the number of turns, μ_0 is the magnetic permeability of the free space, i is the current through the winding, α and

β are two constant parameters. As demonstrated in [54], neglected the parameter δ has no significant effect on the behavior of the circuit. Thus, to simplify the analysis during this work, the parameter δ will be taken equal to zero.

- **Inductor without ferromagnetic material**

  When the magnetic circuit can be subjected to the magnetic flux more than its ability, its inductance follows a nonlinear behaviour, and its expression is:

$$L = L_0 \left[(1+\gamma) - \gamma \tanh^2 \left(\frac{i}{i_0} \right) \right] \tag{1.6}$$

  with L_0 the normalization inductance, γ the saturation parameter and i_0 the normalization current [55, 56].

1.3.3 Mathematical modelling of QZS mechanism

The Quazi Zero Stiffness (QZS) mechanism under consideration is schematically shown in Figure 1.1, where the device to be isolated is not included. The system comprises a vertical spring with linear stiffness k_v which is connected at point P with two linear springs with identical stiffness and initial length L_0 mounted obliquely. The two springs are initially inclined with a slope of an angle θ_0 from the horizontal plane and hinged at points M and N respectively. Consider a loading force f at point P downwards. The loading point P is initially located at height h_0 above the points M, N and at horizontal distance a_0 apart from these points respectively. It is assumed that $L_0 \geq a_0$. The application of the force f causes a vertical displacement Y_0 and when the system is loaded with a suitably force, the springs are compressed from the initial unloaded position P to the equilibrium position O where the oblique springs are compressed in the horizontal position and the static load is only supported by the vertical spring. When k_v and k_0 match, the positive

stiffness of the vertical spring and negative stiffness formed by the oblique springs will cancel with each other to achieve zero stiffness at the equilibrium position. In this way the system is developed into a QZS system. The geometry of the system is defined by the parameters a_0 and h_0. Provided the coordinate Y_0 defines the displacement from the initial unloaded position, a loading force f given by the following equation, leads to a resulting displacement Y_0 [50, 57–59].

$$f = f_v + f_0 \tag{1.7}$$

where the term f_v denotes the contribution from the vertical spring and the term f_0 denotes the contribution from the two oblique sprigs given as follows:

$$f_v = k_v Y_0 \tag{1.8}$$

and

$$f_0 = 2k_0(L_0 - L)\sin\theta_0 \tag{1.9}$$

where $\sin\theta_0 = \frac{(h_0 - Y_0)}{L}$. It should be noticed that when $\theta_0 = 0$ the springs lie horizontally and do not exert any vertical force, i.e f_0 . Thus, the force-displacement relationship can be rewritten as:

$$f_0 = 2k_0(h_0 - Y_0)(\frac{L_0}{L} - 1). \tag{1.10}$$

It can also be seen that

$$L = \sqrt{a_0^2 + (h_0 - Y_0)^2} \tag{1.11}$$

$$f_0 = 2k_0(h_0 - Y_0)\left(\frac{L_0}{\sqrt{a_0^2 + (h_0 - Y_0)^2}} - 1\right) \tag{1.12}$$

If the variable Y defines the downward displacement of the slider from the equilibrium position, when the oblique springs are placed horizontally after applying the loading force f can be rewritten as:

$$f = k_v Y - 2k_0 Y\left(\frac{L_0}{\sqrt{a_0^2 + Y^2}} - 1\right) + k_v h_0. \tag{1.13}$$

1.4 Rotational and translational electromechanical systems

1.4.1 Rotational electromechanical systems

Rotational electromechanical systems are widely used in many domains due to the fact that they are capable to operate in a large power range: from microwatt power to gigawatt power [60]. Amoung those systems we can found rotary electric motor and electromechanical pendulum.

a) Rotary electric motor

A rotary electric motor or rotary electric actuator (REA) consists of two mechanical parts: the stator which is fixed and the rotor which moves. It also has two electrical components, magnets set and an armature, one of them is attached to the stator and the other to the rotor, together making a magnetic circuit. One distinguish two principle types: Direct Current motors (DC motors) and alternating Current motors (AC motors). Numerous devices including home appliances and industrial automation systems function with AC/DC motors with a large variety of delivered output power.

- **DC motor**

  DC motors take electrical power through direct current and convert this energy into mechanical rotation. It use magnetic fields that occur from the electrical currents generated, which powers the movement of a rotor fixed within the output shaft. By the manner to connect the stator with rotor, one distinguishes many type of DC motor among them one distinguishes separately-excited DC motors (SEDC) which

is of interest since we can obtain the other from it changing simply the manner to connect the rotor with stator. The schematic representation of SEDC motor is shown in figure 1.2 where L_a and R_a are respectively the self-inductance and resistance of the rotor, $U_a(t)$ is the external voltage and $i_a(t)$ the current across the roor. $\theta(t)$ is the angular displacement of rotor and $\omega(t)$ its angular velocity. $\Phi(t) = k_f i_f(t)$ is the magnetic inductor flux, $i(t)$ is the current across the inductor and k_f a constant. Using the Kirchhof's voltage law, the equation of the electrical part is given by the following relation [61]:

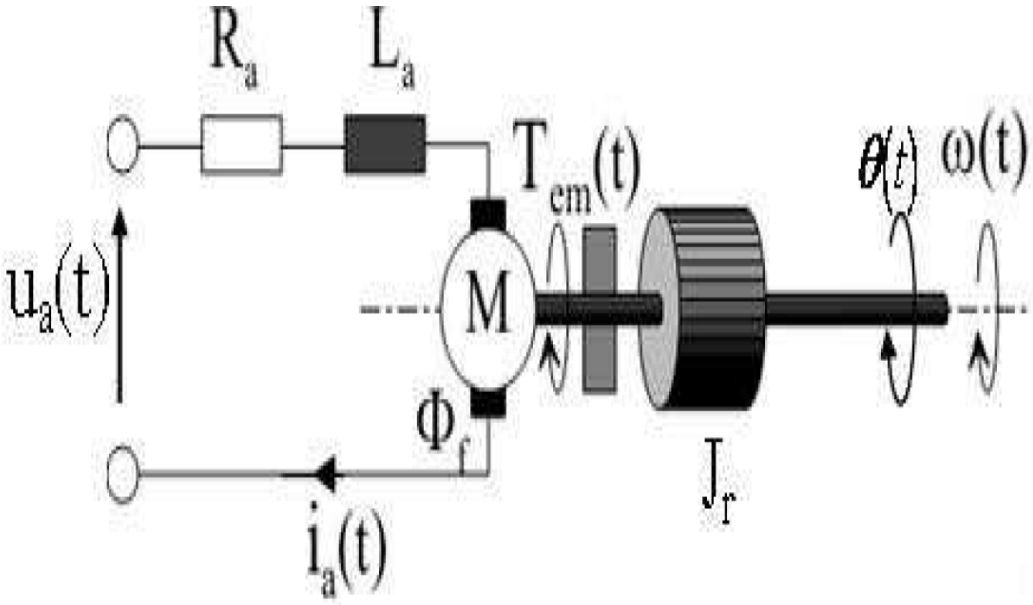

Figure 1.2: Schematic representation of SEDC motor [61].

$$L_a \frac{di_a}{dt} + R_a i_a + e_m(t) = u_a(t) \tag{1.14}$$

where, in the left, the first term is the voltage across the inductor, the second term is the ohmic voltage and the third term $e_m(t) = k_E \Phi_f(t) w(t)$ is the back electromotive force (BEF) which represents the coupling term between the electrical part and mechanical part of the device and k_E the BEF constant. Using the Newton second

law of dynamics for rotary motions and taking into account the Laplace force, the equation of the mechanical part is obtained as:

$$\begin{cases} \frac{d\theta(t)}{dt} = w(t) \\ J_r \frac{dw(t)}{dt} + C_v w(t) + T_f sign(w(t)) = T_{em}(t) - T_L \end{cases} \tag{1.15}$$

where J_r is the rotor inertia coefficient, C_v the viscous friction coeffcient, T_f the dry friction torque and $T_{em}(t) = k_T \Phi_f(t) i_a$ the electromagnetic torque due to the Laplace force, k_T the torque constant and T_L the load torque. $T_{em}(t)$ represents also the coupling term between the mechanical part and the electrical part of the device.

Using Kirchhoff's voltage law for the electrical part and Newton second Law of dynamics for rotating motions and taking into account Laplace force for the mechanical part, the electromechanical equations of the SEDC motor are written as:

$$\begin{cases} \frac{d\theta(t)}{dt} = w(t) \\ L_a \frac{di_a}{dt} + R_a i_a + k_E \Phi_f(t) w(t) = u_a(t) \\ J_r \frac{dw(t)}{dt} + C_v w(t) + T_f sign(w(t)) = k_T \Phi_f(t) i_a - T_L \end{cases} \tag{1.16}$$

- **AC motor**

An AC motor is an electric motor drive by an alternating current motor. There are two type of AC motor which are synchronous and induction. In a synchronous motor, the rotation of the shaft is at the same place as the frequency of the applied current with multiphase AC electromagnets on the stator that produce a rotating magnetic field. An induction motor or asynchronous motor is a single excited motor where current is applied to one part of the motor, the stator. Flux from the stator circuited coil in the rotor, which feels torque that makes the rotor rotate. AC motor

are power source for a wide variety of applications due to their flexibility, efficiency and noiseless operation. They are used on pumps, water, heaters, garden equipment and are commonly found in many appliances, equipment and tools.

b) Electromechanical pendulum

Pendulum system is a simple mechanical system made with a thin rod which supports a proof mass and a fixed point at its terminal. It is capable on back-and-forth or complete rotation according to the chosen parameter values. They can be coupled to the electrical part and become electromechanical pendulums. Electromechanical pendulums is the subject of interest for several scientist since they have important applications in many engineering objects and in space exploration, manufacturing automation, construction, mining, hazardous operations, and many other areas.

Researchers use the analytical, numerical and experimental tools to analyse the time evolution characteristics of the pendulum electromechanical systems in several configuration. Amongst them:

- Notué and *al* [62], studied the dynamics and control of an electromechanical robot arm manipulator pushing periodically a load. The pendulum is coupled to an electrical part through an electromagnetic link. The author investigated firstly the effect of a periodic impulsive force due to the instantaneous shock between the pendulum arm and external load masses arriving periodically. Secondly he evaluated the critical electrical signal amplitude leading to the displacement of the mass, afterward a pulse like activation signal acts periodically on the pendulum arm in view of optimizing the action of the pendulum arm by counterbalancing the collision effects due to the arriving loads and finally an adaptive back stepping method, based on the automatic variation of an intrinsic parameter, has been developed. See figure 1.3.

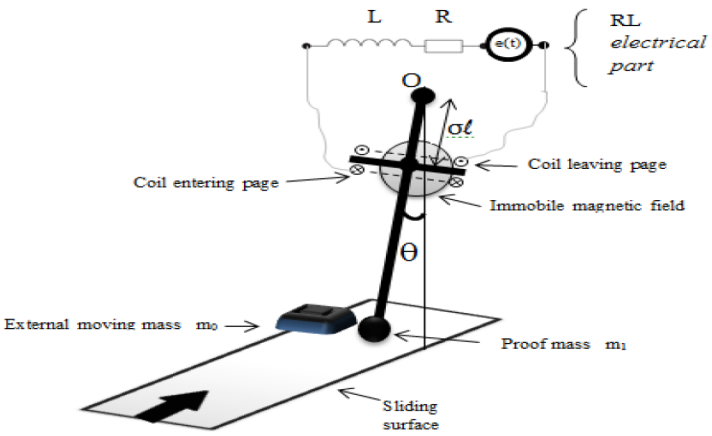

Figure 1.3: Schematic representation of the electromechanical system [62].

- Nana Bonaventure and *al* [63] investigated the dynamic of an EMS consisting of DC motor, a physical pendulum with the repulsive magnets. The author investigations show that both periodic and chaotic behaviors are observed, depending on the frequency and amplitude of the driver and the distance between the two magnets. Amplitude jumps, hysteresis and bistable states occur for a range of frequencies near the natural frequency of the physical system are also observed. See figure 1.4

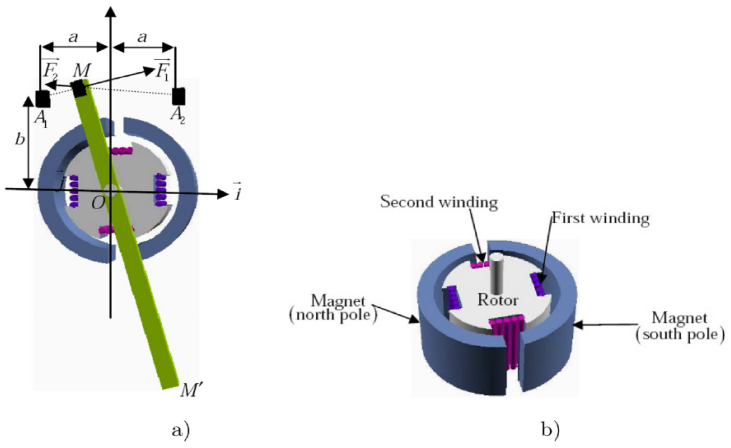

Figure 1.4: a)Schematic representation of the pendulum system and b) schematic representation of the motor with windings to measure the angular velocity and the rotational angular of the rotor [63].

- Kouam and *al* [64] investigated the dynamics of an EMS consisting of a DC motor-driving arm within a circular periodic potential created by three permanent magnets. Two different forms of input signal are used: DC and AC voltage sources. The author studied the condition under which the mechanical arm can perform a complete rotation. The result have shown that for voltage lower than a critical value, the mechanical arm oscillates and then stabilizes at the equilibrium position in the case of DC voltage while in the case of AC voltage, the arm exhibits oscillations with amplitude less than one turn. When the voltage amplitude is higher than the critical value, the mechanical arm undergoes large amplitude motion (complete rotation) for DC voltage source and displays angular oscillations with amplitude greater than one turn for AC source. The bifurcation diagrams have shown that the system exhibit chaotic dynamics. See figure 1.5.

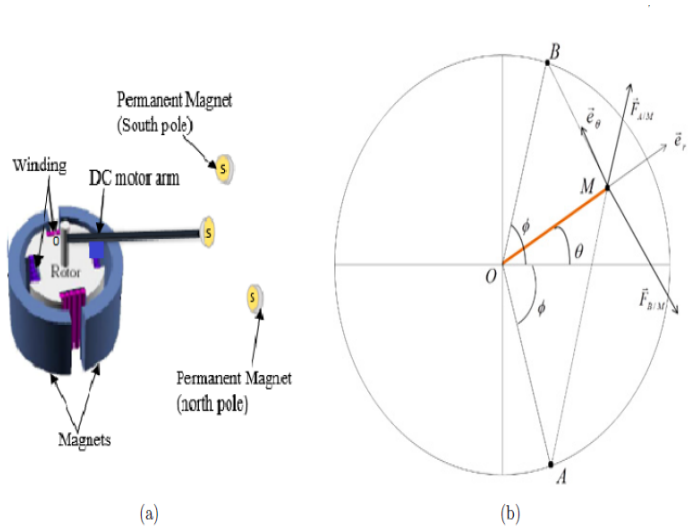

Figure 1.5: a)Schematic representation of the DC motor arm and (b) geometric representation of the magnetic forces acting on DC motor arm (in red) [64].

1.4.2 Translational electromechanical systems

Translational electromechanical systems move along a straight line. Many if not most applications require translational motion as the end product. Some searchers have studied those systems. We can list:

- Yamapi and *al* [65] have studied the electromechanical device which is composed of an electrical part coupled magnetically to a mechanical part. The coupling is realized through the electromagnetic force due to a permanent magnet. It creates a Laplace force in the mechanical part and the Lenz electromotive voltage in the electrical part. The electrical part is a self-excited electrical system described by the Rayleigh-Duffing oscillator, consisting of a nonlinear resistor NLR, a condenser C and an inductor L, all connected in series, while the mechanical part is composed of a mobile beam which can move along the z-axis on both sides. Rod T, which has a similar motion, is bound to a mobile beam with a spring. See figure 1.6.

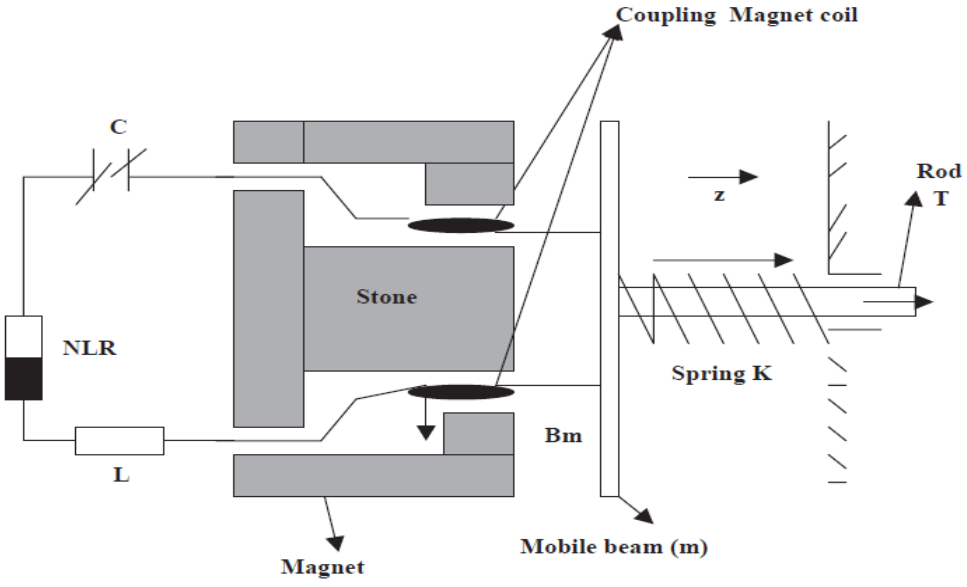

Figure 1.6: Self-sustained electromechanical device [65].

- Tchetchoua and Woafo [66] studied the dynamic of an electromechanical device

consisting of a mobile plate with variable contents fixed to a spring and activated by an induction motor. The asynchronous motor used is a three-phase one with two parts: a stator (inductor) and a rotor mobile around a revolution axis. The electromagnetic torque which is produced by the electromotor is transmitted to the plate by the connecting-track rod system which is mechanically fixed to the rotor. See figure 1.7.

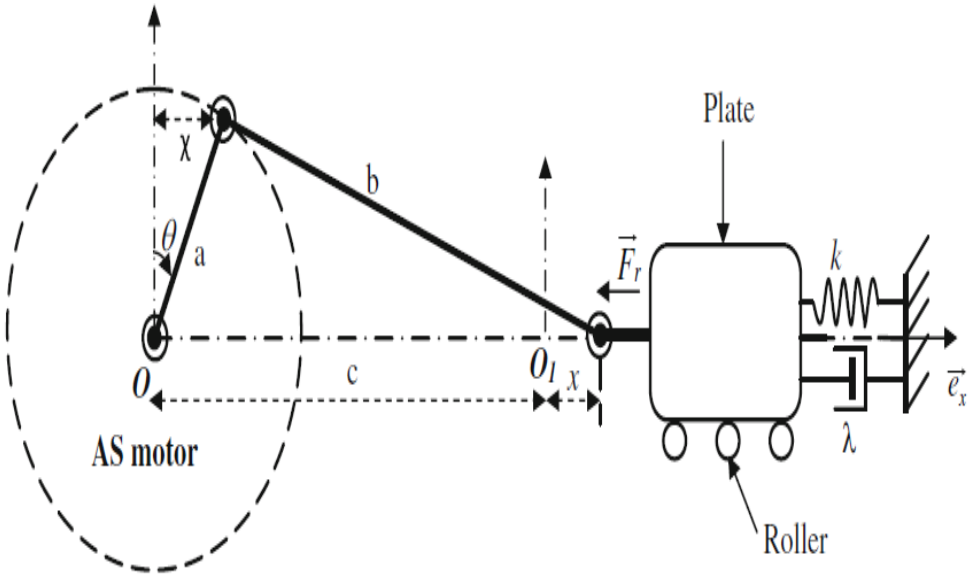

Figure 1.7: Self-sustained electromechanical device [66].

1.5 Problem statement of the work

The main purpose of this thesis is to design and study the dynamics of different electromechanical systems which combine both translational and rotational motion. Ours models consist on one hand to the rotational motion of a motor combined to the translational motion of a plate carrying the motor through Laplace's rails and in another hand to the rotational motion of a pendulum combined to the translation of a rod free to move on Laplace's rails to which it is connected. To induce the chaotic dynamic in our system,

we have introduced the nonlinear spring in the mechanical part and the hysteretic iron-core inductor in the electrical parts. Therefore, studying the dynamical response, both theoretically and numerically, of these structural components would help in understanding and explaining the behavior of more complex real structures for various applications. The complex behaviors of this device can find applications in various branches of electromechanical engineering such as boring machine and drilling machine. They can also find application in the sieving and actuation processes

1.6 Conclusion

We have reported in this chapter a review of literature on EMS. Starting by some generalities on autonomous and non-autonomous electromechanical systems, we have presented different types of electromechanical system and we have ended by stating the problem of this thesis. The next Chapter will be devoted to the mathematical and numerical methods used to analyze the dynamical states of physical devices proposed in this work.

Chapter II

Mathematical formalism, numerical methods and modelling of the mechanical systems

2.1 Introduction

This chapter focuses on the mathematical formalism, numerical methods and modelling of the electromechanical sytems studied in this thesis. Section 2.2 and section 2.3 deal respectively with mathematical analysis and numerical methods used to solve the equations obtained from the mathematical modeling. In section 2.4 numerical tools used to study the dynamical behaviors of the devices proposed are presented. In section 2.5, we describe the different EMSs of this work. Section 2.6 concludes the chapter.

2.2 Mathematical formalism

2.2.1 Lagrange's formalism

A complex system dynamic can be described in efficient way using Lagrange's equation. The complicated vector analysis that needed for describing forces applied on a mechanical system can be reduced by Langrange's equation [67].

A set of generalised coordinate $q = \{q_1, .., q_i, .., q_n\}$ is a representation of the fundamental principle of Lagrange's equation, where q_i is an independent degree of freedom of the system which combines the constraints unique to the system, i.e., the communication

between parts of the system. The total generalised coordinates is do noted by nn.

The Lagrange's equation is expressed by the system's kinetic K and potential energy P which described as follows:

$$L = K\left(q, \dot{q}\right) - P\left(q\right) \tag{2.1}$$

where the function of kinetic energy in terms of the generalised coordinate q and $\dot{q}$ its derivative . The function of potential energy is described in terms of only the generalised coordinate q.

The equations of desired motion are derived using

$$\frac{d}{dt}\left(\frac{\partial L}{\partial \dot{q}_i}\right) - \frac{\partial L}{\partial q_i} + \frac{\partial D_f}{\partial \dot{q}_i} = Q_i \tag{2.2}$$

where Q_i shows the external force that applied in term of q_i coordinate and D_f designates the energy dissipated by friction. This method is used in chapter 3 for the establishment of the equation of the system dynamic.

2.2.2 Linear Stability analysis of ordinary differential equations

Equilibria are not always stable. Since stable and unstable equilibria play quite different roles in the dynamics of a system. That is why the study of stability analysis of steady state solutions and fixed point is an important issue for any dynamical systems. Linear Stability analysis tells us how a system behaves near an equilibrium point. The stability describes the way in which the system reacts to a small perturbation that moves the system slightly away from its steady state. Toward this end, suppose that we have a set of first order autonomous ordinary differential equation, written in vector form

$$\frac{dY(t)}{dt} = F(Y(t), \mu) \tag{2.3}$$

where $Y(t) = (y_1(t), y_2(t), ..., y_n(t))$ is the vector of the n dynamical variables of the system, a set of parameters μ and $F = (F_1, F_2..., F_n)$ is a differentiable vector function.

Suppose that Y_0 is the steady state or fixe point. The linear stability analysis is based on analyzing the time-dependent trajectory of a system slightly perturbed from a steady state Y_0. Therefore, the solution $Y(t)$ can be represented as a sum of the steady state Y_0 and a small perturbation $\delta Y(t)$:

$$Y(t) = Y_0 + \delta Y(t) \tag{2.4}$$

Inserting (2.4) in (2.3) and linearizing around the steady state Y_0 leads to the variational equation for the variable $\delta Y(t)$.

$$\frac{d\delta Y(t)}{dt} = J\delta Y(t) \tag{2.5}$$

where J is nYn matrix of the partial derivatives called the Jacobian matrix. The eigenvalues of the linear system of the equations (2.4) can be found from the following characteristic equation of the system

$$\det(\lambda I - J) = 0 \tag{2.6}$$

where I is the unit matrix and λ are the eigenvalues of the system (2.6) and roots of the characteristic equation. The stability of the steady state X_0 is determined by the eigenvalues of the system (2.6), as follows:

- If all eigenvalues of the Jacobian matrix have real parts less than zero, then the steady state is stable;
- If at least one eigenvalues of the Jacobian matrix has real part greater than zero, then the steady state is unstable.

This mathematical formalism is the basic principle of linear stability analysis for ODEs.

2.2.3 Principle of Harmonic Balance Methods

Harmonic balance method is widely used in the literature for analyzing the periodic solutions of nonlinear differential equation of nonlinear mechanical system. Let consider the following differential equation [68, 69].

$$\ddot{x} + x = \mu f(x, \dot{x}, t) \tag{2.7}$$

where the dot over x refers to differentiation with respect to time t the function $f(x, \dot{x}, t)$ contains explicitly the time t.

$$f(x, \dot{x}, t + T) = f(x, \dot{x}, t) \tag{2.8}$$

The harmonic solution of this equation is expressed in the form

$$x = A\cos(wt + \varphi). \tag{2.9}$$

where A is the maximum amplitude of oscillations and φ the phase difference. Replacing equation (2.9) into equation (2.8) and equating separately the coefficient of sine and cosine terms which have the same harmonics, one obtains (neglecting harmonics order greater than one) a system of algebraic equations which are the amplitude equations. This procedure is the basic principle of harmonic balance. It will be used in chapter 3 to obtain the amplitude and frequency response curves of the devices.

2.3 Numerical Methods

2.3.1 Fourth-order Runge-Kutta method for ordinary differential equations

To solve numerically ordinary differential equations, there exists several numerical analysis techniques as the Verlet method, Euler method, Taylors method, Adams-Bashforth

methods, Runge Kutta metods just to name a few. The Runge Kutta methods is widely used because of its stability. It has been elaborated for the first time in 1894 by Carle Runge and has been improved by Martin W. Kutta in 1901. Modern developments are mostly due to John Butcher in the 1960s. This methods combines both trapezium numerical integration and Simpson methods. Such methods use discretization to calculate the solutions in small steps. The approximation of the next step is calculated from the previous one, by adding terms. Consider the ordinary first order differential equation as

$$\frac{dy}{dt} = f(t, y) \tag{2.10}$$

with the initial condition $y(t_0) = y_0$.

The aims of the RK4 is to find solutions after each time step, the next solution as a function of the previous one. This method establishes the relations [70, 71]:

$$y(t+h) = y(t) + \frac{1}{6}(K_1 + 2K_2 + 2K_3 + K_4) \tag{2.11}$$

The coefficients K_1, K_2, K_3 and K_4 are express as follows:

$$\begin{aligned} K_1 &= hf(t, y(t)) \\ K_2 &= hf(t + \tfrac{h}{2}, y(t) + \tfrac{K_1}{2}) \\ K_3 &= hf(t + \tfrac{h}{2}, y(t) + \tfrac{K_2}{2}) \\ K_4 &= hf(t + h, y(t) + K_3) \end{aligned} \tag{2.12}$$

This iteration procedure needs only the initial value y_0 , to calculate all the other values taken by the function y at other times separated by the time step h.

In the case of second-order differential equation :

$$\begin{cases} \frac{d^2y}{dt^2} = f(t, y, \frac{dy}{dt}) \\ y(t_0) = y_0, \frac{dy}{dt}|_{t=t_0} = y_0 \end{cases} \tag{2.13}$$

It can be divided in order to obtain two first order equations written as follows,

$$\begin{cases} \frac{dy}{dt} = z \\ \frac{dz}{dt} = f(t, y, z) \\ y(t_0) = y_0, z(t_0) = z_0 \end{cases} \tag{2.14}$$

The fourth Order Runge Kutta iterations are given by the following relations:

$$\begin{cases} y(t+h) = y(t) + \frac{1}{6}(K_1 + 2K_2 + 2K_3 + K_4) \\ z(t+h) = Z(t) + \frac{1}{6}(L_1 + 2L_2 + 2L_3 + L_4) \end{cases} \tag{2.15}$$

where

$$\begin{aligned} K_1 &= hz(t) \\ L_1 &= hf(t, y, z) \\ K_2 &= h(z(t) + \tfrac{L_1}{2}) \\ L_2 &= hf(t + \tfrac{h}{2}, y(t) + \tfrac{K_1}{2}, z(t) + \tfrac{L_1}{2}) \\ K_3 &= h(z(t) + \tfrac{L_2}{2}) \\ L_3 &= hf(t + \tfrac{h}{2}, y(t) + \tfrac{K_2}{2}, z(t) + \tfrac{L_2}{2}) \\ K_4 &= h(z(t) + L_3) \\ L_4 &= hf(t + \tfrac{h}{2}, y(t) + K_3, z(t) + L_3) \end{aligned} \tag{2.16}$$

2.3.2 Hardware and software

During the course of this work, we used a Laptop computer running Windows 10 operating system and two major software's: Fortran and Matlab.

2.4 Numerical tools for characterization of the dynamical states

Dynamical states of the nonlinear systems are usually investigated with a number of numerical tools such as the time histories diagram, phase portraits diagrams, Poincare

section, Power spectrum, bifurcation diagrams and Lyapunov exponent. In this section, we present brief information on the numerical tools which are used for characterizing different dynamical states of nonlinear plate in the different study cases considered in this thesis.

2.4.1 Time traces and phase portrait

The first approach of the detection of different dynamics states is visual and it is based to the computer simulation of nonlinear ordinary differential equations(NODE). The time trace of a dynamical system is a representation of the system evolution state in time. Phase portrait is a geometric representation of the trajectories of a dynamical system in the phase plane. Each set of initial conditions is represented by different curve or point. Phase portraits are an invaluable tool in studing dynamical systems. They consist of a plot of typical trajectories in the state space. This reveals information such as whether, an attractor, a limit cycle is present for the chosen parameter values. This reveals information such as whether an attractor, a repellor or limit cycle is present for the chosen parameter value. However the drawback of this computational tool is that it can be hard to distinguish the quasi-periodicity and chaos phenomena by using the phase portrait diagram.

2.4.2 Bifurcation Diagram

Varying the parameter values of NODE, one observes carefully the time histories and phase portraits. The chaotic behavior is distinguished from others by its extremely irregularity. Another approach of the detection of dynamical states is the bifurcation diagram. Bifurcation diagram is helpful to understand how the long term behavior of a model changes as parameter values change [72]. Points on the diagram that represent change in

the behavior are called bifurcation points. The method consists in representing in abscissa on a diagram the values of one parameter of the system and the projection on a vertical straight line the figurative symbols of amplitudes points of the corresponding Poincare section [73]. In the bifurcation phenomena, attractors may appear, disappear or be replaced by another one. Bifurcation diagrams help us to visualize these transitions. We can identify various routes to chaos taken by dynamical systems. The most common are: the period doubling route, the quasi-periodic route and intermittency route. But the Achilles heel of this method is the confusion between the quasi-periodicity and chaos phenomena. The most reliable indicator of chaos phenomenon is the Lyapunov exponent or the Lyapunov number.

2.4.3 Lyapunov exponent

Chaotic behavior needs to be properly identified in dynamical systems. In this regard, diagnostic tools are essential and system invariants are good alternative for this aim. Attractor dimension and Lypunov exponent are usually employed to identified chaos.
Lyapunov exponent evaluates the sensitive dependence on initial conditions estimating the exponential divergence of nearby orbit. These exponents have been used as the most useful diagnostic tool for chaotic system analysis and can also been used for the calculation of other invariant quantities as the attractor dimension. The signs of these exponents provide a qualitative picture of the system's dynamics. The existence of positive Lyapunov exponents defines directions of local instabilities in the system dynamics and any system containing at least one positive exponent presents chaotic behavior. When the Lyapunov exponent is negative or vanishes, trajectories do not diverge. On the other hand, when the exponent is positive, it indicates that trajectories diverge, characterizing chaos. The

maximum one-dimensional Lyapunov exponent is defined as:

$$\lambda_{\max} = \lim \left\{ (\frac{1}{t}) \ln [D(t)] \right\}, \tag{2.17}$$

with

$$D(t) = \sqrt{\delta_1^2 + \delta_2^2 + \delta_3^2}, \tag{2.18}$$

Where $D(t)$ is the distance between neighbouring trajectories. It is computed from the variationally equations obtained by pertubing the solutions of equations as follows:

$$x \to x + \delta_1, y \to y + \delta_2, \dot{y} \to \dot{y} + \delta_3 \tag{2.19}$$

2.5 Modelling of the mechanical systems

2.5.1 Systems delivering rotation and translation motion

a) Presentation and functionning

The electromechanical device represented in Figure 2.1 consists of an electrical motor (inductance L_2 and internal winding resistor R_2) carried by a plate which is fixed to a mobile and conducting rod. Two parallel and straight conducting rails of negligible resistance handle both ends of the mobile rod. These rails are linked to their ends by a resistor R, an inductor L, all connected in series with a sinusoidal voltage source. The mobile rod is free to move along the rails due to the effect of the Laplace's force. The whole system is immerged in a magnetic field $\vec{B}$. A special spring mechanism is fixed to the plate carrying the motor. This spring mechanism consists of an horizontal spring with linear stiffness k_v connected at the point P to two other linear springs of identical stiffness k_0 and initial length l_0 mounted so that during the motion, they occupy oblique configuration. The current, delivered by the generator flows through the two rails, the

mobile rod and the motor. The parameters values and units of this system are listed in tables 2.1, 2.2, 2.3 and 2.4.

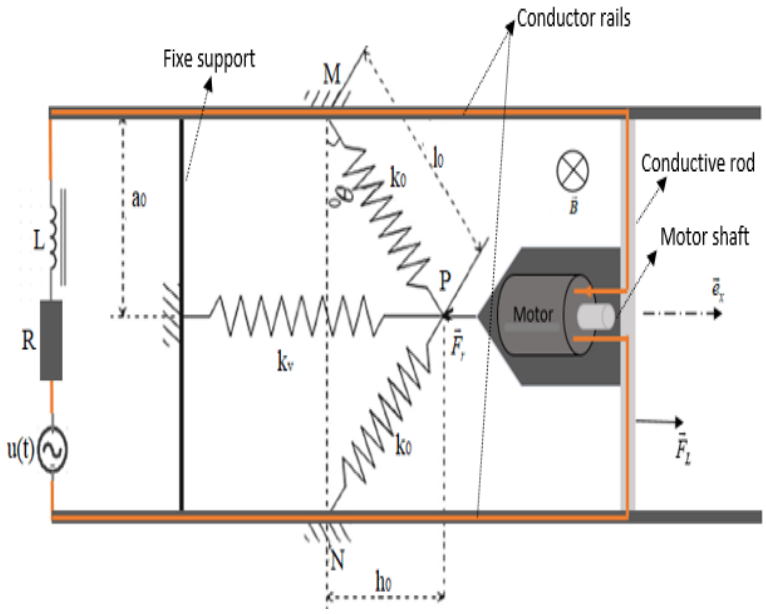

Figure 2.1: Schematic representation of the electromechanical system

Table 2.1: Values of the electrical components in the circuit

Parameters	**Notation**	**Value**	**Unit**
Inductance	L_0	323.18×10^{-3}	H
Resistance	R	5	Ω

Table 2.2: Values of the spring constants, lengths and that of the rails

Parameters	**Notation**	**Value**	**Unit**
Horizontal sprint stiffness	k_v	10	$N.m$
Oblique sprint stiffness	k_0	9	$N.m$
Initial length of the oblique springs	l_0	0.1	m
Distance between the two rails	l_r	0.134	m
Viscous damping	λ	0.4×10^{-2}	$N.s/m$
The middle distance between the two rails	a_0	0.067	m

Table 2.3: Values of the motor parameters

Parameters	**Notation**	**Value**	**Unit**
Height of the rotor	h	9.85×10^{-2}	m
Diameter of the rotor	D	8.12×10^{-2}	m
Magnetic field intensity	B	0.73	T
Relative permeability	μ_r	985	
Thickness of the winding	l_g	5×10^{-3}	m
Resistivity of the wire	φ	1.72×10^{-8}	Ωm
Diameter of the wire in the winding	d	0.15×10^{-3}	m
Number of turns	N	20	
Rotor inertia moment	J_r	9.5×10^{-7}	$Kg.m^2$
Back electromotive force constant	K_E	2.8×10^{-5}	$V.s/rad$
Torque constant	K_T	2.8×10^{-5}	$N.m/A$
Viscous friction coefficient	C_v	0.2×10^{-3}	$N.s$
Mass of the motor, the plate and rod	M	0.068	kg

Table 2.4: Parameter of the nonlinear inductance

Parameters	**Notation**	**Value**	**Unit**
Cross sectional area	A	176.71	mm^2
Saturation flux density	B_s	130×10^{-3}	T
Number of turns	N	1000	
Parameter	α	88.23×10^{-4}	m/A
Parameter	β	88.42×10^{-2}	

For the electrical circuits, the values come from the experimental work conducted by Nana et *al* in [63]. For the mechanical systems, we have considered values of DC motors and the physical dimensions are fixed by us. For the nonlinear spring system, it has been used for several investigations both for theoretical and experimental investigations (see [50, 74]).

b) Equations of motion

In regard to the mechanical part, the motion is studied with two dimensions respectively, x the translational displacement of the mobile rod and, θ the rotor angular displacement. According to the Newtown's second law for translational motion, the dynamical equation of the mobile rod is written as:

$$M\frac{d^2x}{dt^2} = -F_r + F_l \tag{2.20}$$

where F_r is the resistance force of the rod due to the spring and F_l is the Laplace force. Both force can be expressed as:

$$F_r = \lambda\dot{X} + k_v X - 2k_0 X\left(\frac{l_0}{\sqrt{a_0^2 + X^2}} - 1\right) + k_v h_0 \tag{2.21}$$

Let us consider in Figure 2.1 that the initial position of the system is taken when the oblique springs are transversal to the longitudinal spring. Then the elastic force becomes:

$$F_r = \lambda\dot{X} + k_v X - 2k_0 X\left(\frac{l_0}{\sqrt{a_0^2 + X^2}} - 1\right) \tag{2.22}$$

And

$$F_l = Bil_r \tag{2.23}$$

Equation (2.20) can be written taking into account equations (2.22) and (2.23) as follows:

$$M\frac{d^2X}{dt^2} + \lambda\frac{dX}{dt} + k_v X - 2k_0 X\left(\frac{L_0}{\sqrt{a_0^2 + X^2}} - 1\right) - Bil_r = 0 \tag{2.24}$$

Using to the Newtown's second law for rotational motion, the second equation for the mechanical part is given by:

$$J_r\frac{d^2\theta}{dt^2} + C_v\frac{d\theta}{dt} - K_T i = 0 \tag{2.25}$$

where: $J_r : [kg.m^2]$ is the rotor inertia coefficient, $C_v : [n.m.s]$ the viscous friction coefficient, and K_T the torque constant. However, the equation of the electrical part is obtained by applying the Kirchhoff's voltage law to the electrical circuit. It is given by:

$$\left(L_0\left((1-\eta)+\frac{2\eta}{1+\cosh\left(\frac{i}{i_0}\right)}\right)+L_2\right)\frac{di}{dt}+(R+R_2)\,i+Bl_r\frac{dX}{dt}+K_E\frac{d\theta}{dt}=u(t) \quad (2.26)$$

In this equation, from left to right the first term is the voltage across the inductor, the second term is the ohmic voltage and the third term is the back electromotive force (BEF) which represents the coupling term between the electrical part and mechanical part of the device and K_E the back electromotive force constant. $u(t)$ is the external excitation source considered as sinusoidal $u(t)=e_0\cos(\omega t)$. The parameters η, L_2 and R have the following expressions:

$$\eta=\frac{\beta_s\alpha}{2\mu_0+\beta_s\alpha};\ L_2=\frac{\mu_0\mu_r N^2hD}{l_g};\ R=\frac{8\varphi(h+D)N}{\pi d^2}.$$

μ_r is the relative permeability of the rotor, l_g is the thickness of the winding, φ and d are respectively the resistivity and diameter of the wire used in the winding, N is the number of turns, h and D are respectively the height and diameter of the rotor, μ_0 is the permeability of vacuum.

The resulting electromechanical equations which govern the system are given as:

$$\begin{cases}\left(L_0\left((1-\eta)+\frac{2\eta}{1+\cosh\left(\frac{i}{i_0}\right)}\right)+L_2\right)\frac{di}{dt}+(R+R_2)\,i+Bl_r\frac{dX}{dt}+K_E\frac{d\theta}{dt}=u(t)\\ M\frac{d^2X}{dt^2}+\lambda\frac{dX}{dt}+k_vX-2k_0X\left(\frac{l_0}{\sqrt{a_0^2+X^2}}-1\right)-Bil_r=0\\ J_r\frac{d^2\theta}{dt^2}+c_v\frac{d\theta}{dt}-K_Ti=0\end{cases} \quad (2.27)$$

The following dimensionless quantities are used in this part of work:

$x_1=\frac{i}{i_0}$, $x_3=\frac{X}{l_0}$, $y=\frac{\theta}{\theta_0}$, $t=\frac{\tau}{w_0}$.

where i_0 and θ_0 are respectively the normalization current and angular displacement. Let us consider $x_4 = \frac{dx_3}{d\tau}$ and $z = \frac{dy}{d\tau}$ respectively as the translational and angular velocity of the rod.

2.5.2 Hybrid translational-pendulum electromechanical system with a nonlinear spring

a) Presentation and functionning

The system is depicted in Figure 2.2. It is an electromechanical system consisting of a pendulum attached to a mobile-conducting rod (support). The system bathes in a magnetic field $\vec{B}$. A special spring mechanism is fixed to the mobile rod. This spring mechanism consists of an horizontal spring with linear stiffness k_v connected at the point P to two other linear springs of identical stiffness k_0 and initial length l_0 mounted so that during the motion, they occupy oblique configuration. Due to the effect of the Laplace's force, the rod is free to displace itself along two parallel and straight conducting rails of negligible resistance. These rails are connected at their ends by an electrical part of the system consisting of a resistor R and a sinusoidal voltage source, all connected in series. The current, delivered by the generator flows through the two rails and the mobile rod. The parameters values and units of this system are listed in tables 2.5.

b) Equations of motion

To determine the equations which derive from figure 2.2, we use Langrangian formalism. Considering figure 2.2, the total kinetic energy of the system can be expressed as:

$$E_k = \frac{1}{2}M_t\dot{x}^2 + \frac{1}{2}m_p v_p^2 \tag{2.28}$$

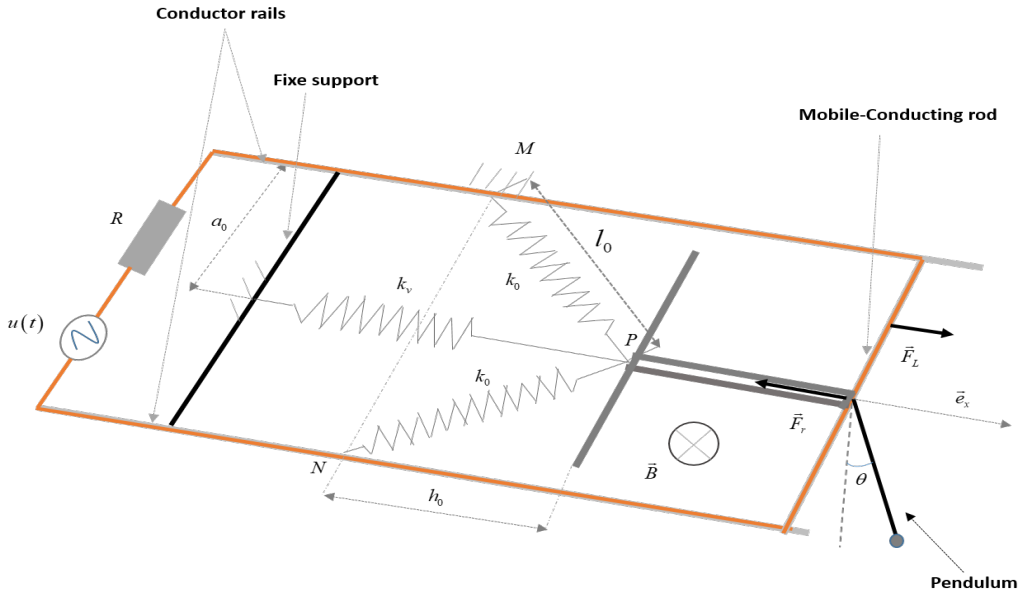

Figure 2.2: Schematic representation of the electromechanical device

Table 2.5: Parameter values

Parameters	**Notation**	**Value**	**Unit**
Resistance	R	5	Ω
Magnetic field intensity	B	0.73	T
Mass of the pendulum	m_p	0.268	kg
Pendulum lenght	l	0.3	m
Pendulum friction constant	ε	5×10^{-3}	$N.m.s/rad$
Mass of the mobile rod	M_t	0.5	kg
Viscous damping	λ	5×10^{-2}	$N.s/m$
Distance between the two rails	l_r	0.198	m
The middle distance between the two rails	a_0	0.099	m
Oblique sprint stiffness	k_0	7	N/m
Horizontal sprint stiffness	k_v	10	N/m
Initial length of the oblique springs	L_0	0.1	m
Gravitational constant	g	9.81	m/s^2

where $\frac{1}{2}M_t\dot{x}^2$ is the kinetic energy of the mobile support due to its linear motion and $\frac{1}{2}m_p v_p^2$ is the kinetic energy of the physical pendulum.

Coordinate of the pendulum mass are:

$$x_p = x + l\sin\theta \tag{2.29}$$

$$y_p = l\cos\theta \tag{2.30}$$

From (2.29) and (2.30) one obtains:

$$v_p^2 = (\dot{x}_p^2 + \dot{y}_p^2) = \dot{x}^2 + 2l\dot{\theta}\dot{x}\cos\theta + l^2\dot{\theta}^2 \tag{2.31}$$

Therefore the kinetic energy becomes:

$$E_k = \frac{1}{2}\dot{x}^2(M_t + m_p) + m_p l\dot{\theta}\dot{x}\cos\theta + \frac{1}{2}m_p l^2\dot{\theta}^2 \tag{2.32}$$

The potential energy of the system is defined as:

$$E_p = E_{p1} + E_{p2} \tag{2.33}$$

where E_{p1} is the potential energy of the pendulum and E_{p2} the one of the mobile rod

$$E_{P1} = m_p gl(1 - \cos\theta) \tag{2.34}$$

The elastic force f can be written as it was given in equation (2.22) thus

$$E_{p2} = \int F_r dx = \int \left(k_v x - 2k_0 x \left(\frac{l_0}{\sqrt{a_0^2 + x^2}} - 1 \right) \right) dx \tag{2.35}$$

Hence the potential energy of the system can be writen as:

$$E_P = m_p gl(1 - \cos\theta) + \frac{1}{2}k_v x^2 - 2k_0 \left(l_0\sqrt{a^2 + x^2} - \frac{1}{2}x^2 \right) \tag{2.36}$$

The Lagrangian of the entire system is given as:

$$L = \frac{1}{2}\dot{x}^2(M_t + m_p) + m_p l\dot{\theta}\dot{x}\cos\theta + \frac{1}{2}m_p l^2\dot{\theta}^2 - m_p gl(1 - \cos\theta) - \frac{1}{2}k_v x^2 + 2k_0 \left(l_0\sqrt{a^2 + x^2} - \frac{1}{2}x^2 \right) \tag{2.37}$$

The Euler Lagrangian equation is given as:

$$\ddot{x}(M_t+m_p)+m_p l\ddot{\theta}\cos\theta-m_p l\dot{\theta}^2\sin\theta+k_v x-2k_0 x\left(\frac{l_0}{\sqrt{a^2+x^2}}-1\right)=-\lambda\dot{x}+Bil_r \quad (2.38)$$

$$m_p l\ddot{x}\cos\theta+m_p l^2\ddot{\theta}+m_p gl\sin\theta=-\varepsilon\dot{\theta} \quad (2.39)$$

The equation of the electrical part is given as:

$$Ri+Bl_r\frac{dx}{dt}=u(t) \quad (2.40)$$

Therefore the electromechanical equations which show the dynamic of the entire system are given as:

$$\begin{cases} \ddot{x}(M_t+m_p)+m_p l\ddot{\theta}\cos\theta-m_p l\dot{\theta}^2\sin\theta+k_v x-2k_0 x\left(\frac{l_0}{\sqrt{a^2+x^2}}-1\right)=-\lambda\dot{x}+Bil_r \\ m_p l^2\ddot{\theta}+m_p l\ddot{x}\cos\theta+m_p gl\sin\theta=-\varepsilon\dot{\theta} \\ Ri+Bl_r\dot{x}=u(t) \end{cases} \quad (2.41)$$

where x is the displacement of the mobile conducting rod, θ is the pendulum angle and i is the electric current. The external excitation source $u(t)$ is considered as a sinusoidal input voltage of the form $u(t)=e_0\cos(wt)$ (e_0, ω and t been respectively the amplitude, frequency and time). By substituting in the first equation the current taken from the last equation, the above equations can be reduced to a set of two coupled differential equations:

$$\begin{aligned} &\ddot{x}(M_t+m_p)+\dot{x}\left(\lambda+\tfrac{1}{R}B^2l_r^2\right)+x\left[k_v-2k_0\left(\tfrac{l_0}{\sqrt{a^2+x^2}}-1\right)\right] \\ &+m_p l\ddot{\theta}\cos\theta-m_p l\dot{\theta}^2\sin\theta=\tfrac{1}{R}Bl_r u(t) \end{aligned} \quad (2.42a)$$

$$\ddot{x}\cos\theta+l\ddot{\theta}+\frac{\varepsilon}{m_p l}\dot{\theta}+g\sin\theta=0 \quad (2.42b)$$

Let us use the following dimensionless parameters:

$$\begin{aligned} &x_3 = \frac{x}{l_0}; y = \frac{\theta}{\theta_0}; t = \frac{\tau}{w_0}; a = \frac{a_0}{l_0}; \alpha = \frac{k_0}{k_v}; \Omega = \frac{w}{w_0}; w_0 = \sqrt{\frac{k_v}{(M_t + m_p)}} \\ &\alpha_1 = \frac{1}{w_0(M_t + m_p)}(\lambda + \frac{1}{R}B^2 l_r^2); \alpha_2 = \frac{m_p l \theta_0}{l_0(M_t + m_p)}; \alpha_3 = \frac{m_p l \theta_0^2}{l_0(M_t + m_p)} \\ &\beta_1 = \frac{\varepsilon}{m_p l^2 w_0}; \beta_2 = \frac{l_0}{\theta_0 l}; \beta_3 = \frac{g}{w_0^2 \theta_0 l}; E = \frac{B l_r e_0}{w_0^2 l_0 R(M_t + m_p)} \end{aligned} \tag{2.43}$$

In this case, the system is modelled as follows:

$$\begin{cases} \ddot{x}_3 + \alpha_1 \dot{x}_3 + \left(1 - 2\alpha\left(\frac{1}{\sqrt{a^2 + x_3^2}} - 1\right)\right) x_3 + \alpha_2 \ddot{y}\cos(\theta_0 y) - \alpha_3 \dot{y}^2 \sin(\theta_0 y) = E\cos(\Omega\tau) \\ \ddot{y} + \beta_1 \dot{y} + \beta_2 \ddot{x}_3 \cos(\theta_0 y) + \beta_3 \sin(\theta_0 y) = 0 \end{cases} \tag{2.44}$$

2.6 Conclusion

In this chapter, we started by the presentation of the mathematical formalisms and the numerical methods used to solve the differential equations as well as the hardware and software used. We have elaborated some dynamical tools that will be useful in the next chapter to characterize the dynamical states of the EMSs. We ended by the presentation of the two electromechanical devices studied in this work and their mathematical models. The next chapter will be based on the dynamic of those two devices.

Chapter III

Results and discussion

3.1 Introduction

This chapter is devoted to the results and discussions on the work carried out in this thesis. It is therefore organized as follows. Section 3.2 presents the dynamical behaviour of an electromechanical system consisting of an electrical motor carried by a mobile conducting rod (support). The attention is focussed on the effects of the nonlinear spring and the hysteretic iron-core inductor introduced in the mechanical and electrical parts respectively. In section 3.3, the dynamical study of a new model of device combining translational and pendulum motion is presented. We end this chapter by a conclusion in section 3.4.

3.2 Dynamical behaviours of a coupled system made of rotary motor and mobile translating support

3.2.1 Oscillatory state in the linear case

In the linear case, it is assumed that the hysteretic inductor inductance is equal to $L_0(\eta = 0)$, and the two oblique springs are absent $k_0 = 0$. In this case, the dimensionless

equations describing the dynamics of the system are as follows:

$$\begin{cases} \dot{x}_1 + \alpha_1 x_1 + \alpha_2 \dot{x}_3 + \alpha_3 \dot{y} = E_0 \cos(\Omega\tau) \\ \ddot{x}_3 + \beta_1 \dot{x}_3 + x_3 - \beta_2 x_1 = 0 \\ \ddot{y} + \gamma_1 \dot{y} - \gamma_2 x_1 = 0 \end{cases} \tag{3.1}$$

with the following rescaling:

$$\begin{aligned} &\Omega = \tfrac{w}{w_0}; w_0 = \sqrt{\tfrac{k_v}{M}}; \alpha_1 = \tfrac{(R+R_2)}{(L_0+L_2)w_0}; \alpha_2 = \tfrac{Bl_r x_0}{(L_0+L_2)i_0}; \alpha_3 = \tfrac{K_E\theta_0}{(L_0+L_2)i_0} \\ &\beta_1 = \tfrac{\lambda}{Mw_0}; \beta_2 = \tfrac{Bl_r i_0}{Mw_0^2 x_0}; \gamma_1 = \tfrac{c_v}{J_r w_0}; \gamma_2 = \tfrac{K_T i_0}{J_r w_0^2 \theta_0}; E_0 = \tfrac{e_0}{(L_0+L_2)w_0 i_0} \end{aligned} \tag{3.2}$$

To derive the amplitude of the oscillatory states delivered by equation (3.1), let us express its solution by the mathematical relations of the form

$$\begin{aligned} &x_1 = A\cos(\Omega\tau - \varphi_1), x_3 = B\cos(\Omega\tau - \varphi_2), x_4 = C\cos(\Omega\tau - \varphi_3), \\ &y = D\cos(\Omega\tau - \varphi_4), z = E\cos(\Omega\tau - \varphi_5) \end{aligned} \tag{3.3}$$

where A, B, C, D and E are unknown maximal amplitudes, Ω the frequency and φ_i $(i = 1, 2, 3, 4, 5)$ the initial phases, all to be determined. Inserting equation (3.3) into equation (3.1) and then equating separately the coefficients of sine and cosine terms, one obtains a set of equations for A, B, C, D and E. This set of equations leads to:

$$A^2 = \frac{E_0^2}{\left[\alpha_1+\frac{\alpha_2\beta_1\gamma_2\Omega^2}{\beta_1^2\Omega^2+(1-\Omega^2)^2}+\frac{\alpha_3\gamma_1\gamma_2\Omega^2}{\Omega^4+\gamma_1^2\Omega^2}\right]^2+\left[\Omega+\frac{\alpha_2\gamma_2\Omega(1-\Omega^2)}{\beta_1^2\Omega^2+(1-\Omega^2)^2}-\frac{\alpha_3\gamma_2\Omega^3}{\Omega^4+\gamma_1^2\Omega^2}\right]^2}$$

$$B^2 = \frac{\beta_2^2E_0^2}{\left[\beta_1^2\Omega^2+(1-\Omega^2)^2\right]\left[\left[\alpha_1+\frac{\alpha_2\beta_1\gamma_2\Omega^2}{\beta_1^2\Omega^2+(1-\Omega^2)^2}+\frac{\alpha_3\gamma_1\gamma_2\Omega^2}{\Omega^4+\gamma_1^2\Omega^2}\right]^2+\left[\Omega+\frac{\alpha_2\gamma_2\Omega(1-\Omega^2)}{\beta_1^2\Omega^2+(1-\Omega^2)^2}-\frac{\alpha_3\gamma_2\Omega^3}{\Omega^4+\gamma_1^2\Omega^2}\right]^2\right]}$$

$$C^2 = \frac{\Omega^2\beta_2^2E_0^2}{\left[\beta_1^2\Omega^2+(1-\Omega^2)^2\right]\left[\left[\alpha_1+\frac{\alpha_2\beta_1\gamma_2\Omega^2}{\beta_1^2\Omega^2+(1-\Omega^2)^2}+\frac{\alpha_3\gamma_1\gamma_2\Omega^2}{\Omega^4+\gamma_1^2\Omega^2}\right]^2+\left[\Omega+\frac{\alpha_2\gamma_2\Omega(1-\Omega^2)}{\beta_1^2\Omega^2+(1-\Omega^2)^2}-\frac{\alpha_3\gamma_2\Omega^3}{\Omega^4+\gamma_1^2\Omega^2}\right]^2\right]} \tag{3.4}$$

$$D^2 = \frac{\gamma_2^2E_0^2}{(\Omega^4+\gamma_1^2\Omega^2)\left[\left[\alpha_1+\frac{\alpha_2\beta_1\gamma_2\Omega^2}{\beta_1^2\Omega^2+(1-\Omega^2)^2}+\frac{\alpha_3\gamma_1\gamma_2\Omega^2}{\Omega^4+\gamma_1^2\Omega^2}\right]^2+\left[\Omega+\frac{\alpha_2\gamma_2\Omega(1-\Omega^2)}{\beta_1^2\Omega^2+(1-\Omega^2)^2}-\frac{\alpha_3\gamma_2\Omega^3}{\Omega^4+\gamma_1^2\Omega^2}\right]^2\right]}$$

$$E^2 = \frac{\Omega^2\gamma_2^2E_0^2}{(\Omega^4+\gamma_1^2\Omega^2)\left[\left[\alpha_1+\frac{\alpha_2\beta_1\gamma_2\Omega^2}{\beta_1^2\Omega^2+(1-\Omega^2)^2}+\frac{\alpha_3\gamma_1\gamma_2\Omega^2}{\Omega^4+\gamma_1^2\Omega^2}\right]^2+\left[\Omega+\frac{\alpha_2\gamma_2\Omega(1-\Omega^2)}{\beta_1^2\Omega^2+(1-\Omega^2)^2}-\frac{\alpha_3\gamma_2\Omega^3}{\Omega^4+\gamma_1^2\Omega^2}\right]^2\right]}$$

Considering equation (3.4), we analyse the behaviours of A, B, C, D and E when the frequency Ω of the external excitation is varied. The results are presented in Figure 3.1. As it appears in Figure 3.1, when the frequency increases from 0.0 to 3.0, A decreases progressively from the maximum amplitude to the amplitude equal to 0.26 ($\Omega = 1$), then increases a bit and finally decreases to a lower amplitude. In the mean-time the amplitudes B and C increase from almost zero to a higher amplitude equal to 0.53 and decreases to small values. When the frequency is equal to 1, an anti-resonance phenomenon in the electrical part and resonance phenomenon in the translation motion are observed in (Figures 3.1a, 3.1b and 3.1c). The amplitude of the angular displacement D decreases when the frequency increases. E have the same behavior as A. The anti-resonance in the electrical current means that when the power dissipated by the Joule effect is minimum, the displacement of the rod is maximal. Due to the linear form of equation (2.27), one

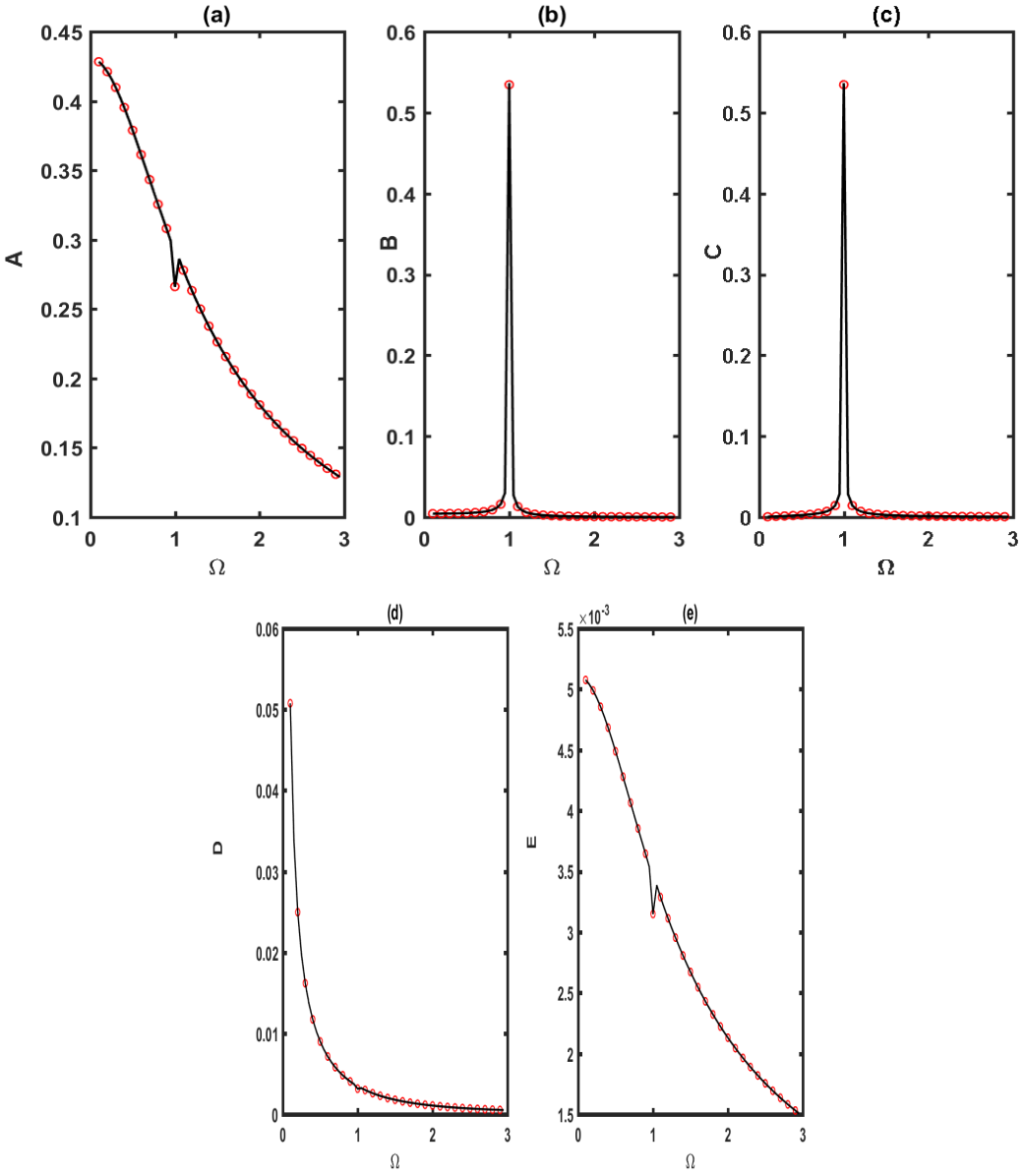

Figure 3.1: Analytical (full line) and numerical (dot line) frequency-response curves: (a) amplitude of the electrical current; (b) amplitude of the rod displacement; (c) amplitude of the rod velocity; (d) amplitude of the angular displacement; (e) amplitude of the angular velocity. With $E_0 = 0.39$.

also observes that the maximal dimensionless value of the translational, the angular displacement and the electrical current increases linearly with the magnitude of the external excitation (Figure not presented here).

3.2.2 Frequency response and bifurcation diagrams

a) Case of linear inductance with nonlinear spring

We remind that this case is described by the following set of equations

$$\dot{x}_1 + \alpha_1 x_1 + \alpha_2 \dot{x}_3 + \alpha_3 \dot{y} = E_0 \cos(\Omega\tau) \tag{3.5a}$$

$$\ddot{x}_3 + \beta_1 \dot{x}_3 + \beta_2 \left[1 - 2\alpha\left(\frac{1}{\sqrt{a^2 + x_3^2}} - 1\right)\right] x_3 - \beta_3 x_1 = 0 \tag{3.5b}$$

$$\ddot{y} + \gamma_1 \dot{y} - \gamma_2 x_1 = 0 \tag{3.5c}$$

The new coefficients are given as follows:

$$\alpha = \frac{k_0}{k_v}; a = \frac{a_0}{l_0}; \beta_2 = \frac{k_v}{M w_0^2}; \beta_3 = \frac{B l_r i_0}{M w_0^2 l_0} \tag{3.6}$$

To conduct more analytical investigations, an approximate cubic expression of the term, which contains the square root, is developed using a Taylor series expansion at the static equilibrium position $x_3 = 0$. One obtains:

$$\left[1 - 2\alpha\left(\frac{1}{\sqrt{a^2 + x_3^2}} - 1\right)\right] x_3 \approx \left[1 - 2\alpha\left(\frac{1-a}{a}\right)\right] x_3 + \frac{\alpha}{a^3} x_3^3 \tag{3.7}$$

Inserting Equation (3.7) in Equation (3.5*b*) and using Equations (3.3), the harmonic balance method is applied. After some algebraic manipulations, it comes that the amplitudes satisfy the following nonlinear algebraic equations:

$$\frac{B^2\left[\beta_1^2\Omega^2+(F+\frac{3\alpha}{4a^3}\beta_2B^2)^2\right]}{\beta_3^2}\left[\begin{array}{c}\left[\alpha_1+\frac{\alpha_2\Omega^2\beta_1\beta_3}{\beta_1^2\Omega^2+(F+\frac{3\alpha}{4a^3}\beta_2B^2)^2}+G\right]^2+\\ \left[\Omega+\frac{\alpha_2\beta_3\Omega(F+\frac{3\alpha}{4a^3}\beta_2B^2)}{\beta_1^2\Omega^2+(F+\frac{3\alpha}{4a^3}\beta_2B^2)^2}-\frac{\Omega}{\gamma_1}G\right]^2\end{array}\right]-E_0^2=0$$

$$\begin{aligned}A^2&=\frac{B^2\left[\beta_1^2\Omega^2+(F+\frac{3\alpha}{4a^3}\beta_2B^2)^2\right]}{\beta_3^2}\\ C^2&=\Omega^2B^2\\ D^2&=\frac{\gamma_2^2B^2}{(\Omega^4+\gamma_1^2\Omega^2)\beta_3^2}\left[\beta_1^2\Omega^2+(F+\frac{3\alpha}{4a^3}\beta_2B^2)^2\right]\\ E^2&=\frac{\Omega^2\gamma_2^2B^2}{(\Omega^4+\gamma_1^2\Omega^2)\beta_3^2}\left[\beta_1^2\Omega^2+(F+\frac{3\alpha}{4a^3}\beta_2B^2)^2\right]\end{aligned}\tag{3.8}$$

with

$F=-\Omega^2+\beta_2\left(1-2\alpha\left(\frac{1-a}{a}\right)\right)$ and $G=\frac{\alpha_3\gamma_1\gamma_2\Omega^2}{\Omega^4+\gamma_1^2\Omega^2}$.

Figure 3.2 presents the frequency-response curves for this nonlinear model. Both the results from equations (3.8) and those obtained from the numerical simulation of equations (3.5) are plotted. The curves show that the amplitude of the electrical current, that of the angular displacement and that of the angular velocity decrease when the frequency increases. Also notice the three values sometimes four of these amplitudes when the frequency is between 0.65 and 1.85. This can be understood as two stable solutions separated by an unstable solution. This effect generally leads to the jump phenomenon and hysteresis as shown in the curves of figures 3.2b and 3.2c.

Numerical simulations are used to illustrate the dynamical behaviours of the system mathematically represented by equations (3.5) through bifurcation diagrams, Lyapunov exponent, and phase portraits. In this subsection, the parameters E_0 is chosen as the control

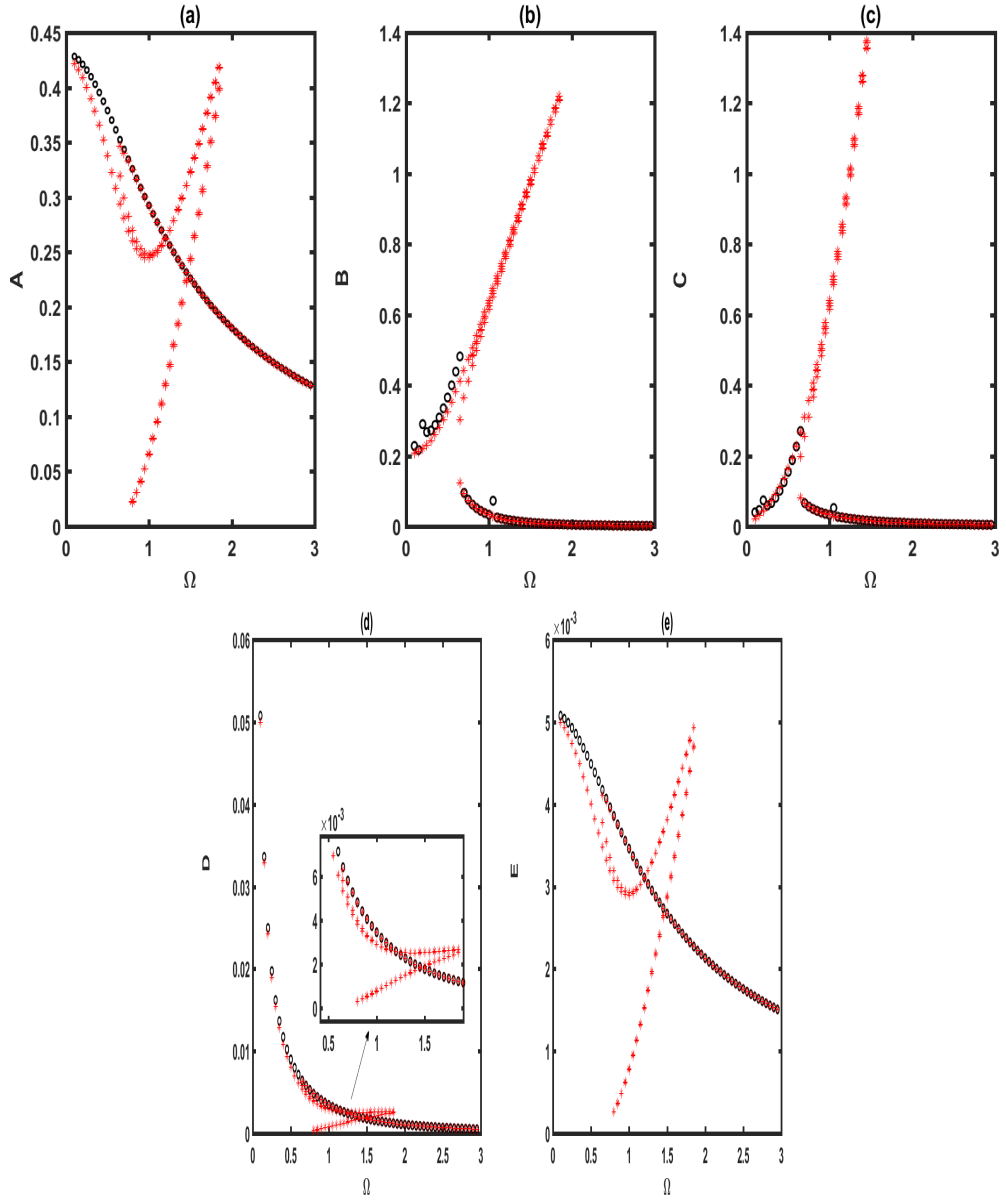

Figure 3.2: Analytical (star line) and numerical (dot line) frequency-response of: (a) amplitude of the electrical current; (b) amplitude of the rod displacement; (c) amplitude of the rod velocity; (d) amplitude of the angular displacement; (e) amplitude of the angular velocity. With $E_0 = 0.39$.

parameter.

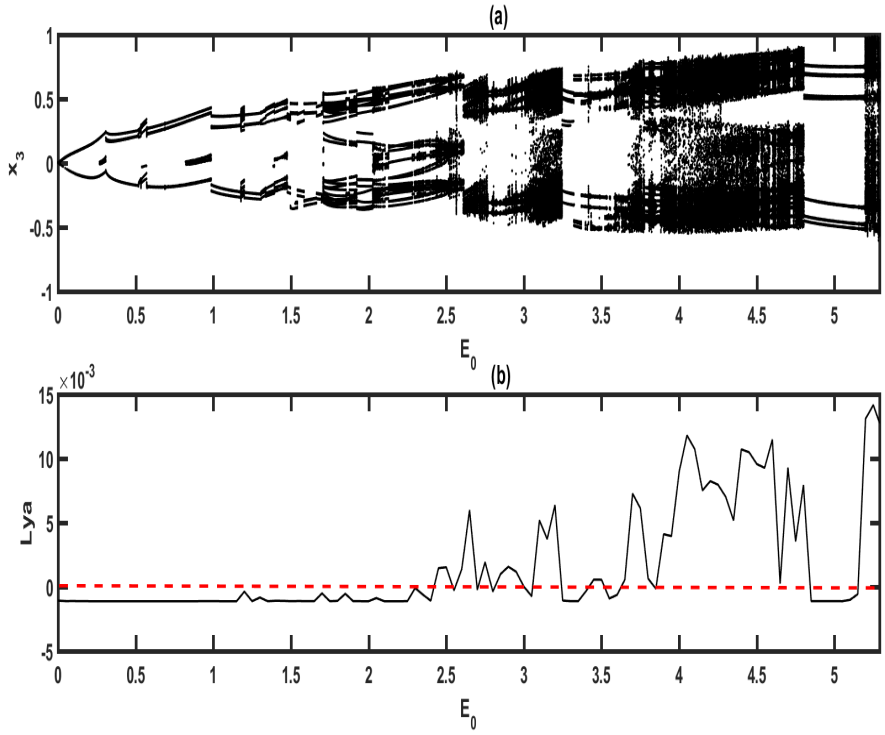

Figure 3.3: (a) Bifurcation diagram, (b) the corresponding Lyapunov exponent, versus the amplitude of the excitation with the parameters of Tables 1,2,3,4 and $\Omega = 0.1$.

From Figure 3.3, one can see that when the maximal value of the external excitation increases, the translational motion of the device firstly presents a periodic and multi periodic motion for $0 \leq E_0 \leq 2.4$. After this range, the system responses exhibit an alternation of chaotic and periodic motions. The chaotic behavior of the system starts when $E_0 = 2.5$. To confirm the results in Figure 3.3, some phase portraits are plotted in Figure 3.4 where one finds chaos (Figure 3. 4(c)) and periodic motions (Figures 3.4a, 3.4b and 3.4d).

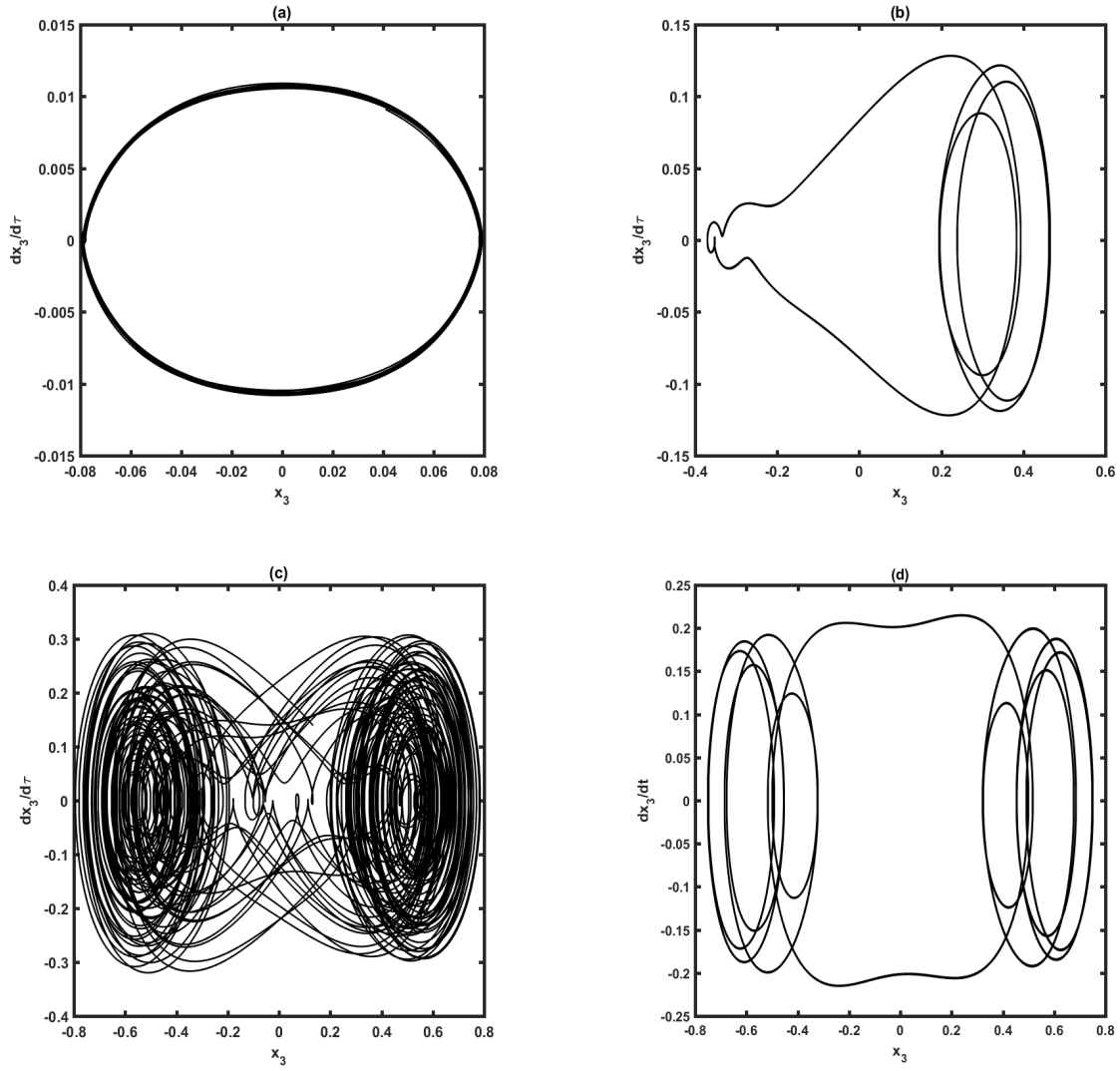

Figure 3.4: Phase portraits obtain with parameter of Figure 3.3 and (a)$E_0 = 0.1$, (b) $E_0 = 1.5$, (c)$E_0 = 4$ and (d)$E_0 = 5$.

b) Case of nonlinear inductance with nonlinear spring

This case is described by the the following equations:

$$\begin{cases} \left(1-\eta+\frac{2\eta}{1+\cosh(x_1)}+\alpha_4\right)\dot{x}_1+\alpha_1 x_1+\alpha_2\dot{x}_3+\alpha_3\dot{y}=E_0\cos(\Omega\tau) \\ \ddot{x}_3+\beta_1\dot{x}_3+\beta_2\left[1-2\alpha\left(\frac{1}{\sqrt{a^2+x_3^2}}-1\right)\right]x_3-\beta_3 x_1=0 \\ \ddot{y}+\gamma_1\dot{y}-\gamma_2 x_1=0 \end{cases} \tag{3.9}$$

with

$$\begin{aligned} &\alpha_1=\tfrac{(R+R_2)}{L_0 w_0};\alpha_2=\tfrac{Bl_r l_0}{L_0 i_0};\alpha_3=\tfrac{K_E\theta_0}{L_0 i_0};\alpha_4=\tfrac{L_2}{L_0};\beta_1=\tfrac{\lambda}{Mw_0} \\ &\beta_2=\tfrac{k_v}{Mw_0^2};\beta_3=\tfrac{Bl_r i_0}{Mw_0^2 L_0};\gamma_1=\tfrac{c_v}{J_r w_0};\gamma_2=\tfrac{K_T i_0}{J_r w_0^2\theta_0};E_0=\tfrac{e_0}{L_0 w_0 i_0} \end{aligned} \tag{3.10}$$

For analytical treatment, the nonlinear spring expression is developed as in Equation (3.7) while

$$\frac{1}{1+\cosh x_1}\approx\frac{1}{2}\left(1-\frac{x_1^2}{4}\right) \tag{3.11}$$

Inserting Equation (3.11) in Equation (3.9), we use the harmonic balance method through Equation (3.3) to establish the equations characterizing the different maximal amplitudes. The amplitudes A, B, C, D and E satisfy the following equations:

$$\begin{aligned} &B^2\left[\beta_1^2\Omega^2+(F+\tfrac{3\alpha}{4a^3}\beta_2B^2)^2\right]\tfrac{1}{\beta_3^2}\left[\begin{array}{l}\left[\alpha_1+\frac{\alpha_2\Omega^2\beta_1\beta_3}{\beta_1^2\Omega^2+(F+\frac{3\alpha}{4a^3}\beta_2B^2)^2}+G\right]^2 \\ +\left[\begin{array}{l}(1+\alpha_4)\,\Omega-\frac{\Omega\eta B^2\left(\beta_1^2\Omega^2+(F+\frac{3\alpha}{4a^3}\beta_2B^2)^2\right)}{16\beta_3^2} \\ +\frac{\alpha_2\beta_3\Omega(F+\frac{3\alpha}{4a^3}\beta_2B^2)}{\beta_1^2\Omega^2+(F+\frac{3\alpha}{4a^3}\beta_2B^2)^2}-\frac{\Omega}{\gamma_1}G\end{array}\right]^2\end{array}\right]-E_0^2=0; \\ &A^2=\tfrac{B^2\left[\beta_1^2\Omega^2+(F+\frac{3\alpha}{4a^3}\beta_2B^2)^2\right]}{\beta_3^2}; \\ &C^2=\Omega^2B^2; \\ &D^2=\tfrac{\gamma_2^2B^2}{(\Omega^4+\gamma_1^2\Omega^2)\beta_3^2}\left[\beta_1^2\Omega^2+(F+\tfrac{3\alpha}{4a^3}\beta_2B^2)^2\right] \\ &E^2=\tfrac{\Omega^2\gamma_2^2B^2}{(\Omega^4+\gamma_1^2\Omega^2)\beta_3^2}\left[\beta_1^2\Omega^2+(F+\tfrac{3\alpha}{4a^3}\beta_2B^2)^2\right] \end{aligned} \tag{3.12}$$

with

$F = -\Omega^2 + \beta_2\left(1 - 2\alpha\left(\frac{1-a}{a}\right)\right)$ and $G = \frac{\alpha_3\gamma_1\gamma_2\Omega^2}{\Omega^4+\gamma_1^2\Omega^2}$

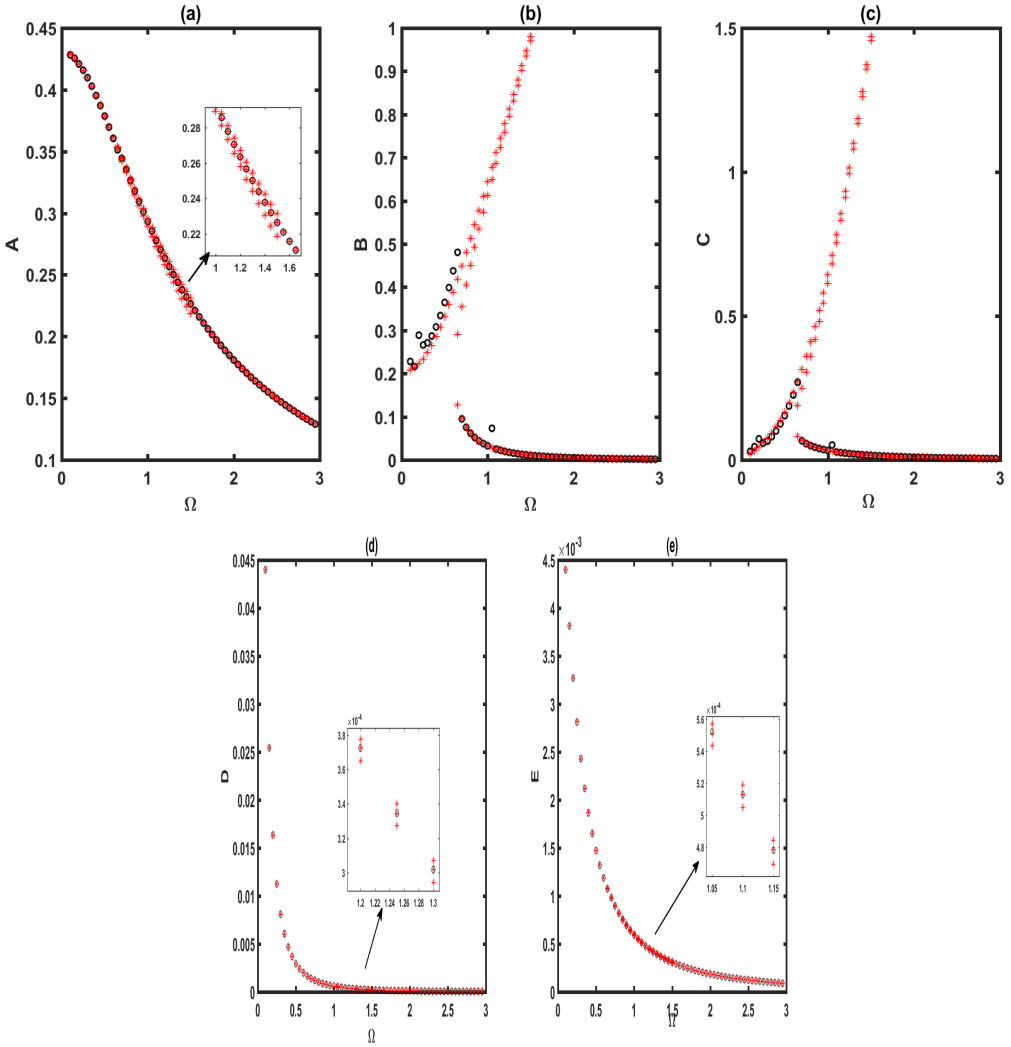

Figure 3.5: Analytical (star line) and numerical (dot line) frequency-response of: (a) amplitude of the electrical current; (b) amplitude of the rod displacement; (c) amplitude of the rod velocity; (d) amplitude of the angular displacement; (e) amplitude of the angular velocity. With $E_0 = 0.39$.

The frequency-response curves of the maximal amplitudes are represented in Figure 3.5. The frequency-response curve of the nonlinear mechanical system shows that when frequency increases, the maximal amplitudes of the electrical current, the angular

displacement and the angular velocity decrease. Multiple amplitudes domain is for frequency between 0.65 and 1.5 and jump phenomenon and hysteresis appear in Figures 3.5b and 3.5c.

The dynamical behaviors of the system mathematically presented by equations (3.9) are illustrated using numerical simulation to present bifurcation diagrams, Lyapunov exponent and phase portraits. In this subsection, parameters E_0 and η are chosen as the control parameters.

The bifurcation diagram versus E_0 is plotted in Figure 3.6(a) in term of non-dimensional displacement of the rod x_3 as E_0 is varies from 0 up to 15. Chaotic behavior of the system begins when $E_0 = 9.7$. Before this value, the system presents a periodic motion for $0 \leq E_0 < 9.7$. After this periodic motion, the system response alternatively comes into chaotic and periodic dynamics as E_0 varies. These behaviors are confirmed by Figure 3.6 (b) which presents the variation of the Lyapunov exponent. Figure 3.7 shows different phase portraits of the rod motion. Period-nT motion is observed in Figure 3.7 (a) and 3.7 (b) while chaotic oscillations is presented in Figure 3.7(c).

Comparing these results to the previous one (see figures 3.3 and 3.4), one finds that when the nonlinearity is introduced in the inductor, chaotic behaviour appears for larger values of the external excitation (i.e. as from $E_0 = 9.5$) than in the case of linear inductance where the chaotic behaviour appears as from $E_0 = 2.5$.

To analyse, the effects of the inductance hysteresis parameter η on the dynamics of the device, a bifurcation diagram and the corresponding Lyapunov exponent are plotted in Figure 3.8 as η varies. One observes that when η increases the system exhibits a chaotic oscillation for $0 \leq \eta < 1.3; 1.37 \leq \eta < 2.17$; $2.23 \leq \eta < 2.66$ and $2.76 \leq \eta < 3$. Non-chaotic behaviors are obtained in the other ranges. These behaviors are confirmed by the phase portraits which present chaotic motions in Figure 3.9a, while Figure 3.9b presents

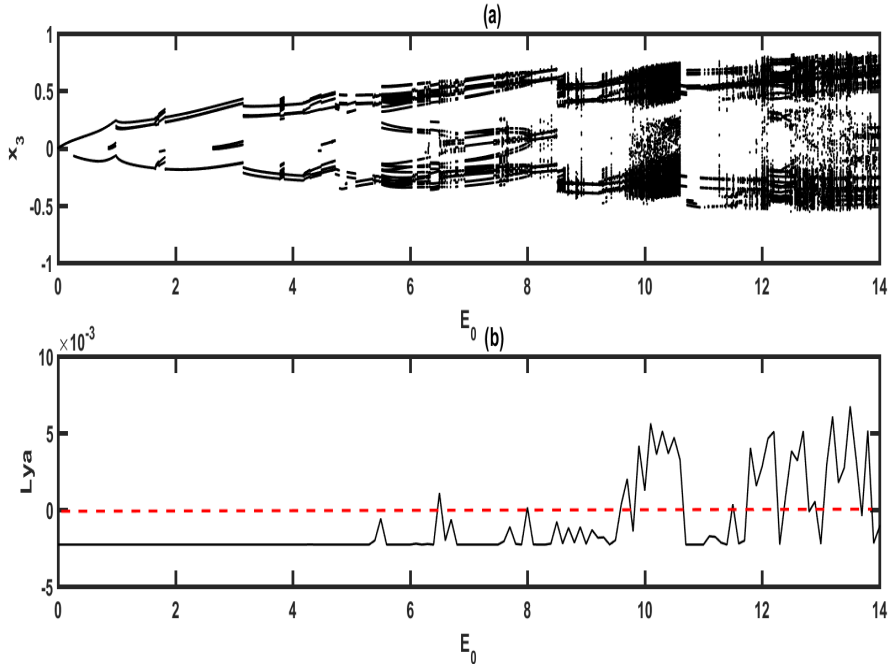

Figure 3.6: ((a)Bifurcation diagram and (b) Lyapunov exponent diagram against the amplitude of the excitation E with the parameter of Figure 3.6 and for $\Omega = 0.1$.

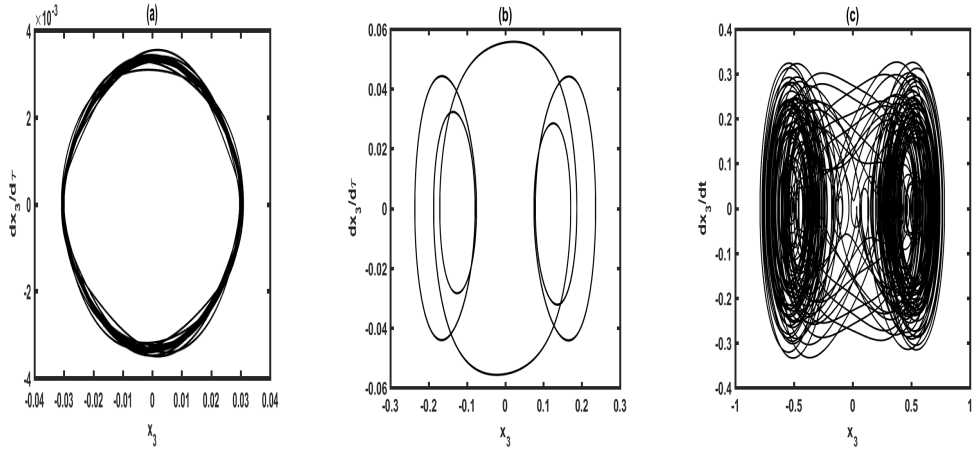

Figure 3.7: Phase portraits with the parameter of Figure 3.6. (a)$E_0 = 0.1$; (b) $E_0 = 1$; (c) $E_0 = 12$.

periodic-nT oscillations.

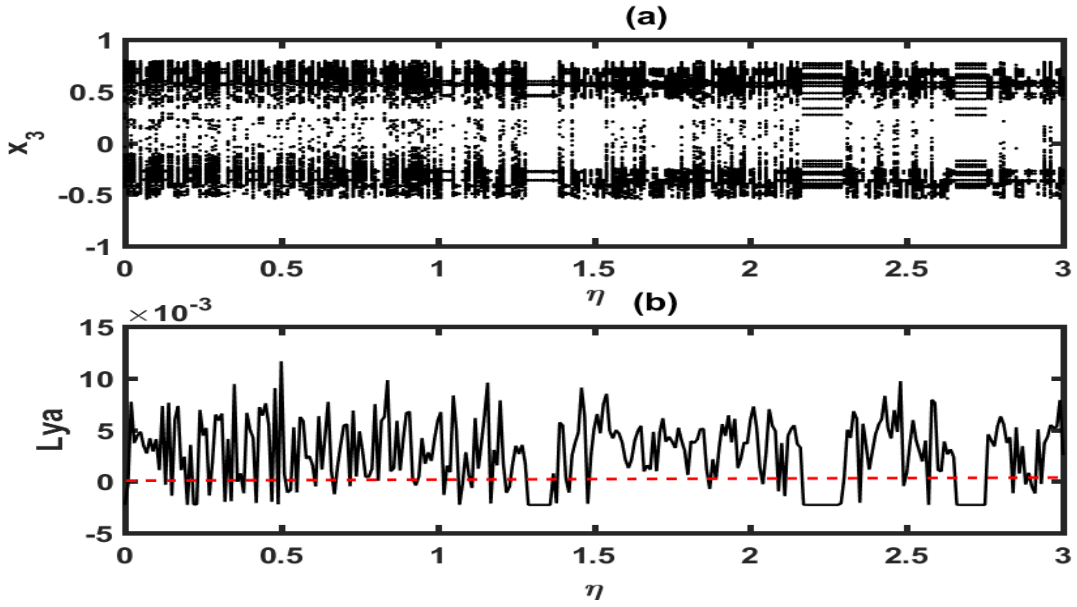

Figure 3.8: (a) Bifurcation diagram and (b) Lyapunov exponent diagram against the control parameter with the parameter of Figure 3.8 and . With $E_0 = 12$.

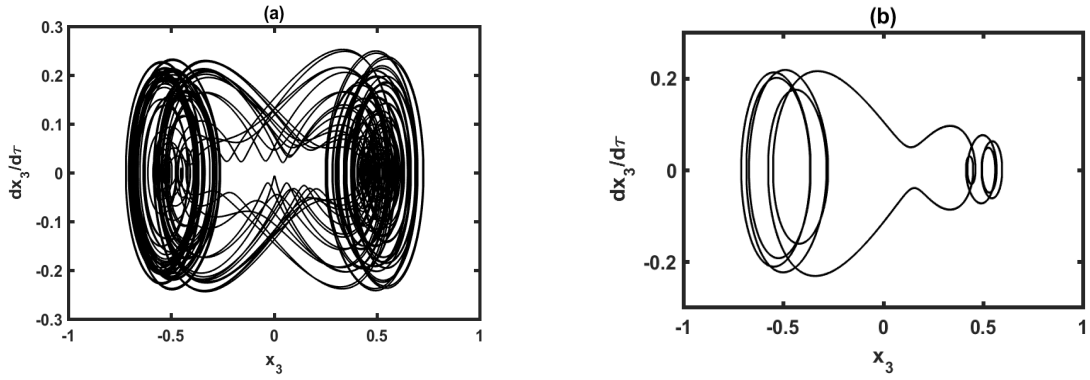

Figure 3.9: Phase portraits obtained with the parameters of figure 3.8 and (a) $\eta = 0.3$; (b) $\eta = 1.33$

The results of the numerical simulation shows that chaotic behavior can be found for very low values of the inductance hysteresis parameter η.

3.3 Complex dynamics of a driven hybrid translational-pendulum electromechanical system subjected to a nonlinear spring

3.3.1 Frequency response

a) Case of linear springs

The dimensionless equations describing the dynamics of the system are as follows:

$$\begin{cases} \ddot{x}_3 + \alpha_1 \dot{x}_3 + x_3 + \alpha_2 \ddot{y}\cos(\theta_0 y) - \alpha_3 \dot{y}^2 \sin(\theta_0 y) = E\cos(\Omega\tau) \\ \ddot{y} + \beta_1 \dot{y} + \beta_2 \ddot{x}_3 \cos(\theta_0 y) + \beta_3 \sin(\theta_0 y) = 0 \end{cases} \tag{3.13}$$

In order to obtain mathematically the approximate solutions of equations (3.13), we use the following expansions considering the case of small and average amplitude of vibrations:

$$\cos\theta_0 y \approx 1; \sin\theta_0 y \approx \theta_0 y; \dot{y}^2 \approx 0 \tag{3.14}$$

Replacing (3.14) in equations (3.13), one obtains equations (3.15).

$$\begin{cases} \ddot{x}_3 + \alpha_2 \ddot{y} = -\alpha_1 \dot{x}_3 - x_3 + E\cos(\Omega\tau) \\ \beta_2 \ddot{x}_3 + \ddot{y} = -\beta_1 \dot{y} - \beta_3 \theta_0 y \end{cases} \tag{3.15}$$

One can therefore apply the linear approximation and then use the harmonic balance method by writing:

$$x_3 = A_1\cos(\Omega\tau) + A_2\sin(\Omega\tau); y = B_1\cos(\Omega\tau) + B_2\sin(\Omega\tau) \tag{3.16}$$

Hence, the unknown parameters A_1, A_2, B_1 and B_2 satisfy the following expression:

$$
\begin{aligned}
B_1 &= E\left[\tfrac{(1-\Omega^2)(-\Omega^2+\beta_3\theta_0)}{\beta_2\Omega^2} - \tfrac{\alpha_1\beta_1}{\beta_2} - \alpha_2\Omega^2\right] \Bigg/ \left[\begin{array}{l} \left(\tfrac{(1-\Omega^2)(-\Omega^2+\beta_3\theta_0)}{\beta_2\Omega^2} - \tfrac{\alpha_1\beta_1}{\beta_2} - \alpha_2\Omega^2\right)^2 \\ + \left(\tfrac{\beta_1(1-\Omega^2)+\alpha_1(-\Omega^2+\beta_3\theta_0)}{\beta_2\Omega}\right)^2 \end{array}\right] \\
B_2 &= E\left[\tfrac{\beta_1(1-\Omega^2)+\alpha_1(-\Omega^2+\beta_3\theta_0)}{\beta_2\Omega}\right] \Bigg/ \left[\begin{array}{l} \left(\tfrac{(1-\Omega^2)(-\Omega^2+\beta_3\theta_0)}{\beta_2\Omega^2} - \tfrac{\alpha_1\beta_1}{\beta_2} - \alpha_2\Omega^2\right)^2 \\ + \left(\tfrac{\beta_1(1-\Omega^2)+\alpha_1(-\Omega^2+\beta_3\theta_0)}{\beta_2\Omega}\right)^2 \end{array}\right] \\
A_1 &= \tfrac{1}{\beta_2\Omega^2}\left(B_1(-\Omega^2+\beta_3\theta_0) + \beta_1\Omega B_2\right) \\
A_2 &= \tfrac{1}{\beta_2\Omega^2}\left(B_2(-\Omega^2+\beta_3\theta_0) - \beta_1\Omega B_1\right)
\end{aligned}
\tag{3.17}
$$

We analyse the behaviours of A and B respectively the maximal amplitude of the rod displacement and the angular displacement. These frequency-responses are plotted for different values of the frequency ratio Q between the oscillation pendulum frequency and the frequency ω_0 due to the elastic coefficient k_v. Q has the following expression:

$$Q = \frac{1}{w_0}\sqrt{\frac{g}{l}} \tag{3.18}$$

One finds the resonance and antiresonance phenomena. Figure 3.10 is plotted for $Q = 1.2$. It appear that when the frequency increase 0.0 to 4.0 maximal amplitude A and B increase progressively from a small value to an maximal one, afterward decrease to an another small value where $\Omega = 1.2$, increase ones more for an maximal amplitude and finally decrease to an minimal value. These behaviours are usualy called resonance and antiresonance. The antiresonance appears at $\Omega = 1.2$. From the figure, one finds that the mathematical derivation of the amplitudes is good since there is a good agreement with the numerical results. We have also plotted the frequency response curves for $Q = 1$ and $Q = 0.8$ (see figures 3.11 and 3.12). One finds that the antiresonance peak appear when the frequency Ω is equal to the ratio Q . When the value of the frequency ratio Q increases, the value of Ω where the first and second resonance pick appear increase too.

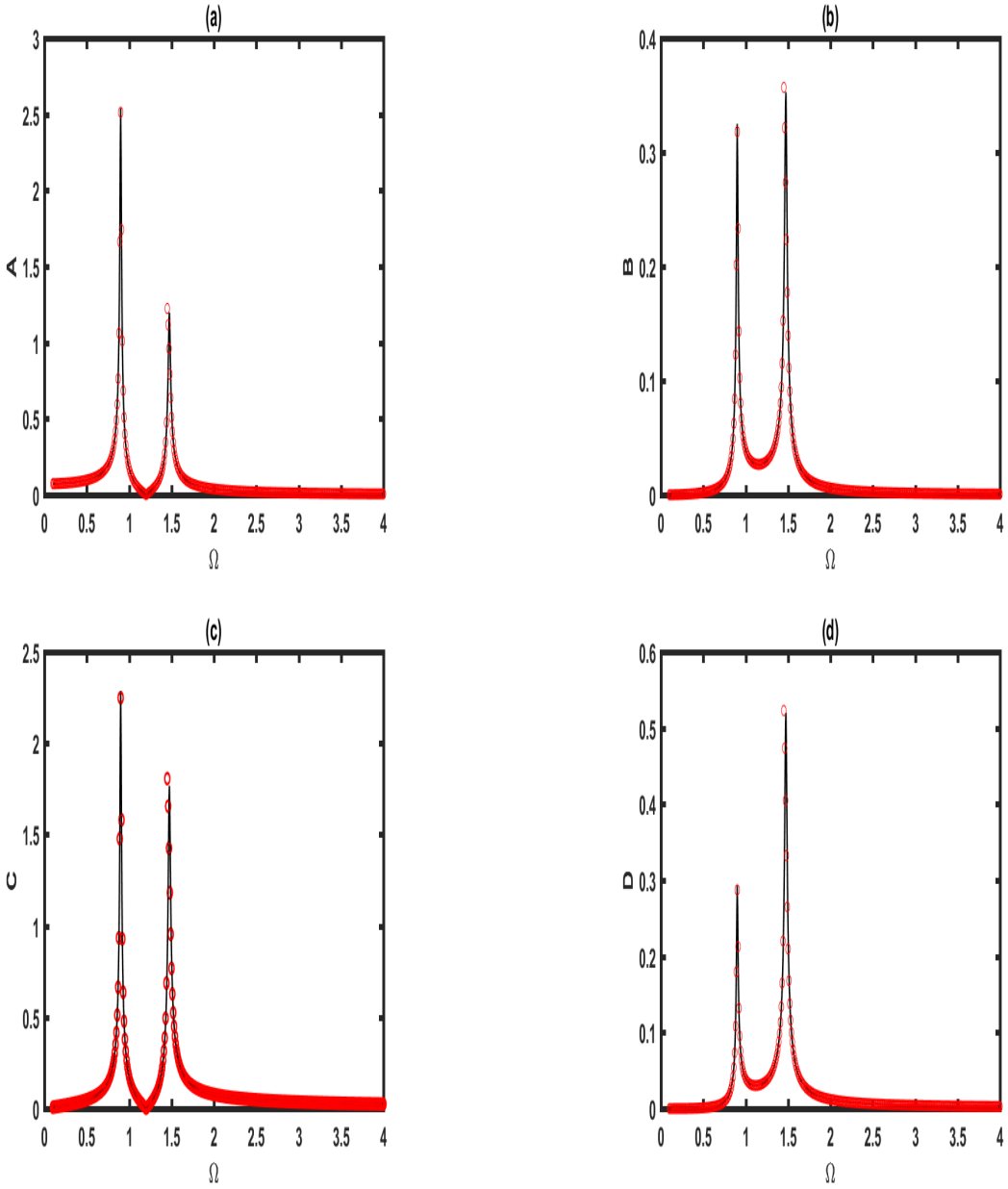

Figure 3.10: Analytical (full line) and numerical (dot line) frequency-response curves: (a) amplitude of the rod displacement;(b) amplitude of the angular displacement; (c) amplitude of the rod velocity; (d) amplitude of the angular velocity. With and $E_0 = 0.07$ and $Q = 1.2$.

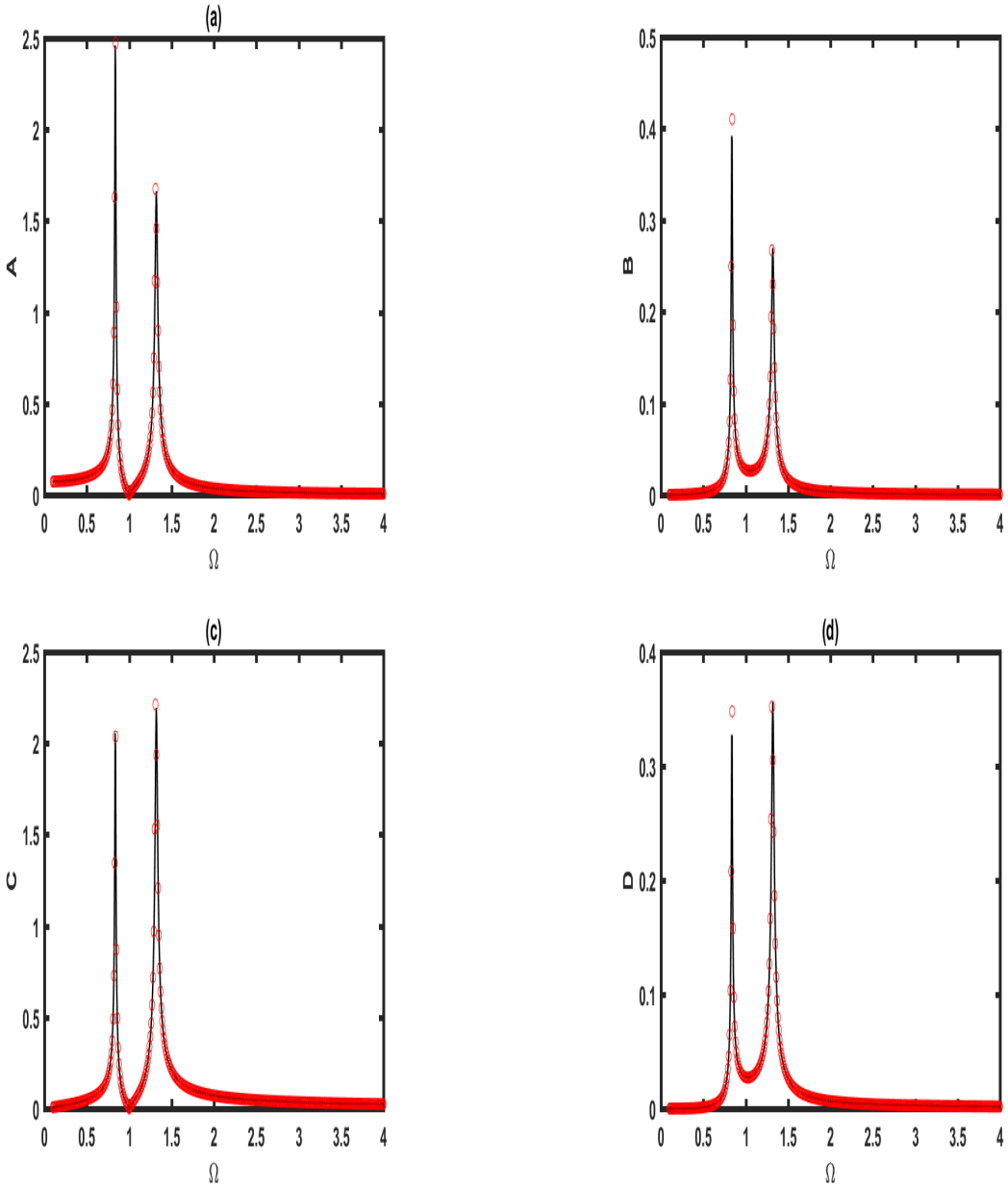

Figure 3.11: Analytical (full line) and numerical (dot line) frequency-response curves: (a) amplitude of the rod displacement;(b) amplitude of the angular displacement; (c) amplitude of the rod velocity; (d) amplitude of the angular velocity. With and $E_0 = 0.07$ and $Q = 1$.

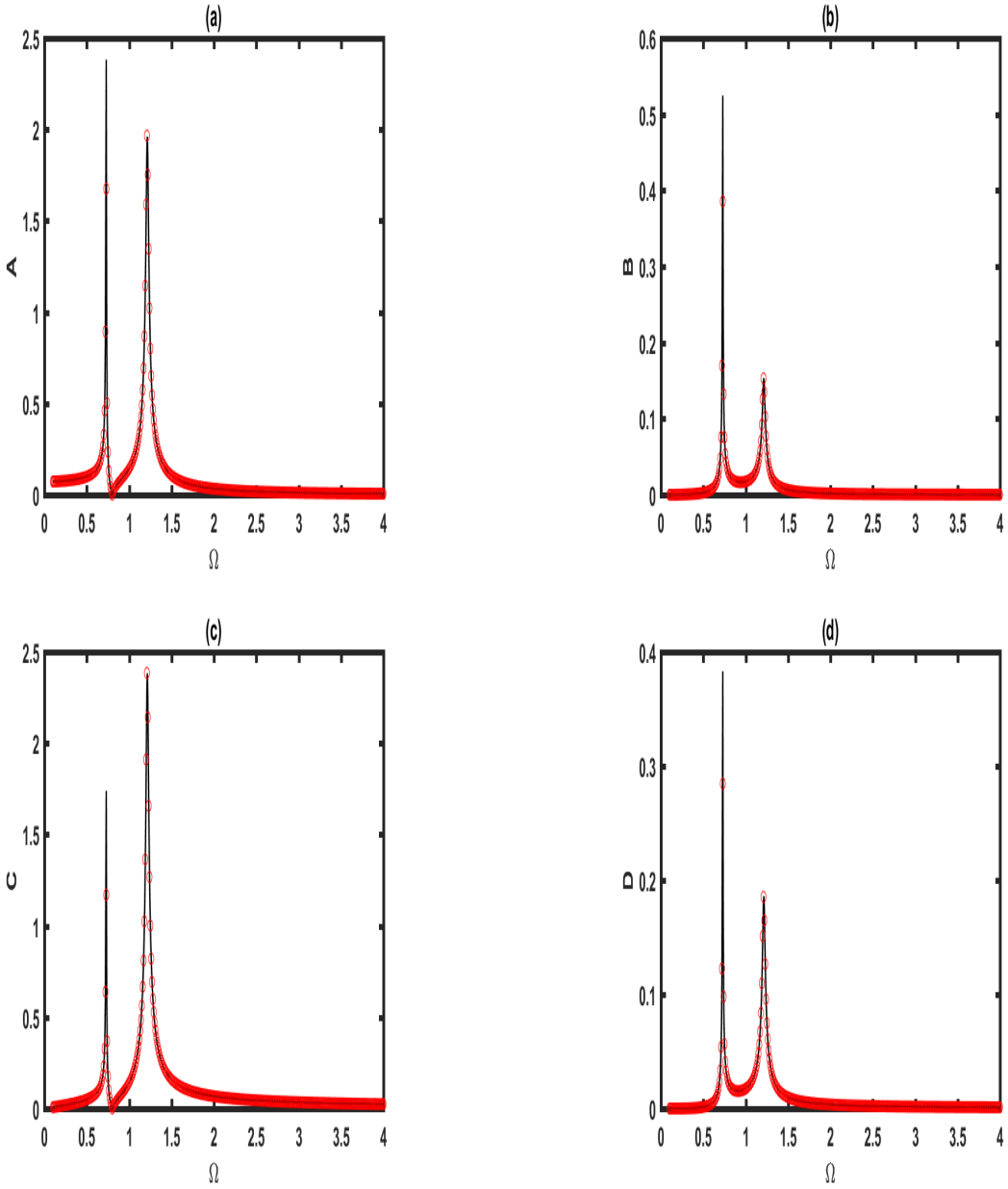

Figure 3.12: Analytical (full line) and numerical (dot line) frequency-response curves: (a) amplitude of the rod displacement;(b) amplitude of the angular displacement; (c) amplitude of the rod velocity; (d) amplitude of the angular velocity. With and $E_0 = 0.07$ and $Q = 0.8$.

b) Case of nonlinear springs

We remind that this case is described by the following equations (2.44):

$$\begin{cases} \ddot{x}_3 + \alpha_1\dot{x}_3 + \left(1 - 2\alpha\left(\frac{1}{\sqrt{a^2+x_3^2}} - 1\right)\right)x_3 + \alpha_2\ddot{y}\cos(\theta_0 y) - \alpha_3\dot{y}^2\sin(\theta_0 y) = E\cos(\Omega\tau) \\ \ddot{y} + \beta_1\dot{y} + \beta_2\ddot{x}_3\cos(\theta_0 y) + \beta_3\sin(\theta_0 y) = 0 \end{cases}$$

In order to obtain mathematically the approximate solutions of these equations, we have considered the case of small and average amplitude of vibrations. The following approximations can thus be used from the Taylor expansion formula:

$$\cos(\theta_0 y) = 1 - \frac{\theta_0^2 y^2}{2}; \sin(\theta_0 y) = \theta_0 y - \frac{\theta_0^3 y^3}{6} \tag{3.19a}$$

$$\left[1 - 2\alpha\left(\frac{1}{\sqrt{a^2+x_3^2}} - 1\right)\right] = \left[1 - 2\alpha\left(\frac{1-a}{a}\right)x_3 + \frac{\alpha}{a^3}x_3^3\right] \tag{3.19b}$$

Replacing (3.19a) and (3.19b) in equations (2.44), one obtains equations (3.20)

$$\ddot{x}_3 + \alpha_2\ddot{y}\left(1 - \frac{\theta_0^2 y^2}{2}\right) = -\left(1 - 2\alpha\left(\frac{1-a}{a}\right)\right)x_3 - \frac{\alpha}{a^3}x_3^3 - \alpha_1\dot{x}_3 + \alpha_3\dot{y}^2\left(\theta_0 y - \frac{\theta_0^3 y^3}{6}\right) + E\cos(\Omega\tau) \tag{3.20a}$$

$$\beta_2\left(1 - \frac{\theta_0^2 y^2}{2}\right)\ddot{x}_3 + \ddot{y} = -\beta_1\dot{y} - \beta_3\left(\theta_0 y - \frac{\theta_0^3 y^3}{6}\right) \tag{3.20b}$$

The approximate solutions for oscillatory states are searched using the harmonic balance scheme which takes

$$x_3 = A\cos(\Omega t - \varphi_1) \tag{3.21a}$$

$$y = B\cos(\Omega t - \varphi_2) \tag{3.21b}$$

The amplitudes A and B satisfy the following algebraic equations:

$$B^2\frac{\left((-\Omega^2+\beta_3\theta_0-\frac{1}{8}\beta_3\theta_0^3B^2)^2+\beta_1^2\Omega^2\right)}{\left(\beta_2\Omega^2-\frac{\beta_2\theta_0^2\Omega^2}{4}B^2\right)^2}\left[\begin{bmatrix}-\Omega^2+\eta+\frac{3\alpha\left((-\Omega^2+\beta_3\theta_0-\frac{1}{8}\beta_3\theta_0^3B^2)^2+\beta_1^2\Omega^2\right)B^2}{4a^3\left(\beta_2\Omega^2-\frac{\beta_2\theta_0^2\Omega^2}{4}B^2\right)^2}- \\ (-\beta_2\Omega^2+\frac{\beta_2\theta_0^2\Omega^2}{4}B^2)(-\Omega^2+\beta_3\theta_0-\frac{1}{8}\beta_3\theta_0^3B^2) \\ \times\frac{(-\alpha_2\Omega^2+\frac{3}{8}\alpha_2\theta_0^2B^2\Omega^2-\frac{\alpha_3\theta_0}{4}B^2\Omega^2+\frac{\alpha_3\theta_0^3}{48}B^4\Omega^2)}{(-\Omega^2+\beta_3\theta_0-\frac{1}{8}\beta_3\theta_0^3B^2)^2+\beta_1^2\Omega^2}\end{bmatrix}^2+\right.$$

$$\left.\begin{bmatrix}\alpha_1+\frac{(-\alpha_2\Omega^2+\frac{3}{8}\alpha_2\theta_0^2B^2\Omega^2-\frac{\alpha_3\theta_0}{4}B^2\Omega^2+\frac{\alpha_3\theta_0^3}{48}B^4\Omega^2)}{(-\Omega^2+\beta_3\theta_0-\frac{1}{8}\beta_3\theta_0^3B^2)^2+\beta_1^2\Omega^2} \\ \times\beta_1\Omega(-\beta_2\Omega^2+\frac{\beta_2\theta_0^2\Omega^2}{4}B^2)\end{bmatrix}^2\right]$$

$$-E^2=0 \tag{3.22a}$$

$$A^2=\frac{\left((-\Omega^2+\beta_3\theta_0-\frac{1}{8}\beta_3\theta_0^3B^2)^2+\beta_1^2\Omega^2\right)}{\left(\beta_2\Omega^2-\frac{\beta_2\theta_0^2\Omega^2}{4}B^2\right)^2}B^2 \tag{3.22b}$$

To check the validity of the mathematical expressions of the oscillations amplitudes, we have also solved numerically the set of equations (2.44) and calculated the amplitude from the discrete data generated by the use of the 4th order Runge- Kutta algorithm. Figure 3.13 presents the variations of the frequency- response for the translational and pendulum oscillations. These frequency-responses are plotted for different values of the frequency ratio Q between the oscillation pendulum frequency and the frequency ω_0 due to the elastic coefficient k_v. One finds the resonance and antiresonance phenomena as well as the hysteresis at the resonance branches. Figure 3.13 is plotted for $Q=1.2$ and the antiresonance appears at $\Omega=1.2$. From the figure, one finds that the mathematical derivation of the amplitudes is good since there is a good agreement with the numerical results. We have also plotted the frequency response curves for $Q=1$ and $Q=0.8$ (see figures 3.14 and 3.15). One finds that the antiresonance peak appear when the frequency Ω is equal to the ratio Q. When the value of the frequency ratio Q decreases, the value of Ω where the first and second resonance pick appear decrease too. The hysteresis curve gradually slopes more to the right and the resonance amplitude of the angular displacement decreases as Q decreases.

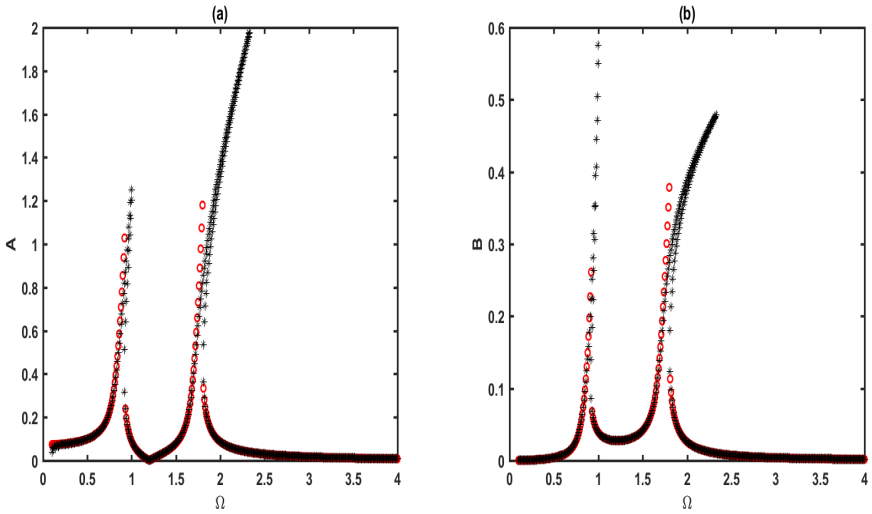

Figure 3.13: Analytical (star line) and numerical (dot line) frequency-response curves: (a) amplitude of the rod displacement, (b) amplitude of the angular displacement with and $E_0 = 0.07$ and $Q = 1.2$.

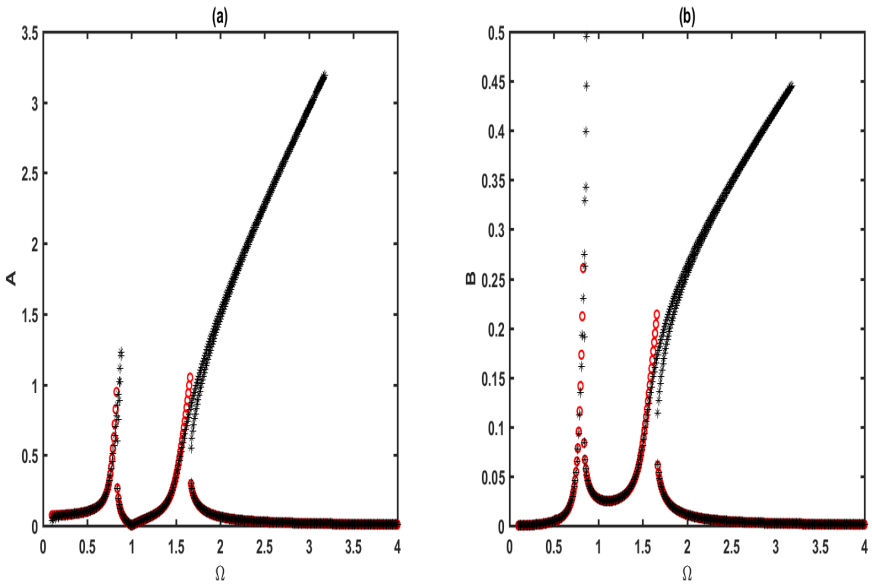

Figure 3.14: Analytical (star line) and numerical (dot line) frequency-response curves: (a) amplitude of the rod displacement, (b) amplitude of the angular displacement with and $E_0 = 0.07$ and $Q = 1$.

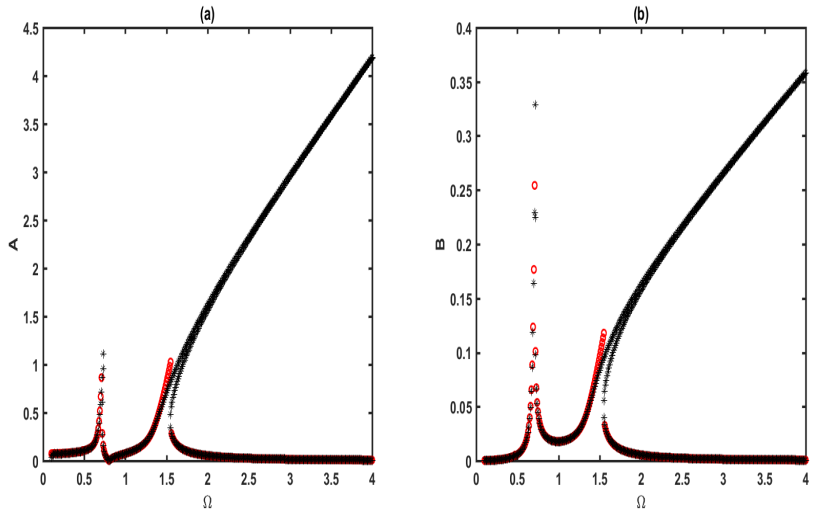

Figure 3.15: Analytical (star line) and numerical (dot line) frequency-response curves: (a) amplitude of the rod displacement, (b) amplitude of the angular displacement with and $E_0 = 0.07$ and $Q = 0.8$.

Figure 3.16 considers the case where the spring is linear $\alpha = 0$. It is plotted for $Q = 1$. One also observed the resonances and antiresonance. There is also an hysteresis branch, but less pronounced as in the case where the spring characteristics is nonlinear.

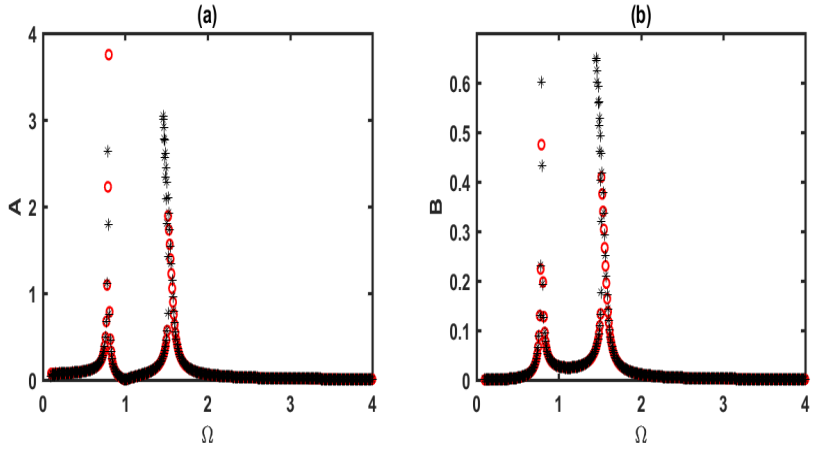

Figure 3.16: Analytical (star line) and numerical (dot line) frequency-response curves: (a) amplitude of the rod displacement, (b) amplitude of the angular displacement with and $E_0 = 0.07$ and $Q = 1$.

We have also analyzed how the nonlinear coefficient α affects the maximal amplitude of oscillations of the translational and pendulum motions. This appears in Figure 3.17 where one finds that the amplitudes descrease when α increases. This descrease is understandable since the increase of α means that the nonlinearity becomes more hard, and consequently the amplitudes of motion become small.

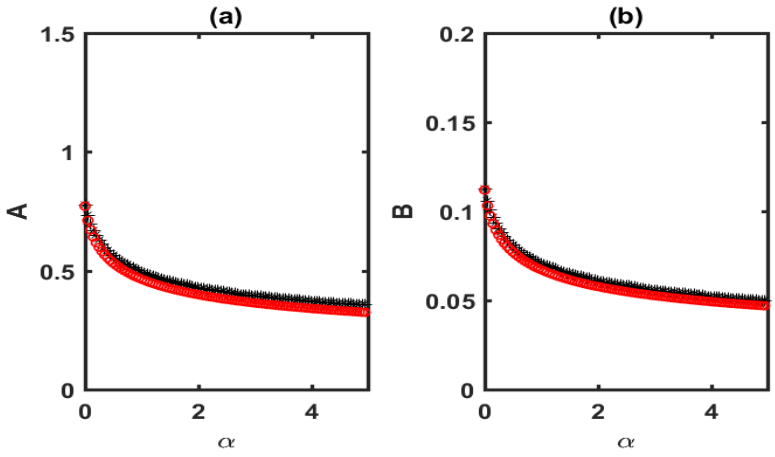

Figure 3.17: Analytical (dot line) and numerical (star line) frequency-response curves: (a) amplitude of the rod displacement, (b) amplitude of the angular displacement with $E_0 = 0.17$, $\Omega = 0.7$ and $Q = 0.8$.

In order to have more information on the dynamical states of the system, bifurcation diagrams have been used. Two control parameters are considered for the bifurcation diagrams: the amplitude E of the voltage source and the ratio α between the constant of the oblique spring and that of the horizontal spring. Q is taken to be equal to 1.
Figure 3.18 presents the bifurcation diagram and the corresponding Lyapunov exponent versus the amplitude of the voltage source. One finds that the behavior of the device shows a period-1T oscillation for $0 \leq E < 1.9$. Chaotic oscillations are obtained for $E \geq 1.9$. These behaviors are confirmed in Figure 3.19 where the corresponding phase potraits are plotted. Figure 3.19 (a) shows a periodic motion and Figure 3.19 (b) chaotic oscillations.

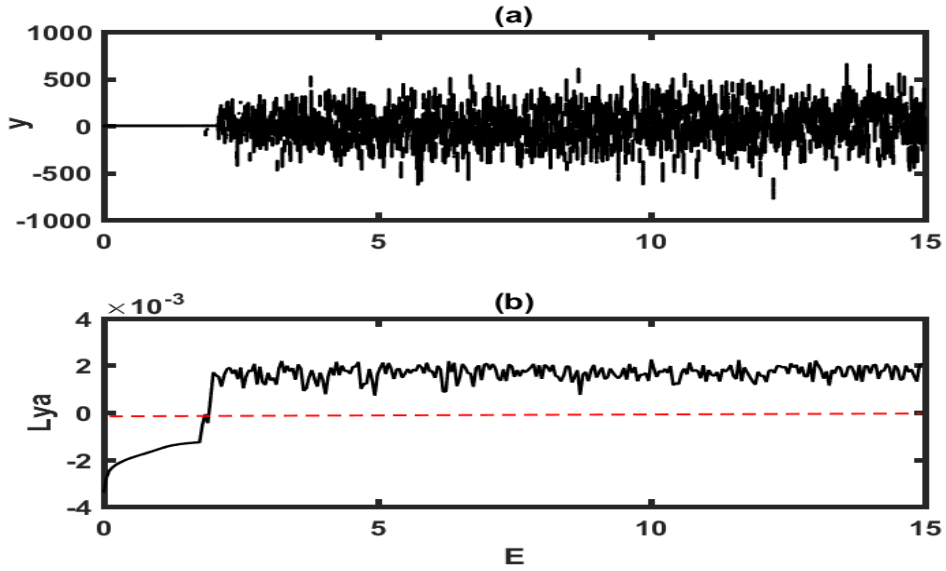

Figure 3.18: (a) Bifurcation diagram, (b) the corresponding Lyapunov exponent, versus the amplitude of the excitation E with the parameters of Tables 1 and $\Omega = 2$ and $Q = 1$.

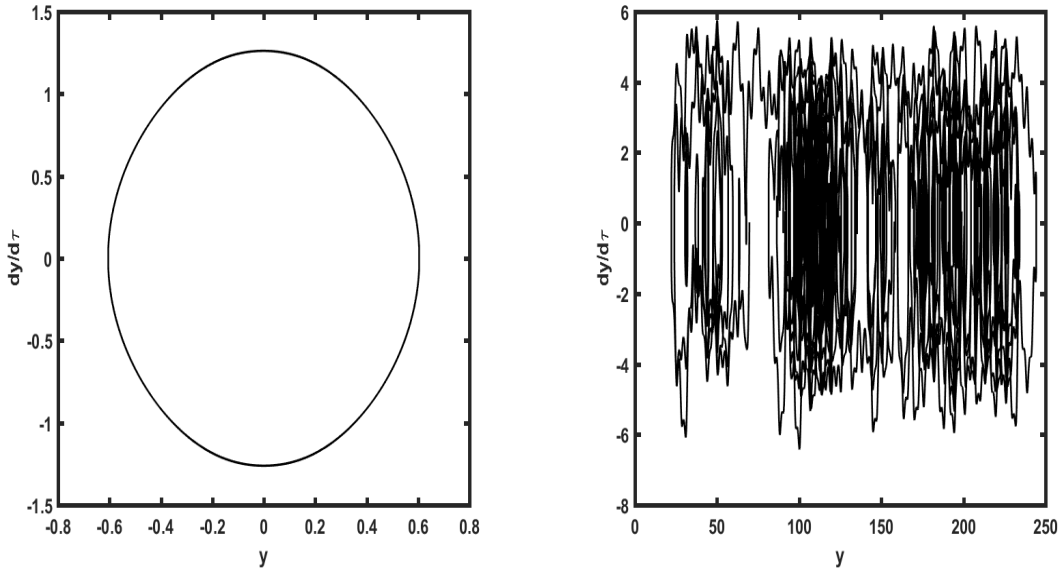

Figure 3.19: Phase portraits obtain with parameter of Figure 3.18 and (a)$E_0 = 2$, (b) $E_0 = 10$.

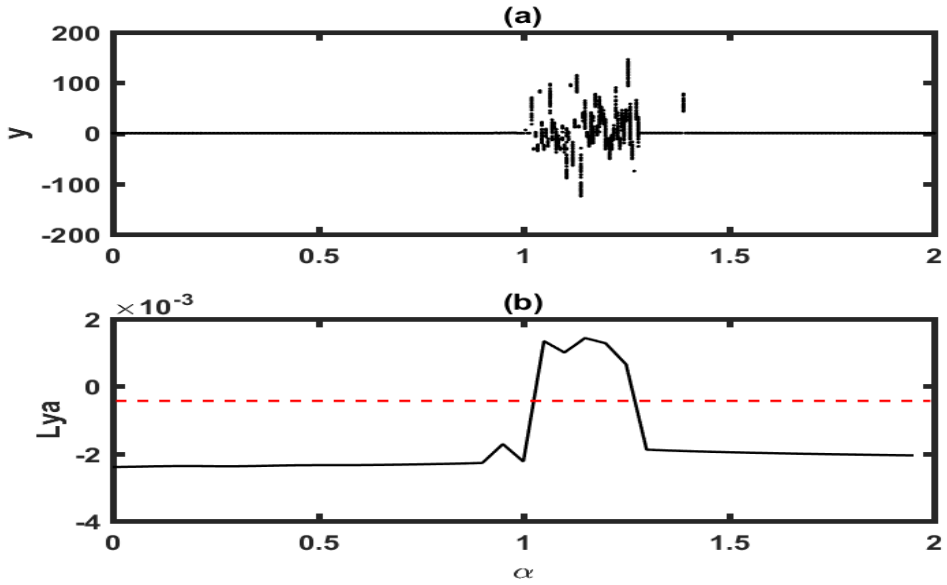

Figure 3.20: (a) Bifurcation diagram, (b) the corresponding Lyapunov exponent, versus the ratio with the parameters of Tables 1, $E_0 = 0.7$, $\Omega = 2$ and $Q = 1$.

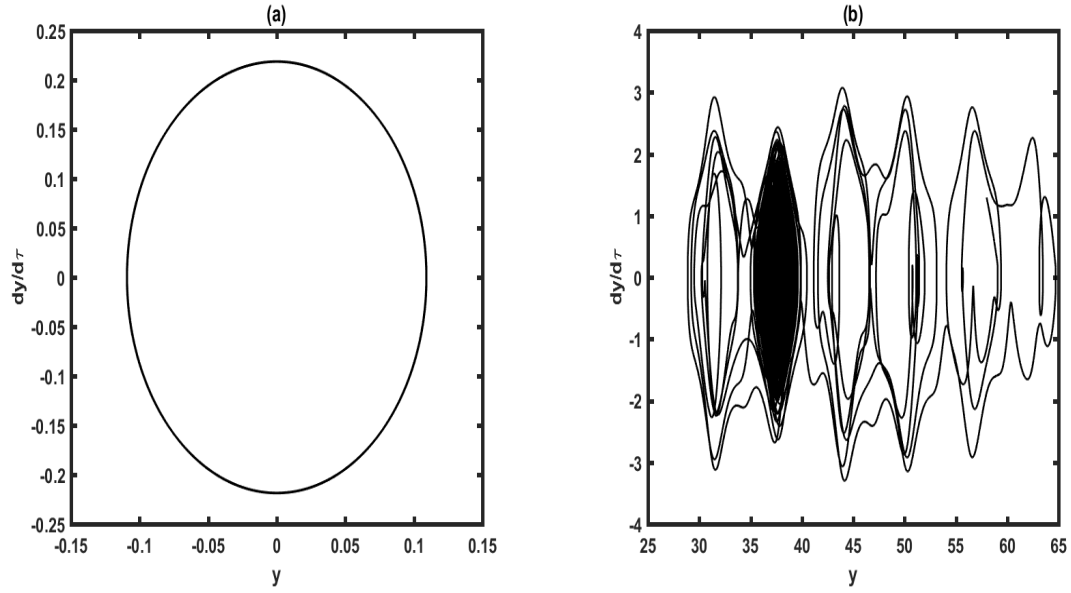

Figure 3.21: Phase portraits obtain with parameter of Figure 3.20 and (a) $\alpha = 0.1$, (b)$\alpha = 1.2$.

In order to find the range of α for which the device exhibits chaos, we present the bifurcation diagram in Figure 3.20(a) and the corresponding variation of the Lyapunov

exponent in Figure 3.20(b) as function of α . One finds that, when $\alpha \in [0,1]\,U\,[1.29,2]$ the device shows period-1T oscillation. For $\alpha \in [1.05,1.28]$ the behavior of the device shows chaotic oscillations. Some phase portraits are plotted in Figure 3.21 to justify the behavior found in figures 3.20. Figure 3.21(a) shows periodic behavior and figure 3.21 (b) chaotic oscillations.

3.4 Conclusion

We have studied the dynamical behaviours of two electromechanical devices combining rotational motion with translational motion. In the case of translational rod and rotational electrical motor presented by section 3.2., in the nonlinear limit, the numerical results show complex dynamical behaviors such as jump phenomenon, periodic motion and chaos. It is seen that when the external excitation amplitude increases, the complexity of the dynamical behaviors increases moving from period-nT oscillations to chaotic oscillations. In presence of the inductance with nonlinear characteristics, it is found that chaotic behaviors appear for larger values of the external excitation than in the case of linear inductance. With the increase of the inductance hysteresis parameter η the behaviour change alternately from chaotic motion to periodic motion and chaotic motions are observed even for very low value of η .

In the case of a driven hybrid translational-pendulum electromechanical system studied in section 3.3, the frequency-response curves show that the rod and angular displacement present resonant and antiresonant points as well as the hysteresis phenomena. When the value of the frequency ratio Q decreases, the resonant hysteresis curve gradually slopes more to the right and the resonance hysteresis amplitude of the angular displacement decreases too. From the bifurcation diagrams, periodic and chaotic oscillations have been

found for appropriate ranges of the amplitude of external voltage and of the spring non-linear coefficient.

The complex behaviors of the first device can find applications in various branches of electromechanical engineering such as boring machine and drilling machine. This device can be also used in home as a mixer in which chaotic oscillations can improve its efficiency while going up and down inside the products to be mixed. The mechanism analyzed in the second work can find applications in the sieving process, but also on actuation processes where one wants two complementary actuators, one being translational while the second is of pendulum type.

GENERAL CONCLUSION

This thesis was motivated by the design of two electromechanical systems having two main particularities. The first one is that they combine rotational and translational motions. The second one is related to the types of nonlinearities used. The first nonlinear component is an inductor whose the current-inductance characteristics shows a highly nonlinear relationship because of the hysteretic iron-core involved. The second nonlinearity is of mechanical nature. It involves the association of three springs, two of which are oblique while one follows the motion direction.

1. Summary of the mains results

Firstly, we have presented a new electromechanical system consisting of an electrical motor carried by a mobile conducting rod (support). We have studied the dynamical behavior of the device in the linear and nonlinear states. Analytical and numerical investigations have been undertaken to present the different dynamical behaviors which can take place in such a complex electromechanical system.

- Assuming small amplitude motion, the nonlinear terms have been linearized to give a set of equations analytically treatable. The mathematical expressions of the oscillations amplitudes have been obtained and the frequency-response curves show that when the power dissipated through the Joule effect is small, the displacement amplitude is high.

- In the nonlinear limit, the numerical results show complex dynamical behaviors such as jump phenomenon, periodic motion and chaos. It is seen that when the external excitation amplitude increases, the complexity of the dynamical behaviors increases moving from period-nT oscillations to chaotic oscillations. In presence of the inductance with nonlinear characteristics, it is found that chaotic behaviors appear for larger values of the external excitation than in the case of linear inductance. With the variation of the inductance hysteresis parameter, the behaviour changes alternately from chaotic motion to periodic motion and chaotic motions are observed even for very low value of the hysteresis parameter.

Secondly, we have considered the dynamical behaviour of an electromechanical system which combines both the rotational motion of a pendulum and the translational motion of a mobile rod on the Laplace's rails. Apart from the intrinsic nonlinearity of the pendulum system, a nonlinear spring component has been added in the mechanical part. Mathematical and numerical investigations have been undertaken to present the different dynamical behaviors which can take place in such a complex electromechanical system. The mathematical expressions of the oscillations amplitudes have been obtained and the frequency-response curves show that the rod and angular displacement present resonant and antiresonant points as well as the hysteresis phenomena. When the value of the frequency ratio Q decreases, the resonant hysteresis curve gradually slopes more to the right and the resonance hysteresis amplitude of the angular displacement decreases too. From the bifurcation diagrams, periodic and chaotic oscillations have been found for appropriate ranges of the amplitude of external voltage and of the spring nonlinear coefficient.

The complex behaviors of the first device can find applications in various branches of electromechanical engineering such as boring machine and drilling machine. This device

can be also used in home as a mixer in which chaotic oscillations can improve its efficiency while going up and down inside the products to be mixed. The mechanism analyzed in the second device can find applications in the sieving process and also on actuation processes where one wants two complementary actuators, one being translational while the second is of pendulum type.

2. Perspectives

In this thesis, some interesting results have been obtained and have opened interesting perspectives for future investigations.

- To complement the results obtained in this thesis for applications purpose, an experimental study of each device must be made where the Laplace's rails could be replaced by two magnet coil in series.
- For the pendulum system, future investigation can concern the case where the pendulum is inverted. The effect of the nonlinear spring on the dynamics of this system will be investigated and a control could be applied to impose the desired dynamics on the system.

Bibliography

Bibliography

[1] W.M. Kuhnert, A. Cammarano and M. Silveira (2021). Synthesis of viscoelastic behavior through electromechanical coupling. *J. Vib. Eng. Technol.* 9:367-379.

[2] B. Nana, S. B Yamgoué, R. Tchitnga and P. Woafo (2017). Dynamics of a pendulum driven by a DC motor and magnetically controlled. *Chaos Solit Frac* 104:18-27.

[3] J.Aditya Khatokar (2021). A study on improved methods in micro-electromechanical systems technology. *Materials today: Proceedings* 43:3784-3790.

[4] C. He, S. Li, K. Shao, W. Meng and H. Zhao (2021). Robust Iterative Feedback Tuning Control of a Permanent Magnet Synchronous Motor with Repetitive Constraints: A UdwadiaKalaba Approach.*J. Vib. Eng. Technol.* 90: 3434-3446.

[5] F. D. Tcheutchoua and P. Woafo (2013). Generation of complex phenomena in a simple electromechanical system using the feedback control. *Commun Nonlinear Sci Numer Simulat.* 18:209-218.

[6] L. Zhe (1995). Chaotic vibration sieve. *Mech. Mach. Theory* 30:608-613.

[7] K.T. Chau, S. Ye, Y. Gao (2004). Application to chaotic-motions motors to industrial mixing processes. *IEEE* 207: 513-530.

[8] F. R. Tsapla and P. Woafo (2016). Chaos in a new bistable rotating electromechanical system. *Chaos, Solit. Frac.* 93:48-57.

[9] A. M. Wahrhaftig, R. M. L. R. F. Brasil, T. B. Groba, J. M. Balthazar and L.S.M.S.C. Nascimento. (2020). Resonance of a rotary machine support beam considering geometric stiffness. *J. Theor. Appl. Mech.*58:1023-1035.

[10] T. Gerach, S. Schuler, L. Lindner and J. Frohlich. (2021). Electromechanical whole-heart digital twins: A fully coupled multi-physics approach. *Mathematics* 9:1247.

[11] A. A. Korobov, S. V. Frolov, N. E. Aliyev and I.E. Rodionova (2020). Dual-contoured model of cardiovascular system regulation. *Journal of Physics conference series*1553: 012006.

[12] F. D. Tcheutchoua, P. Woafo (2011). Dynamics of an electromechanical system with angular and ferroresonant non linearities. *J. Sound Vib.*133:1-7.

[13] J. M. Ottino, F. J. Muzzio, M. Tjahjadi (1992). Chaos, symmetry, and self-similarity: exploiting order and disorder in mixing process. *Science* 257:754-760.

[14] C. A. Kitio Kwuimy and P. Woafo (2010). Experimental realization and simulations a self-sustained Macro ElectroMechanical System. *Mech. Res. Commun.* 37: 106 - 110.

[15] Z. Wang, K. T. Chau (2008). Anti-control of chaos of a permanent magnet DC motor system for vibratory compactors. *Chaos Solit Frac.* 36:694-708.

[16] A. I. Ismael (2021). A new pendulum motion with a suspended point near infinity. *Sci Rep* 11:13199.

[17] A. D. Myers, R. T. Joshua, D. Petrushenko and F. A. Khasawneh (2020). Low-cost double pendulum for high-quality data collection with open-source video tracking and analysis. *HardwareX* 8:e00138.

[18] M. P. Calvo and J. M. Sanz-Serma (2010). Carring an inverted pendulum on a bumpy road. *J Discret Contin. Dyn. Syst. -B* 14: 429-438.

[19] D.B. Marghitu and J. Zhao (2020).Impact of a multiple pendulum with a non-linear contact force. *Mathematics* 8:1202.

[20] A. K. Notué, P. R. Nwagoum and P. Woafo (2017). An electromechanical pendulum robot arm in action: Dynamics and control. *Shock vib.* 2017:1-13.

[21] J.B. Mogo and P. Woafo (2007). Dynamics of a Nonlinear Electromechanical Device with a Pendulum Arm. *J.Comput. Nonl. Dyn.* 2:374-378.

[22] D. Sequeira, J. Little and B.P. Mann (2019). Investigating threshold escape behavior for the gimballed horizontal pendulum system.*J. Sound Vib.* 450:47-60.

[23] N. Han and Q. Cao (2017). Rotating pendulum with smooth and discontinuous dynamics. *Int. J. Mech.Sci.* 127:91-102.

[24] M. E. Semenov, A. M Solovyov and P. A. Meleshenko (2021). Stabilization of the coupled inverted pendula: from discrete to continuous case. *J. Vib. control* 27: 1-2.

[25] B. lui, B. Zhan, C. Zhang and L.Yang (2020). Research on visual control system of inverted pendulum based on pixel displacement. *J. Phys. Conf. Ser.* 1550:062006.

[26] H. Simo, U. S. Domguia, J. K. Dutt and P. Woafo (2019). Analysis of vibration of pendulum arm under bursting oscillation excitation.*Pramana- J. Phys.* 92:1-11.

[27] Y. Kraftmakher (2007). Experiments with a magnetically controlled pendulum. *Eur. J. Phys.* 28:1007.

[28] Khalid El Rifai, G. Haller and A.N. Bajaj (2007) .Global dynamics of an autoparametric spring-mass-pendulum system. *Nonlinear Dyn.*49:105-116.

[29] M. C. Nuci (2017). The nonlinear pendulum always oscillates.*J.Nonlinear Math.Phys.* 24:1146-156.

[30] X.Chen, Z. Jing and X. Fu (2015). Chaos control in a pendulum system with excitations, Discret Contin. *Dyn. Syst.-B* 20:373-383.

[31] J.B. Mogo and P. Woafo (2011). Dynamics of a cantilever arm actuated by a nonlinear electrical circuit. *Nonl. Dynamics* 63:807-818.

[32] A. Nalin, Chaturvedi, Taeyoung Lee, M. Leok and N.H. McClamroch (2011). Nonlinear Dynamics of the 3D Pendulum. *J Nonlinear Sci.* 21:3-32.

[33] T. Sze-Hon, D. Hazem (2015). Rotating a pendulum with an electromechanical exitation. *Int. J. Nonlinear Mech.* 70:73-83.

[34] C.A. Kitio Kwuimy and P. Woafo (2008), Dynamics, chaos and synchronization of self-sustained electromechanical systems with clamped-free flexible arm. *Nonl. Dynamics* 53:201-203.

[35] A.M. Tusset, V. Piccirillo, A.M. Bueno, J.M. Balthazar, D. Sado, J.L.P. Felix and R.M.L.R. Bresil (2015). Chaos control and sensitivity analysis of a double pendulum arm excited by an RLC circuit based nonlinear shaker. *Journal of Vibration and Control* 1-17.

[36] T. Sze-Hong, C. Kok-Hong, W. Ko-Choong and D. Hazem (2015). Rotating a pendulum with an electromechanical excitation. Int. J. Non-linear Mech. 70:73-83.*Int J Adv Manuf Technol* 36: 516-524.

[37] M. Monir (2018). Analyzing and designing control system for an inverted pendulum on a car. *Eu. Sci. J.* 14(6):387.

[38] D. Komali, D. Smritilekha, B. Prabha and V.V.S. Sasank (2020). Enhancement for the position of inverted pendulum using linear quadratic regulator based fuzzy system. *Eur. J. Mol. Clin. Med.* 7(4):757-765.

[39] A. A Kolesnikov (2000). Modern applied control theory: new classes of technical systems regulators. *TSURE press, Taganrog.*

[40] B. Nana, S.B. Yamgoue and P. Woafo (2021). Dynamics of an autonomous electromechanical pendulum-like system with experimentation. *Chaos Solit. Fractals* 152:111475.

[41] E. Grassl and F.Schmidt (2006). Energy-autonomous electromechanical wireless switch.*Patent US 7,019,241 B2.*

[42] H. Simo and P. Woafo (2011). Bursting oscillations in electromechanical systems.*Mech. Res. Commun* 38: 537-541.

[43] J. Cai and M. Lin (2010), finite time of non-autonomous chaotic systems with unknown parameters. *international Workshop on Chaos-Fractal Theories and Applications* 2010:8-13.

[44] X. M. Huang, C. Zorman and M. L. Roukes (2002). Nanoelectromechanical systems. *Nature (London)* 421:496.

[45] M. L. Roukes (1999). Yoctocalorimetry: Phonon Counting in Nanostructures. *Physica B: Condensed Matter* 1:263-264.

[46] K. L. Ekinci, X. M. H. Huang and M. L. Roukes (2002). Ultrasensitive nanoelectromechanical mass detection. *Appl. Phys. Lett.* 84(22):4469-4471.

[47] V. Sazonova, Y. Yaish, H. Ustunel, D. Roundy , T. A. Arias, Mc Euen PL (2004). A tunable carbon nanotube electromechanical oscillator. *Nature* 431:284-287.

[48] M. A. Seyed, J. H. Boske and N. Behdad (2016). Macro-Electro-Mechanical systems(MAEMS) based concept for microwave beam steering in reflectarry antennas. *Journal of Apllied Physics*, 120: 054901.

[49] C. A. Kitio Kwuimy and P.Woafo (2010). Experimental bifurcations and chaos in a modified self-sustained macro electromechanical system. *Journal of Sound and Vibration* 329:3137-3148.

[50] B. H. Sonfack, B. R. Nana and P. Woafo (2020). Isolation performance of a quasi-zero stiffness isolator in vibration isolation of a multi-span continuous beam bridge under pier base vibrating. *Nonlinear Dyn.* 100:125-141.

[51] A. Notué Kadjie and P. Woafo (2014). Effect of springs on a pendulum electromechanical energy harvester. *Theor. Appl. Mech. Lett* 4:2-7.

[52] G. S. Mbouna Ngueuteu , R. Yamapi and P. Woafo (2008). Effects of higher nonlinearity on the dynamics and synchronization of two coupled electromechanical devices. *Communications in Nonlinear Science and Numerical Simulation* 13:1213-1240.

[53] P. Oksasoglu and D. Vavriv (1994). Interaction of low- and high-frequency oscillations in a nonlinearrlc circuit. *IEEE Transactions on Circuits and Systems I: Fundamental Theory and Applications* 41(10):669-672.

[54] B. Nana, S. B. Yamgoué, I. Kemajou, R. Tchitnga and P. Woafo (2018). Dynamics of a RLC series circuit with hysteretic iron-core inductor. *Chaos Solit. Frac.* 106:184-921.

[55] D. O. Tcheutchoua Fossi (2011). Sieving Devices based on Nonlinear Dynamics of Electromechanical Systems with Rotary Electric Actuator: Theory and Experiment. *Ph.D. Thesis, Faculty of Science, University of Yaounde 1, Cameroon.*

[56] R. Tsapla Fotsa (2017). Rotating electromechanical systems with bistable potential, histeretic iron-core inductor and delay. *Ph.D. Thesis, Faculty of Science, University of Yaounde 1, Cameroon.*

[57] A. Carrella (2008). Passive Vibration Isolators with High-Static-Low-Dynamic-Stiffness. *Ph.D. thesis, University of Southampton, Institute of Sound and Vibration Research.*

[58] A. Carrella, M.J. Brennan, T.P. Waters (2007). Static analysis of a passive vibration isolator with quasi-zero-stiffness characteristic. *J. Sound Vib.* 301:678-689.

[59] Cobelli C, Renard E and Kovatchev B, Artificial Pancreas: Past, Present, Future, D. Xu, Y. Zhang, J. Zhou, J. Lou (2014).

On the analytical and experimental assessment of the performance of a quasi-zerostiffness isolator. *J. Vib. Control* 20:2314-2325.

[60] S.E. Lyshevski (2008). Electromechanical Systems and Devices. *CRC Press.*

[61] F. Kreith, and D.Y. Goswami (2005). The mechanical engineering handbook series. *CRC Press, New York.*

[62] A. Notué Kadjie, I. Kemajou and Paul Woafo (2018). Control of an electromechanical pendulum subjected to impulsive disturbances using the Melnikov theory approach. *Journal of Mechanical Science and Technology* 32(2):865-874.

[63] B.Nana and all (2018). Nonlinear dynamics of a sinusoidally driven lever in repulsive magnetic fields. *Nonlinear Dyn* 91:55-66.

[64] R. F. Kouam Tagne, R. Tsapla Fotsa and P. Woafo (2021). Dynamic of a DC motor-driving arm with a circular periodic Potential and DC/AC voltage input.*Int J Bifurcat Chaos* 31:2150178

[65] R. Yamapi and P. Woafo (2005). Dynamics and synchronization of coupled self-sustained electromechanical devices. *Journal of Sound and Vibration* 285:1151-1170.

[66] D. O. Tcheutchoua Fossi and P. Woafo (2010). Dynamical behaviors of a plate activated by an induction motor. *Journal of Sound and Vibration* 329: 3507-3519.

[67] I. Siradjuddin and al (2018). Stabilising a cart inverted pendulum with an augmented PID control scheme. *MATEC Web of Conferences* 197: 11013.

[68] C. Hayashi (1964). Nonlinear Oscillations in Physical Systems. *New York : McGraw-Hill* 392.

[69] A. H. Nayfeh and D. T. Mook (1979). *Nonlinear oscillations. Wiley.*

[70] P. Frolkovic (1990). *Numerical recipes: The art of scientific computing* 19:297-299.

[71] W. H. Press, S. A. Teukolsky, W. T. Vetterling and B. P. Flannery (2007). Numerical Recipes: The Art of Scientific Computing. *Cambridge University Press, New York.*

[72] D. R. J. Chillingworth and P. Glendinning (1997). Stability, Instability and Chaos. *Cambridge Press.*

[73] J. E. Ott (2002), Chaos in Dynamical Systems. Cambridge. *Cambridge University Press*.

[74] L. Yan, and X. Gong (2018). Experimental study of vibration isolation characteristics of a geometric anti-spring isolator. *App Sci* 711: 1-20.

List of publications

1- **N. D. Ngatcha Tanly**, R. Tsapla Fotsa and P. Woafo (2022). Complex Dynamics of a Mechanical Mechanism Combining Translational and Rotational Motions. *Journal of Vibration Engineering and Technologies* 10: 1753-1764.

Journal of Vibration Engineering & Technologies
https://doi.org/10.1007/s42417-022-00481-4

ORIGINAL PAPER

Complex Dynamics of a Mechanical Mechanism Combining Translational and Rotational Motions

N. D. Ngatcha Tanly[1] · R. Tsapla Fotsa[2] · P. Woafo[1]

Received: 8 October 2021 / Revised: 16 March 2022 / Accepted: 18 March 2022

Abstract

Purpose In this paper, the dynamics of a mechanical mechanism, which combines the rotational motion of a motor and the translational motion of a plate carrying the motor through Laplace's rails is considered. The attention is focussed on the effects of the nonlinear spring and the hysteretic iron-core inductor introduced in the mechanical and electrical parts, respectively.

Methods The modelling of the system is conducted leading to nonlinear differential equations. These equations are solved both analytically and numerically using the harmonic balance method and the fourth-order Runge–Kutta method. As software used for conducting simulations, FORTRAN 95 version PLATO is used for numerical simulation and MATLAB for plotting curves using the data generated from FORTRAN simulations.

Results and Conclusion The dynamical study, based on time traces, phase portraits and bifurcation diagrams, shows that the device exhibits behaviors like jump amplitude phenomenon, hysteresis phenomenon, periodic and chaotic oscillations. The mechanism can be useful for several tasks such as drilling and boring.

Keywords Laplace rail · Motor · Nonlinear spring · Hysteretic iron-core inductor · Chaos

Introduction

In recent years, many efforts have been focused on the development and improvement of electromechanical systems (EMS) [1–7]. Due to their various configurations, EMS are used in a variety of applications in industries and at home. At home, EMS are used as machine tools for some laborious tasks such as mixing and sieving processes [3, 5, 7]. In these EMS, nonlinear dynamics can result as the consequence of inherent or introduced nonlinear components. In the modelling, nonlinear terms can arise from a mechanical part (material, geometric or inertial nonlinearities), from an electrical circuit (nonlinear self, nonlinear condenser, nonlinear resistance) and from the coupling (coupling between the electromagnets, saturation, hysteresis, nonlinear magnetic force, time delay). This leads to complex dynamical behaviors such as the jump, the hysteresis, subharmonic and superharmonic oscillations, frequency division or multiplication, multistability, grazing, switching, quasi-periodicity and chaos. Some of these behaviors resulting from nonlinear dynamics can improve the processes in which the electromechanical systems are engaged such as industrial mixing processes [8], industrial shaking processes [9] and monitoring compaction [10, 11].

Almost all of the studies on EMS have paid attention either on EMS with only translational motion or on EMS with only rotational motions. But, there are industrial automation, domestic appliances and even medical tasks where the electromechanical systems actions required both rotation and translation. This might for instance be the case of some mixers which may translate and rotate during the mixing processes to cover the whole space occupied by the products to be mixed. Another application of interest is an electromechanical perforator which has many applications in

✉ R. Tsapla Fotsa
rtsapla@yahoo.com

[1] Laboratory of Modelling and Simulation in Engineering, Biomimetics and Prototypes, Faculty of Science, University of Yaoundé I, P.O. Box 812, Yaoundé, Cameroon

[2] Mechanical Engineering Department, College of Technology, University of Buea, P.O.Box 63, Buea, South West Region, Republic of Cameroon

Published online: 06 April 2022

mechanical and civil engineering (for instance for the digging of wells for water, gas or petrol). As a research contribution, this paper presents a new electromechanical device which undergoes both rotation and translation movement. One of the objective of this paper is to design a new electromechanical device which is able to perform both rotational and translational motion. Same as it has been demonstrated that nonlinear dynamical behaviors present some benefits in increasing the efficiency of some activities, one can expect that mechanisms delivering combined complex rotational and translational motions can improve the efficiency while performing the targeted tasks. In the same line, the second objective of this paper is to generate complex behaviours in the dynamics of the designed electromechanical system.

Thus, this work aims to design and study the dynamics of a new electromechanical mechanism which undergoes both translation and rotation. To generate nonlinear dynamical behaviors, two nonlinear components are inserted in the system. A hysteretic iron-core inductor [12] where the inductance is a function of the electric current is introduced in the electric part. In the mechanical part, we insert a nonlinear spring mechanism which was recently used for vibration control and termed as quasi-zero stiffness vibration mechanism [13–16]. The structure of the work is as follows: the next section deals with the materials and methods. The subsequent section deals with the results and discussion. The final section concludes the paper.

Materials and Methods

Description of the Designed Electromechanical System

The electromechanical device represented in Fig. 1 consists of an electrical motor (inductance L_2 and internal winding resistor R_2) carried by a plate which is fixed to a mobile and conducting rod. Two parallel and straight conducting rails of negligible resistance handle both ends of the mobile rod. These rails are linked to their ends by a resistor R, an inductor L, all connected in series with a sinusoidal voltage source. The mobile rod is free to move along the rails due to the effect of the Laplace's force. The whole system is immerged in a magnetic field $\vec{B}$. A special spring mechanism is fixed to the plate carrying the motor. This spring mechanism consists of an horizontal spring with linear stiffness k_v connected at the point P to two other linear springs of identical stiffness k_0 and initial length l_0 mounted so that during the motion, they occupy oblique configuration. The current, delivered by the generator flows through the two rails, the mobile rod and the motor. Most of the studies so far undertaken do not consider such a hybrid motion mechanism which can be found or introduced in new equipment, for instance boring and drilling machines with automatically moving parts. It can also be inserted in mixers and improve its efficiency while autonomously going up and down inside the products to be mixed in a regular or chaotic manner.

Nonlinear Components

Considering the device presented in Fig. 1, the inductor L and the spring system are the nonlinear components.

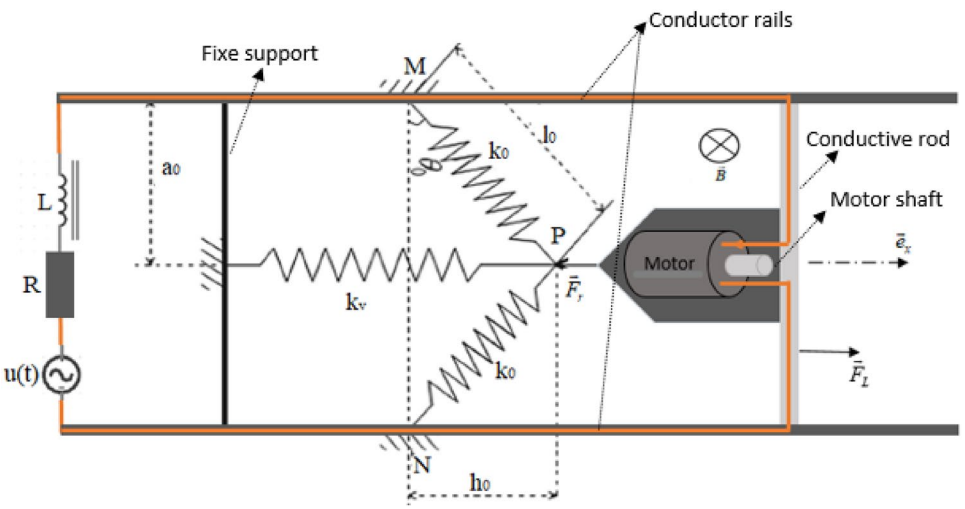

Fig. 1 Coupled system made of rotary motor and mobile translating support

The following subsections will present their mathematical expressions.

Inductor

Nana et al. in [12] demonstrated experimentally that under some conditions, the inductance of an inductor with a magnetic core can depend on the current and has the following mathematical expression:

$$L = \frac{\mu_0 N^2 A}{l} + \frac{B_s NA}{i} \tanh\left(\frac{\alpha N i}{2l} - \frac{\delta}{2}\right) \tag{1}$$

with $\delta = \beta \text{sign}\left(\frac{di}{dt}\right)$,

B_s is the saturation flux density. A and l are, respectively, the cross-sectional area and the average length of the magnetic material. N is the number of turns, μ_0 is the magnetic permeability of the free space, i is the current through the winding, α and β are two constant parameters. As demonstrated in [12], neglecting the parameter δ has no significant effect on the behavior of the circuit. Thus, to simplify the analysis during this work, the parameter δ will be taken equal to zero.

Spring with Nonlinear Response

The schematic representation of the spring force is displayed in Fig. 2.

As indicated above, the spring system comprises a longitudinal spring with linear stiffness k_v which is connected at point P with two linear springs with identical stiffness k_0 and initial length l_0 mounted obliquely. The two springs are initially inclined with a slope of angle θ_0 from the horizontal plane and hinged at points M and N, respectively. The loading point P is initially located at height h_0 above the points M, N and at horizontal distance a_0 apart from these points. The elastic force f can be written as it was given in [12]:

$$f = k_v X - 2k_0 X\left(\frac{l_0}{\sqrt{a_0^2 + X^2}} - 1\right) + k_v h_0. \tag{2}$$

Let us consider in Fig. 1 that the initial position of the system is taken when the oblique springs are transversal to the longitudinal spring. Then the elastic force becomes

$$f = k_v X - 2k_0 X\left(\frac{l_0}{\sqrt{a_0^2 + X^2}} - 1\right). \tag{3}$$

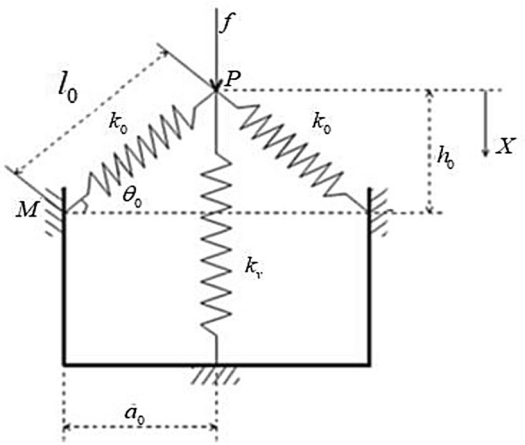

Fig. 2 Schematic representation of the spring system

System Modeling

Using the Kirchhoff's voltage law and the Newton's second law of dynamics for rotary and translational motions and taking into account the Laplace force, the electromechanical equations of the device are as follows:

$$\begin{cases} \left(L_0\left((1-\eta) + \frac{2\eta}{1+\cosh\left(\frac{i}{i_0}\right)}\right) + L_2\right)\frac{di}{dt} + (R+R_2)i + Bl_r\frac{dX}{dt} + K_E\frac{d\theta}{dt} = u(t) \\ M\frac{d^2X}{dt^2} + \lambda\frac{dX}{dt} + k_v X - 2k_0 X\left(\frac{l_0}{\sqrt{a_0^2+X^2}} - 1\right) - Bil_r = 0 \\ J_r\frac{d^2\theta}{dt^2} + c_v\frac{d\theta}{dt} - K_T i = 0, \end{cases} \tag{4}$$

where $u(t)$ is the external excitation source considered as sinusoidal ($u(t) = e_0\cos(\omega t)$),t is the time, X the translational displacement of the rod, θ is the rotor angular displacement.

Table 1 Values of the electrical components in the circuit

Parameter	Notation	Value	Unit
Inductance	L_0	323.18×10^{-3}	H
Resistance	R	5	Ω

Table 2 Values of the motor parameters

Height of the rotor	h	9.85×10^{-2}	m
Diameter of the rotor	D	8.12×10^{-2}	m
Magnetic field intensity	B	0.73	T
Relative permeability	μ_r	985	
Thickness of the winding	l_g	5×10^{-3}	m
Resistivity of the wire	φ	1.72×10^{-8}	Ω m
Diameter of the wire in the winding	d	0.15×10^{-3}	m
Number of turns	N	20	
Rotor inertia moment	J_r	9.5×10^{-7}	Kg m^2
Back electromotive force constant	K_E	2.8×10^{-5}	V s/rad
Torque constant	K_T	2.8×10^{-5}	N m/A
Viscous friction coefficient	C_v	0.2×10^{-3}	N s
Mass of the motor, the plate and rod	M	0.068	Kg

Table 3 Values of the spring constants, lengths and that of the rails

Horizontal sprint stiffness	k_v	10	N/m
Oblique sprint stiffness	k_0	9	N/m
Initial length of the oblique springs	l_0	0.1	m
Distance between the two rails	l_r	0.134	m
Viscous damping	λ	0.4×10^{-2}	N s/m
The middle distance between the two rails	a_0	0.067	m

Table 4 Parameter of the nonlinear inductance

Cross sectional area	A	176.71	mm^2
Saturation flux density	B_s	130×10^{-3}	T
Number of turns	N	1000	
Parameter	α	88.23×10^{-4}	m/A
Parameter	β	88.42×10^{-2}	

The parameters η, L_2 and R have the following expressions:

$$\eta=\frac{\beta_s\alpha}{2\mu_0+\beta_s\alpha};L_2=\frac{\mu_0\mu_r N^2hD}{l_g};R=\frac{8\varphi(h+D)N}{\pi d^2},$$

μ_r is the relative permeability of the rotor, l_g is the thickness of the winding, φ and d are, respectively the resistivity and diameter of the wire used in the winding, N is the number of turns, h and D are respectively the height and diameter of the rotor, μ_0 is the permeability of vacuum.

Values of the Parameters

Tables 1, 2, 3 and 4 give the values of the electrical and mechanical components of the systems. For the electrical circuits, the values come from the experimental work conducted by Nana et al. [17]. For the mechanical systems, we have considered values of DC motors and the physical dimensions are fixed by us. For the nonlinear spring system, it has been used for several investigations both for theoretical and experimental investigations (see [13, 18]).

Dimensionless Form of the Equations

The following dimensionless quantities are used: $x_1=\frac{i}{i_0}$, $x_3=\frac{X}{l_0}$, $y=\frac{\theta}{\theta_0}$, $t=\frac{\tau}{w_0}$,

where i_0 and θ_0 are, respectively, the normalization current and angular displacement. Let us consider $x_4=\frac{dx_3}{d\tau}$ and $z=\frac{dy}{d\tau}$ respectively as the translational and angular velocity of the rod.

Linear Case

In the linear case, it is assumed that the hysteretic inductor inductance is equal to $L_0(\eta=0)$, and the two oblique springs are absent $(k_0=0)$. In this case, the dimensionless equations describing the dynamics of the system are as follows:

$$\begin{cases}\dot{x}_1+\alpha_1x_1+\alpha_2\dot{x}_3+\alpha_3\dot{y}=E_0\cos(\Omega\tau)\\ \ddot{x}_3+\beta_1\dot{x}_3+x_3-\beta_2x_1=0\\ \ddot{y}+\gamma_1\dot{y}-\gamma_2x_1=0\end{cases}\tag{5}$$

with the following rescaling

$$\Omega=\frac{w}{w_0};w_0=\sqrt{\frac{k_v}{M}};\alpha_1=\frac{(R+R_2)}{(L_0+L_2)w_0};\alpha_2=\frac{Bl_rx_0}{(L_0+L_2)i_0};\alpha_3=\frac{K_E\theta_0}{(L_0+L_2)i_0}$$
$$\beta_1=\frac{\lambda}{Mw_0};\beta_2=\frac{Bl_ri_0}{Mw_0^2x_0};\gamma_1=\frac{c_v}{J_rw_0};\gamma_2=\frac{K_Ti_0}{J_rw_0^2\theta_0};E_0=\frac{e_0}{(L_0+L_2)w_0i_0}.\tag{6}$$

Linear Inductance with Nonlinear Spring

Considering now the case where the inductance in series with the generator remains linear with the value L_0 and the nonlinear spring mechanism is present $(k_0\neq0)$, the differential equations are given as

$$\dot{x}_1+\alpha_1x_1+\alpha_2\dot{x}_3+\alpha_3\dot{y}=E_0\cos(\Omega\tau),\tag{7a}$$

$$\ddot{x}_3+\beta_1\dot{x}_3+\beta_2\left[1-2\alpha\left(\frac{1}{\sqrt{a^2+x_3^2}}-1\right)\right]x_3-\beta_3x_1=0,\tag{7b}$$

$$\ddot{y} + \gamma_1 \dot{y} - \gamma_2 x_1 = 0. \tag{7c}$$

The new coefficients are given as follows

$$\alpha = \frac{k_0}{k_v}; a = \frac{a_0}{l_0}; \beta_2 = \frac{k_v}{M w_0^2}; \beta_3 = \frac{B l_r i_0}{M w_0^2 l_0}. \tag{8}$$

Nonlinear Inductance with Nonlinear Spring

Let us use the following dimensionless parameters:

$$\alpha_1 = \frac{(R+R_2)}{L_0 w_0}; \alpha_2 = \frac{B l_r l_0}{L_0 i_0}; \alpha_3 = \frac{K_E \theta_0}{L_0 i_0}; \alpha_4 = \frac{L_2}{L_0}; \beta_1 = \frac{\lambda}{M w_0}$$
$$\beta_2 = \frac{k_v}{M w_0^2}; \beta_3 = \frac{B l_r i_0}{M w_0^2 L_0}; \gamma_1 = \frac{c_v}{J_r w_0}; \gamma_2 = \frac{K_T i_0}{J_r w_0^2 \theta_0}; E_0 = \frac{e_0}{L_0 w_0 i_0}. \tag{9}$$

In this more general case, the system is modelled as follows:

$$\begin{cases} \left(1 - \eta + \dfrac{2\eta}{1+\cosh(x_1)} + \alpha_4\right)\dot{x}_1 + \alpha_1 x_1 + \alpha_2 \dot{x}_3 + \alpha_3 \dot{y} = E_0 \cos(\Omega\tau) \\ \ddot{x}_3 + \beta_1 \dot{x}_3 + \beta_2 \left[1 - 2\alpha\left(\dfrac{1}{\sqrt{a^2 + x_3^2}} - 1\right)\right] x_3 - \beta_3 x_1 = 0 \\ \ddot{y} + \gamma_1 \dot{y} - \gamma_2 x_1 = 0. \end{cases} \tag{10}$$

Mathematical and Numerical Methods

Harmonic Balance Method

To predict the behaviour of the system in terms of amplitude, the corresponding modelling equations are solved analytically using the harmonic balance method restricting to the first harmonics. In this spirit, assuming that the device performs small angular and tranlational displacement, the harmonic solutions of equations are expressed under the following form:

$$x_1 = A\cos(\Omega t - \varphi_1), x_3 = B\cos(\Omega t - \varphi_2), x_4 = C\cos(\Omega t - \varphi_3),$$
$$y = D\cos(\Omega t - \varphi_4), z = E\cos(\Omega t - \varphi_5), \tag{11}$$

where A, B, C, D and E are unknown maximal amplitudes, Ω the frequency and $\varphi_i (i = 1, 2, 3, 4, 5)$ the initial phases, all to be determined. Replacing Eq. (11), into the differential equations, then equating separately the coefficient of sine and cosine terms, one obtains a system of algebraic equations, which give the values of the unknown amplitudes.

Numerical Methods for Differential Equation

To obtain numerically the dynamical behaviours of the electromechanical device, the fourth-order Runge–Kutta (RK4) algorithm is used to solve by computer simulation the differential equations.

Bifurcation Diagram and Lyapunov Exponent

Bifurcation diagram and Lyapunov exponent help to characterize the different dynamical states in the system. The Largest Lyapunov exponent is defined as

$$\lambda_{\max} = \lim_{t \to \infty} \left[\frac{1}{t} \ln(D(t))\right], \tag{12}$$

where $D(t) = \sqrt{\xi_1^2 + \xi_2^2 + \xi_3^2 + \xi_4^2 + \xi_5^2}$, and is computed from the following variational equations:

$$\dot{\xi}_1 = -\alpha_1 \xi_1 - \alpha_2 \xi_3 + \alpha_3 \xi_5, \dot{\xi}_2 = \xi_3,$$
$$\dot{\xi}_3 = -\beta_1 \xi_3 - \beta_2 \xi_2 \left[1 - 2\alpha\left(\frac{1}{\sqrt{a^2 + x_3^2}} - 1\right) + \frac{2\alpha x_3^2}{\left(a^2 + x_3^2\right)^{3/2}}\right] + \beta_3 \xi_1,$$
$$\dot{\xi}_4 = \xi_5, \dot{\xi}_5 = -\gamma_1 \xi_5 + \gamma_2 \xi_1. \tag{13}$$

Equation (3) is obtained by adding some perturbations on the solutions of Eqs. (7a)–(7c) as follows: $x_1 \to x_1 + \xi_1$, $x_3 \to x_3 + \xi_2$, $x_4 \to x_4 + \xi_3$, $y \to y + \xi_4$, $z \to z + \xi_5$. $D(t)$ is thus the distance between neighboring trajectories. The hysteretic behavior of the inductance was discarded when writing Eq. (13).

Results and Discussion

Frequency Response Curves in the Linear Case

In this case, we replace Eq. (11) into Eq. (5) and then equate separately the coefficients of sine and cosine terms, one obtains a set of algebraic Eq. (14) where the unknowns are A, B, C and the phase φ_1, φ_2, and φ_3.

$$\begin{cases} \alpha_1 A\cos\varphi_1 + \Omega A\sin\varphi_1 + \alpha_2 \Omega B\sin\varphi_2 + \alpha_3 \Omega C\sin\varphi_3 = E \\ -\Omega A\cos\varphi_1 + \alpha_1 A\sin\varphi_1 - \alpha_2 \Omega B\cos\varphi_2 - \alpha_3 \Omega C\sin\varphi_3 = 0 \\ -B\Omega^2\cos\varphi_2 - \beta_1 \Omega B\sin\varphi_2 + B\cos\varphi_2 - \beta_2 A\cos\varphi_1 = 0 \\ \beta_1 \Omega B\cos\varphi_2 - B\Omega^2\sin\varphi_2 + B\sin\varphi_2 - \beta_2 A\sin\varphi_1 = 0 \\ -C\Omega^2\cos\varphi_3 + \gamma_1 \Omega C\sin\varphi_3 - \gamma_2 A\cos\varphi_1 = 0 \\ -\gamma_1 \Omega C\cos\varphi_3 - C\Omega^2\sin\varphi_3 - \gamma_2 A\cos\varphi_1 = 0 \end{cases} \tag{14}$$

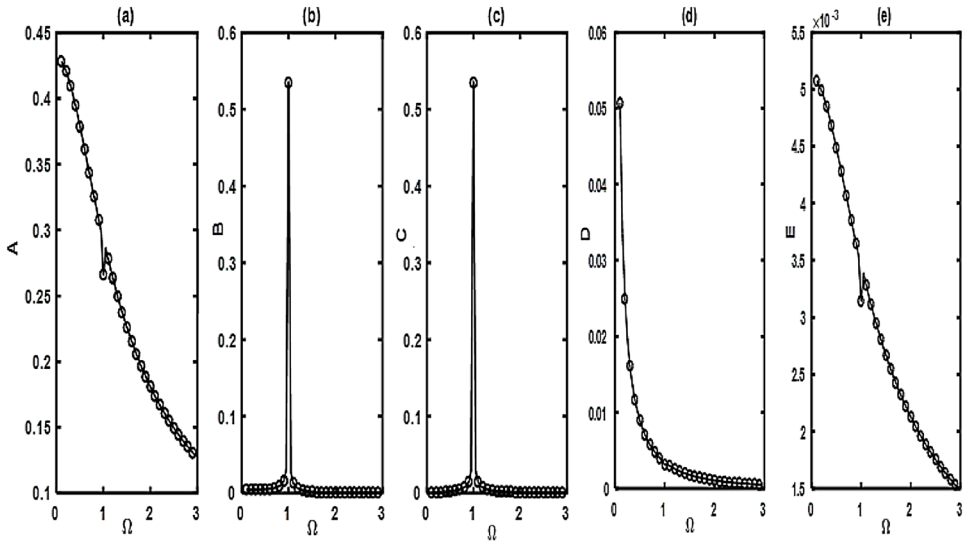

Fig. 3 Analytical (full line) and numerical (dot line) frequency–response curves: **a** amplitude of the electrical current; **b** amplitude of the rod displacement; **c** amplitude of the rod velocity; **d** amplitude of the angular displacement; **e** amplitude of the angular velocity. With $E = 0.39$

From this set of equations, one obtains the mathematical expressions of the unknown amplitudes as given in Eq. (15).

$$
\begin{aligned}
A^2 &= \frac{E_0^2}{\left[\alpha_1 + \frac{\alpha_2\beta_1\gamma_2\Omega^2}{\beta_1^2\Omega^2+(1-\Omega^2)^2} + \frac{\alpha_3\gamma_1\gamma_2\Omega^2}{\Omega^4+\gamma_1^2\Omega^2}\right]^2 + \left[\Omega + \frac{\alpha_2\gamma_2\Omega(1-\Omega^2)}{\beta_1^2\Omega^2+(1-\Omega^2)^2} - \frac{\alpha_3\gamma_2\Omega^3}{\Omega^4+\gamma_1^2\Omega^2}\right]^2},\\
B^2 &= \frac{\beta_2^2 E_0^2}{\left[\beta_1^2\Omega^2 + (1-\Omega^2)^2\right]\left[\left[\alpha_1 + \frac{\alpha_2\beta_1\gamma_2\Omega^2}{\beta_1^2\Omega^2+(1-\Omega^2)^2} + \frac{\alpha_3\gamma_1\gamma_2\Omega^2}{\Omega^4+\gamma_1^2\Omega^2}\right]^2 + \left[\Omega + \frac{\alpha_2\gamma_2\Omega(1-\Omega^2)}{\beta_1^2\Omega^2+(1-\Omega^2)^2} - \frac{\alpha_3\gamma_2\Omega^3}{\Omega^4+\gamma_1^2\Omega^2}\right]^2\right]},\\
C^2 &= \frac{\Omega^2\beta_2^2 E_0^2}{\left[\beta_1^2\Omega^2 + (1-\Omega^2)^2\right]\left[\left[\alpha_1 + \frac{\alpha_2\beta_1\gamma_2\Omega^2}{\beta_1^2\Omega^2+(1-\Omega^2)^2} + \frac{\alpha_3\gamma_1\gamma_2\Omega^2}{\Omega^4+\gamma_1^2\Omega^2}\right]^2 + \left[\Omega + \frac{\alpha_2\gamma_2\Omega(1-\Omega^2)}{\beta_1^2\Omega^2+(1-\Omega^2)^2} - \frac{\alpha_3\gamma_2\Omega^3}{\Omega^4+\gamma_1^2\Omega^2}\right]^2\right]},\\
D^2 &= \frac{\gamma_2^2 E_0^2}{(\Omega^4+\gamma_1^2\Omega^2)\left[\left[\alpha_1 + \frac{\alpha_2\beta_1\gamma_2\Omega^2}{\beta_1^2\Omega^2+(1-\Omega^2)^2} + \frac{\alpha_3\gamma_1\gamma_2\Omega^2}{\Omega^4+\gamma_1^2\Omega^2}\right]^2 + \left[\Omega + \frac{\alpha_2\gamma_2\Omega(1-\Omega^2)}{\beta_1^2\Omega^2+(1-\Omega^2)^2} - \frac{\alpha_3\gamma_2\Omega^3}{\Omega^4+\gamma_1^2\Omega^2}\right]^2\right]},\\
E^2 &= \frac{\Omega^2\gamma_2^2 E_0^2}{(\Omega^4+\gamma_1^2\Omega^2)\left[\left[\alpha_1 + \frac{\alpha_2\beta_1\gamma_2\Omega^2}{\beta_1^2\Omega^2+(1-\Omega^2)^2} + \frac{\alpha_3\gamma_1\gamma_2\Omega^2}{\Omega^4+\gamma_1^2\Omega^2}\right]^2 + \left[\Omega + \frac{\alpha_2\gamma_2\Omega(1-\Omega^2)}{\beta_1^2\Omega^2+(1-\Omega^2)^2} - \frac{\alpha_3\gamma_2\Omega^3}{\Omega^4+\gamma_1^2\Omega^2}\right]^2\right]}.
\end{aligned}
\tag{15}
$$

We analyse the behaviours of A, B, C and D when the frequency Ω of the external excitation is varied and the results are presented in Fig. 3.

As it appears in Fig. 3, when the frequency increases from 0.0 to 3.0, A decreases progressively from the maximum amplitude to the amplitude equal to 0.26 ($\Omega = 1$), then increases a bit and finally decreases to a lower amplitude. In the mean time, the amplitudes B and C increase from almost zero to a higher amplitude equal to 0.53 and decreases to small values. When the frequency is equal to 1, an anti-resonance phenomenon in the electrical part and resonance phenomenon in the translation motion are observed in (Fig. 3a–c). The amplitude of the angular displacement D decreases when the frequency

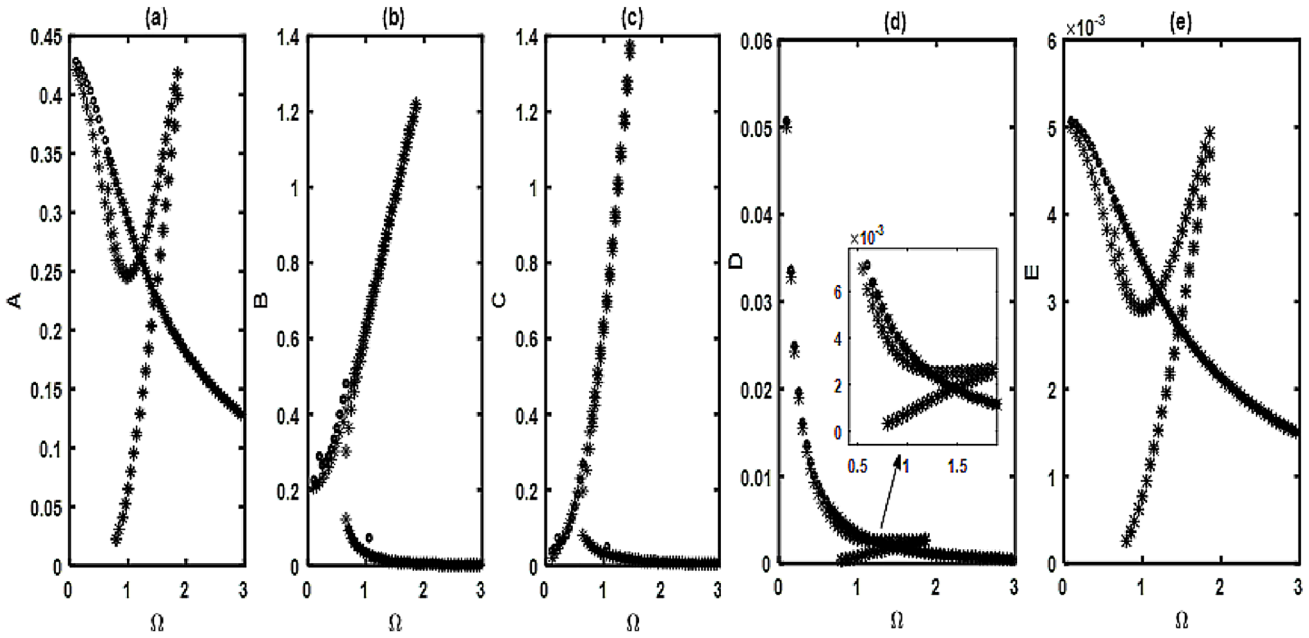

Fig. 4 Analytical (star line) and numerical (dot line) frequency–response of: **a** amplitude of the electrical current; **b** amplitude of the rod displacement; **c** amplitude of the rod velocity; **d** amplitude of the angular displacement; **e** amplitude of the angular velocity. With $E = 0.39$

increases. D has the same behavior as A. The anti-resonance in the electrical current means that when the power dissipated by the Joule effect is minimum, the displacement of the rod is maximal.

Frequency Response Curves in the System with Linear Inductance and Nonlinear Spring

To conduct more analytical investigations, an approximate cubic expression of the term, which contains the square root, is developed using a Taylor series expansion at the static equilibrium position $x_3 = 0$. One obtains:

$$F(x_3) = \left[1 - 2\alpha\left(\frac{1}{\sqrt{a^2 + x_3^2}} - 1\right)\right]x_3 = \left[1 - 2\alpha\left(\frac{1-a}{a}\right)\right]x_3 + \frac{\alpha}{a^3}x_3^3. \tag{16}$$

Inserting Eq. (16) in Eq. (7b) and using Eq. (11), the harmonic balance method is used. After some algebraic manipulations, it comes that the amplitudes satisfy the following nonlinear algebraic equations:

$$\frac{B^2\left[\beta_1^2\Omega^2 + \left(F + \frac{3\alpha}{4a^3}\beta_2 B^2\right)^2\right]}{\beta_3^2}\left[\left[\alpha_1 + \frac{\alpha_2\Omega^2\beta_1\beta_3}{\beta_1^2\Omega^2 + \left(F + \frac{3\alpha}{4a^3}\beta_2 B^2\right)^2} + G\right]^2 + \left[\Omega + \frac{\alpha_2\beta_3\Omega\left(F + \frac{3\alpha}{4a^3}\beta_2 B^2\right)}{\beta_1^2\Omega^2 + \left(F + \frac{3\alpha}{4a^3}\beta_2 B^2\right)^2} - \frac{\Omega}{\gamma_1}G\right]^2\right] - E_0^2 = 0$$

$$A^2 = \frac{B^2\left[\beta_1^2\Omega^2 + \left(F + \frac{3\alpha}{4a^3}\beta_2 B^2\right)^2\right]}{\beta_3^2};$$

$$D^2 = \frac{\gamma_2^2 B^2}{(\Omega^4 + \gamma_1^2\Omega^2)\beta_3^2}\left[\beta_1^2\Omega^2 + \left(F + \frac{3\alpha}{4a^3}\beta_2 B^2\right)^2\right]; C^2 = \Omega^2 B^2$$

$$E^2 = \frac{\Omega^2\gamma_2^2 B^2}{(\Omega^4 + \gamma_1^2\Omega^2)\beta_3^2}\left[\beta_1^2\Omega^2 + \left(F + \frac{3\alpha}{4a^3}\beta_2 B^2\right)^2\right];$$

$$F = -\Omega^2 + \beta_2\left(1 - 2\alpha\left(\frac{1-a}{a}\right)\right); G = \frac{\alpha_3\gamma_1\gamma_2\Omega^2}{\Omega^4 + \gamma_1^2\Omega^2}. \tag{17}$$

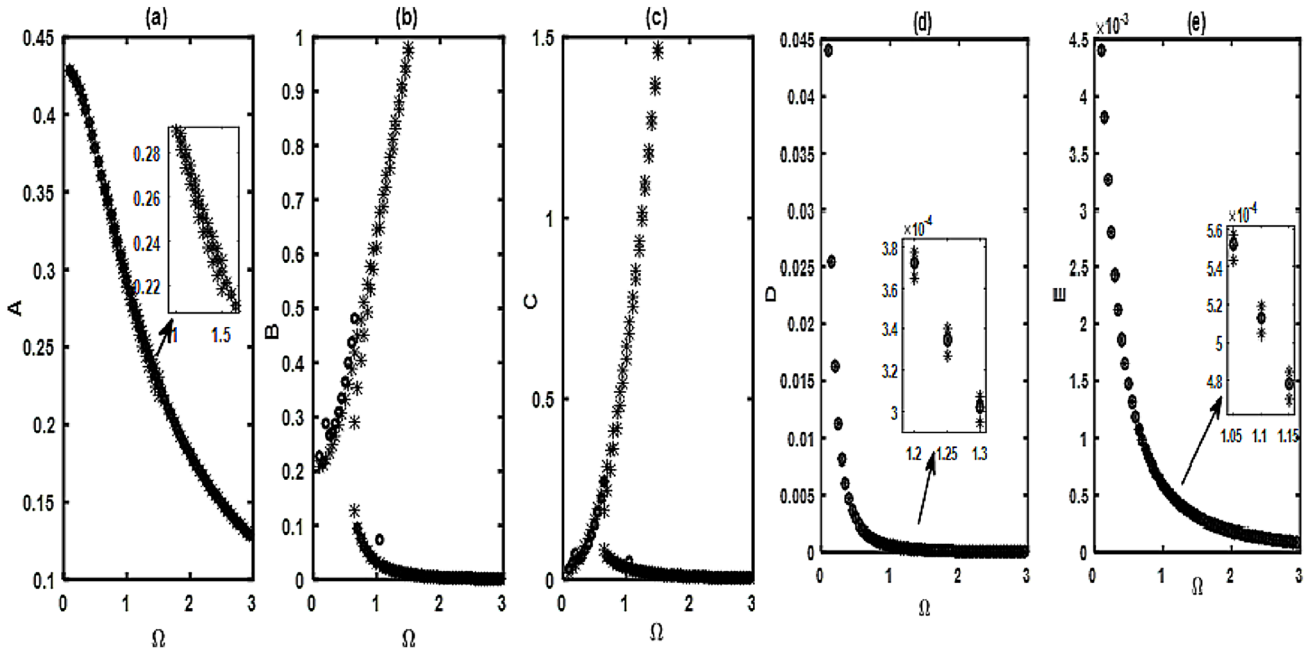

Fig. 5 Analytical (star line) and numerical (dot line) frequency–response of: **a** amplitude of the electrical current; **b** amplitude of the rod displacement; **c** amplitude of the rod velocity; **d** amplitude of the angular displacement; **e** amplitude of the angular velocity. With $E = 0.39$

Figure 4 presents the frequency–response curves for this nonlinear model. Both the results from Eq. (17) and those obtained from the numerical simulation of Eqs. (7a)–(7c) are plotted. The curves show that the amplitude of the electrical current, that of the angular displacement and that of the angular velocity decrease when the frequency increases. Also notice the three values sometimes four of these amplitudes when the frequency is between 0.65 and 1.85. This can understood as two stable solutions separated by an unstable solution. This effect generally leads to the jump phenomenon and hysteresis as shown in the curves of Fig. 4b and c.

Frequency–Response Curves in the System with Nonlinear Inductance and Nonlinear Spring

For analytical treatment, the nonlinear spring expression is developed as in Eq. (16) while

$$\frac{1}{1+\cosh x_1} \approx \frac{1}{2}\left(1-\frac{x_1^2}{4}\right) \tag{18}$$

Considering Eqs. (10) and (11), the amplitudes A, B, C, D and E satisfy the following equations:

$$B^2\left[\beta_1^2\Omega^2+\left(F+\frac{3\alpha}{4a^3}\beta_2B^2\right)^2\right]\frac{1}{\beta_3^2}\left[\left[\alpha_1+\frac{\alpha_2\Omega^2\beta_1\beta_3}{\beta_1^2\Omega^2+\left(F+\frac{3\alpha}{4a^3}\beta_2B^2\right)^2}+G\right]^2+\left[(1+\alpha_4)\Omega-\frac{\Omega\eta B^2\left(\beta_1^2\Omega^2+\left(F+\frac{3\alpha}{4a^3}\beta_2B^2\right)^2\right)}{16\beta_3^2}+\frac{\alpha_2\beta_3\Omega\left(F+\frac{3\alpha}{4a^3}\beta_2B^2\right)}{\beta_1^2\Omega^2+\left(F+\frac{3\alpha}{4a^3}\beta_2B^2\right)^2}-\frac{\Omega}{\gamma_1}G\right]^2\right]-E_0^2=0 \tag{19}$$

$$A^2=\frac{B^2\left[\beta_1^2\Omega^2+\left(F+\frac{3\alpha}{4a^3}\beta_2B^2\right)^2\right]}{\beta_3^2};C^2=\Omega^2B^2;E^2=\frac{\Omega^2\gamma_2^2B^2}{(\Omega^4+\gamma_1^2\Omega^2)\beta_3^2}\left[\beta_1^2\Omega^2+\left(F+\frac{3\alpha}{4a^3}\beta_2B^2\right)^2\right].$$

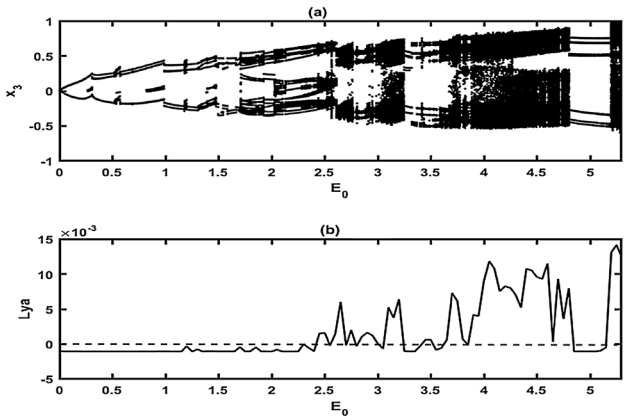

Fig. 6 **a** Bifurcation diagram, **b** the corresponding Lyapunov exponent, versus the amplitude of the excitation E_0 with the parameters of Tables 1, 2, 3, 4 and $\Omega = 0.1$

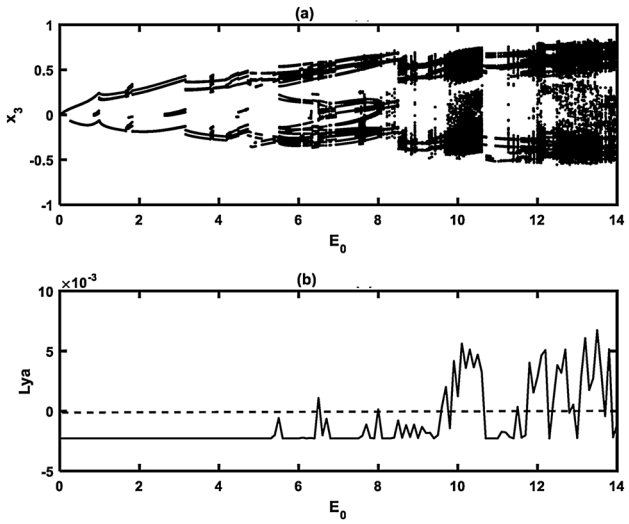

Fig. 8 **a** Bifurcation diagram and **b** Lyapunov exponent diagram against the amplitude of the excitation E with the parameter of Fig. 7 and for $\Omega = 0.1$

The frequency–response curves of the maximal amplitudes are represented in Fig. 5.

The frequency–response curve of the nonlinear mechanical system shows that when frequency increases, the maximal amplitudes of the electrical current, the angular displacement and the angular velocity decrease. Multiple amplitudes domain is for frequency between 0.65 and 1.5 and jump phenomenon and hysteresis appear in Fig. 5b and c.

Bifurcation Diagram in the System with Linear Inductance and Nonlinear Spring

Numerical simulations are used to illustrate the dynamical behaviours of the system mathematically represented by Eqs. (7a)–(7c) through bifurcation diagrams, Lyapunov exponent, and phase portraits. In this subsection, the parameters E_0 *is* chosen as the control parameter.

From Fig. 6, one can see that when the maximal value of the external excitation increases, the translational motion of the device firstly presents a periodic and multi periodic motion for $0 \leq E_0 \leq 2.4$. After this range, the system responses exhibit an alternation of chaotic and periodic motions. The chaotic behavior of the system starts when $E_0 = 2.5$. To confirm the results in Fig. 6, some phase portraits are plotted in Fig. 7 where one finds chaos (Fig. 7c) and periodic motions (Fig. 7a, b and d).

Bifurcation Diagrams in the System with Nonlinear Inductance and Nonlinear Spring

The dynamics of the system mathematically represented by Eq. (10) is analysed through bifurcation diagrams, Lyapunov exponent, and phase portraits.

Control Parameter E_0.

The bifurcation diagram versus E_0 is plotted in Fig. 8a in term of non-dimensional displacement of the rod x_3 as E_0 is varies from 0 up to 15. Chaotic behavior of the system begins when $E_0 = 9.7$. Before this value,

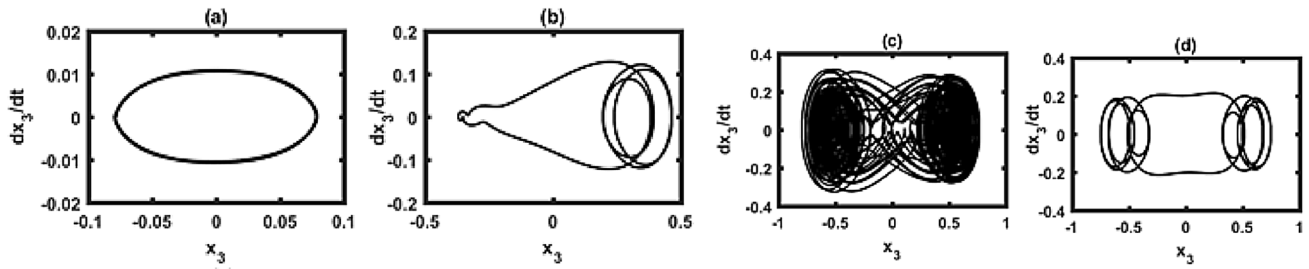

Fig. 7 Phase portraits obtain with parameter of Fig. 6 and **a** $E_0 = 0.1$, **b** $E_0 = 1.5$, **c** $E_0 = 4$, **d** $E_0 = 5$

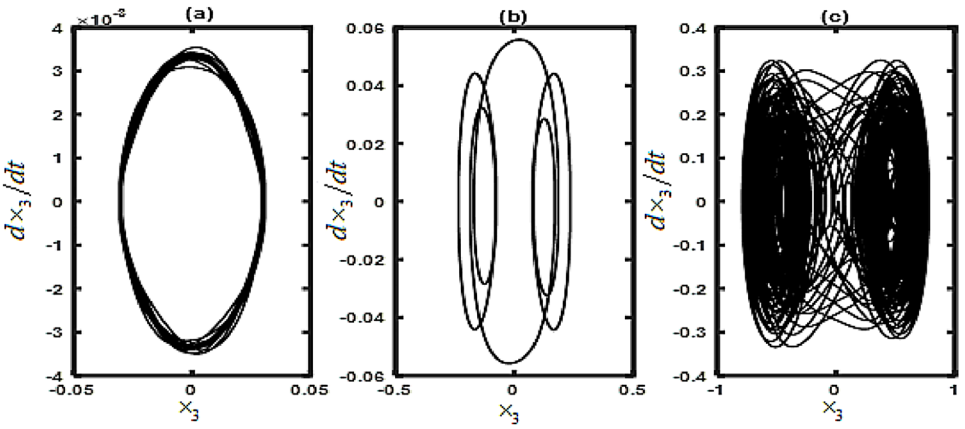

Fig. 9 Phase portraits with the parameter of Fig. 8. **a** $E_0 = 0.1$; **b** $E_0 = 1$; **c** $E_0 = 12$

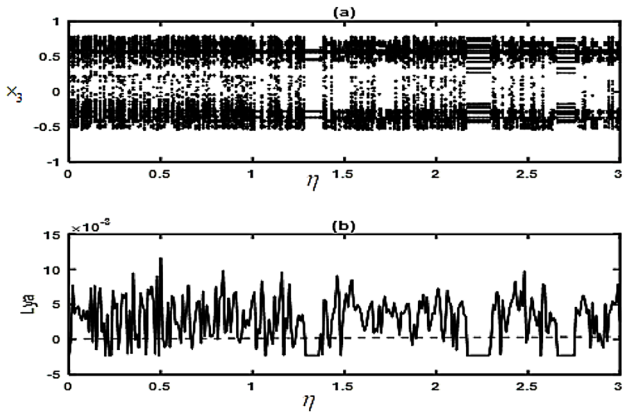

Fig. 10 **a** Bifurcation diagram and **b** Lyapunov exponent diagram against the control parameter η with the parameter of Fig. 9 and $E_0 = 12$

the system presents a periodic motion for $0 \leq E_0 < 9.7$. After this periodic motion, the system response alternatively comes into chaotic and periodic dynamics as E_0 varies. These behaviors are confirmed by Fig. 8b which presents the variation of the Lyapunov exponent.

Figure 9 shows different phase portraits of the rod motion. Period-nT motion is observed in Fig. 9a and b while chaotic oscillations is presented in Fig. 9c.

Comparing these results to the previous one (see Figs. 6 and 7), one finds that when the nonlinearity is introduced in the inductor, chaotic behaviour appears for larger values of the external excitation (i.e. as from $E_0 = 9.5$) than in the case of linear inductance where the chaotic behaviour appears as from $E_0 = 2.5$.

Control Parameter η

To analyse, the effects of the inductance hysteresis parameter η on the dynamics of the device, a bifurcation diagram and the corresponding Lyapunov exponent are plotted in Fig. 10 as η varies. One observes that when η increases the system exhibits a chaotic oscillation for $0 \leq \eta < 1.3; 1.37 \leq \eta < 2.17$; $2.3 \leq \eta < 2.66$ and $2.76 \leq \eta < 3$. Non-chaotic behaviors are obtained in the other ranges. These behaviors are confirmed by the phase portraits which present chaotic motions

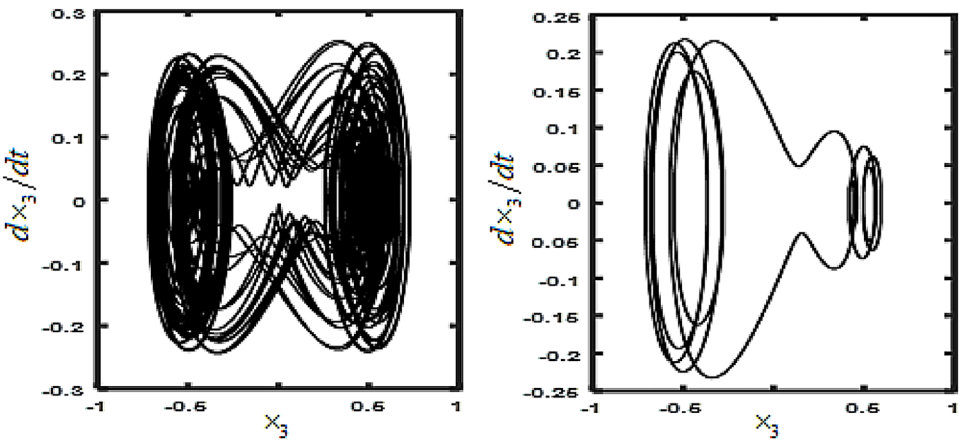

Fig. 11 Phase portraits obtained with the parameters off Fig. 10 and **a** $\eta = 0.3$; **b** $\eta = 1.33$

in Fig. 11a, while Fig. 11b presents periodic-nT oscillations.

The results of the numerical simulation show that chaotic behavior can be found for very low values of the inductance hysteresis parameter η.

Conclusion

In this work, the dynamics of an electromechanical device having two main particularities. The first one is that it combines rotational and translational motions indicating that the mechanical system rotates while undergoing translation. The second one is related to the types of nonlinearities used. The first nonlinear component is an inductor chose the current–inductance characteristics show a highly nonlinear relationship because of the hysteretic iron-core involved. The second nonlinearity is of the mechanical nature. It involves the association of three springs two of which are oblique while one follows the motion direction. Because of the oblique position, geometric nonlinearity appears in the system. Analytical and numerical investigations have been undertaken to present the different dynamical behaviors which can take place in such a complex electromechanical system.

Assuming small amplitude motion, the nonlinear terms have been linearized to give a set of equations analytically treatable. The mathematical expressions of the oscillations amplitudes have been obtained and the frequency–response curves show that when the power dissipated through the Joule effect is small, the displacement amplitude is high.

In the nonlinear limit, the numerical results show complex dynamical behaviors such as jump phenomenon, periodic motion and chaos. It is seen that when the external excitation amplitude increases, the complexity of the dynamical behaviors increases moving from period-nT oscillations to chaotic oscillations. In presence of the inductance with nonlinear characteristics, it is found that chaotic behaviors appear for larger values of the external excitation than in the case of linear inductance. With the increase of the inductance hysteresis parameter η the behaviour change alternately from chaotic motion to periodic motion and chaotic motions are observed even for very low value of η.

These results are interesting since they give the parameter ranges where the device can be used either in the regular dynamics or in the chaotic states. The complex behaviors of this device can find applications in various branches of electromechanical engineering such as boring machine and drilling machine. This device can be also used in home as a mixer in which chaotic oscillations can improve its efficiency while going up and down inside the products to be mixed.

Declarations

Conflict of interest On behalf of all authors, the corresponding author states that there is no conflict of interest.

References

1. Kuhnert WM, Cammarano A, Silveira M (2021) Synthesis of viscoelastic behavior through electromechanical coupling. J Vib Eng Technol 9:367–379. https://doi.org/10.1007/s42417-020-00235-0
2. Nana B, Yamgoué SB, Tchitnga R, Woafo P (2017) Dynamics of a pendulum driven by a DC motor and magnetically controlled. Chaos Solit Frac 104:18–27. https://doi.org/10.1016/j.chaos.2016.09.025
3. Kindly provide complete details for the Ref. [3], if possible.
4. He C, Li S, Shao K, Meng W, Zhao H (2021) Robust iterative feedback tuning control of a permanent magnet synchronous motor with repetitive constraints: a Udwadia-Kalaba approach. J Vib Eng Technol. https://doi.org/10.1007/s42417-021-00365-z
5. Tcheutchoua FD, Woafo P (2013) Generation of complex phenomena in a simple electromechanical system using the feedback control. Commun Nonlinear Sci Numer Simulat 18:209–218. https://doi.org/10.1016/j.cnsns.2012.06.021
6. Zhe L (1995) Chaotic vibration sieve. Mech Mach Theory 30:608–613. https://doi.org/10.1016/0094-114X(94)00061-O
7. Chau KT, Ye S, Gao Y (2004) Application to chaotic-motions motors to industrial mixing processes. IEEE 1AS:1874–1880. https://doi.org/10.1109/IAS.2004.1348725
8. Tcheutchoua FD, Woafo P (2011) Dynamics of an electromechanical system with angular and ferroresonant non linearities. J Sound Vib 133:1–7. https://doi.org/10.1115/1.4004938
9. Ottino JM, Muzzio FJ, Tjahjadi M (1992) Chaos, symmetry, and self-similarity: exploiting order and disorder in mixing process. Science 257:754–760. https://doi.org/10.1126/science.257.5071.754
10. Kitio KCA, Woafo P (2010) Experimental realization and simulation of a self-sustained macro electromechanical system. Mech Res Commun 37:106–110. https://doi.org/10.1115/1.4000827
11. Wang Z, Chau KT (2008) Anti-control of chaos of a permanent magnet DC motor system for vibratory compactors. Chaos Solit Frac 36:694–708. https://doi.org/10.1016/j.chaos.2006.06.105
12. Nana B, Yamgoué SB, Kemajou I, Tchitnga R, Woafo P (2018) Dynamics of a RLC series circuit with hysteretic iron-core inductor. Chaos Solit Frac 106:184–191. https://doi.org/10.1016/j.chaos.2017.11.014
13. Sonfack BH, Nana NBR, Woafo P (2020) Isolation performance of a quasi-zero stiffness isolator in vibration isolation of a multi-span continuous beam bridge under pier base vibrating. Nonlinear Dyn 100:1125–1141. https://doi.org/10.1007/s11071-020-05580-z
14. Ghodssi R, Lin P (2011) MEMS materials and processes handbook. Springer, Berlin, pp 925–1044

15. Sun X, Xu J, Jing X, Cheng L (2014) Beneficial performance of a quasi-zero-stiffness vibration isolator with time-delayed active control. Int J Mech Sci 82:32–40. https://doi.org/10.1016/j.ijmessci.2014.03.002
16. Balaji PS, Karthik Selvakuma K (2021) Application of nonlinearity in passive vibration control. J Vib Eng Technol 9:183–213. https://doi.org/10.1007/s42417-020-00216-3
17. Nana B, Yamgoué SB, Tchitnga R, Woafo P (2018) Nonlinear dynamics of a sinusoidally driven lever in repulsive magnetic fields. Nonlinear Dyn 91:55–66. https://doi.org/10.1007/s11071-017-3839-9
18. Yan L, Gong X (2018) Experimental study of vibration isolation characteristics of a geometric anti-spring isolator. Appl Sci 7(7):1–20. https://doi.org/10.3390/app7070711